2020-03

EVALUATION OF UNSCHEDULED INTENTIONAL ISLANDING METHODS FOR SINGLE PHASE GRID-CONNECTED INVERTERS IN COMPLIANCE WITH IEEE STANDARD 1547-2018

Tencate, Timothy

Monterey, CA; Naval Postgraduate School

NAVAL POSTGRADUATE SCHOOL

MONTEREY, CALIFORNIA

THESIS

EVALUATION OF UNSCHEDULED INTENTIONAL ISLANDING METHODS FOR SINGLE PHASE GRID-CONNECTED INVERTERS IN COMPLIANCE WITH IEEE STANDARD 1547-2018

by

Timothy Tencate

March 2020

Thesis Advisor: Giovanna Oriti
Co-Advisor: Roberto Cristi

THIS PAGE INTENTIONALLY LEFT BLANK

REPORT DOCUMENTATION PAGE	*Form Approved OMB No. 0704-0188*

1. AGENCY USE ONLY *(Leave blank)*	**2. REPORT DATE** March 2020	**3. REPORT TYPE AND DATES COVERED** Master's thesis

4. TITLE AND SUBTITLE
EVALUATION OF UNSCHEDULED INTENTIONAL ISLANDING METHODS FOR SINGLE PHASE GRID-CONNECTED INVERTERS IN COMPLIANCE WITH IEEE STANDARD 1547-2018

5. FUNDING NUMBERS

6. AUTHOR(S) Timothy Tencate

7. PERFORMING ORGANIZATION NAME(S) AND ADDRESS(ES)
Naval Postgraduate School
Monterey, CA 93943-5000

8. PERFORMING ORGANIZATION REPORT NUMBER

9. SPONSORING / MONITORING AGENCY NAME(S) AND ADDRESS(ES)
N/A

10. SPONSORING / MONITORING AGENCY REPORT NUMBER

11. SUPPLEMENTARY NOTES The views expressed in this thesis are those of the author and do not reflect the official policy or position of the Department of Defense or the U.S. Government.

12a. DISTRIBUTION / AVAILABILITY STATEMENT
Approved for public release. Distribution is unlimited.

12b. DISTRIBUTION CODE
A

13. ABSTRACT (maximum 200 words)

A power electronics-based Energy Management System (EMS) is a key component of a microgrid; it manages loads, controls power flow to improve overall efficiency, and disconnects Distributed Energy Resources (DER) from the main grid in the event of a grid fault. The latter is the focus of the research conducted in this thesis. IEEE Standard 1547-2018 provides the requirements relevant to the connection of a microgrid to the main grid. The standard requires that the disconnection control method maintains connection for a specified time, known as voltage ride-through time, during voltage disturbances in the main grid voltage.

This thesis explores five different methods of EMS control and their respective algorithm for disconnection from the grid. The response times of disconnection from the grid are simulated using a physics-based model validated by experimental measurements on a laboratory prototype. The simulations are compared against the IEEE Standard 1547-2018 voltage ride-through times to determine if the different controller dynamic responses meet the requirements. Of the five methods tested, all were in compliance with IEEE Standard 1547-2018 grid disconnection times but only the two best performing methods, extended Multiple Second Order Generalized Integrator (MSOGI) and true root mean squared (RMS), were able to comply with the voltage ride-through requirements.

14. SUBJECT TERMS microgrid, supercapacitors, IEEE Standard 1547, Distributed Energy Resources	**15. NUMBER OF PAGES** 133
	16. PRICE CODE

17. SECURITY CLASSIFICATION OF REPORT	**18. SECURITY CLASSIFICATION OF THIS PAGE**	**19. SECURITY CLASSIFICATION OF ABSTRACT**	**20. LIMITATION OF ABSTRACT**
Unclassified	Unclassified	Unclassified	UU

NSN 7540-01-280-5500

Standard Form 298 (Rev. 2-89)
Prescribed by ANSI Std. 239-18

THIS PAGE INTENTIONALLY LEFT BLANK

Approved for public release. Distribution is unlimited.

EVALUATION OF UNSCHEDULED INTENTIONAL ISLANDING METHODS FOR SINGLE PHASE GRID-CONNECTED INVERTERS IN COMPLIANCE WITH IEEE STANDARD 1547-2018

Timothy Tencate
Lieutenant, United States Navy
BSME, University of Oklahoma, 2012

Submitted in partial fulfillment of the
requirements for the degree of

MASTER OF SCIENCE IN ELECTRICAL ENGINEERING

from the

NAVAL POSTGRADUATE SCHOOL
March 2020

Approved by: Giovanna Oriti
Advisor

Roberto Cristi
Co-Advisor

Douglas J. Fouts
Chair, Department of Electrical and Computer Engineering

THIS PAGE INTENTIONALLY LEFT BLANK

ABSTRACT

A power electronics-based Energy Management System (EMS) is a key component of a microgrid; it manages loads, controls power flow to improve overall efficiency, and disconnects Distributed Energy Resources (DER) from the main grid in the event of a grid fault. The latter is the focus of the research conducted in this thesis. IEEE Standard 1547-2018 provides the requirements relevant to the connection of a microgrid to the main grid. The standard requires that the disconnection control method maintains connection for a specified time, known as voltage ride-through time, during voltage disturbances in the main grid voltage.

This thesis explores five different methods of EMS control and their respective algorithm for disconnection from the grid. The response times of disconnection from the grid are simulated using a physics-based model validated by experimental measurements on a laboratory prototype. The simulations are compared against the IEEE Standard 1547-2018 voltage ride-through times to determine if the different controller dynamic responses meet the requirements. Of the five methods tested, all were in compliance with IEEE Standard 1547-2018 grid disconnection times but only the two best performing methods, extended Multiple Second Order Generalized Integrator (MSOGI) and true root mean squared (RMS), were able to comply with the voltage ride-through requirements.

THIS PAGE INTENTIONALLY LEFT BLANK

TABLE OF CONTENTS

LIST OF FIGURES

THIS PAGE INTENTIONALLY LEFT BLANK

LIST OF TABLES

THIS PAGE INTENTIONALLY LEFT BLANK

LIST OF ACRONYMS AND ABBREVIATIONS

BPS	Bulk Power System
DER	Distributed Energy Resources
DR	Distributed Resources
EMS	Energy Management System
EPS	Electrical Power System
FLL	Frequency Locked Loop
HDN	Harmonics Decoupling Network
IEEE	Institute of Electrical and Electronics Engineers
IID	Island Interconnection Device
IGBT	Insulated-Gate Bipolar Transistor
JTAG	Joint Action Test Group
LAPES	Local Area Power and Energy System
MSOGI	Multiple Second Order Generalized Integrator
NPS	Naval Postgraduate School
PCC	Point of Common Coupling
PWM	Pulse Width Modulation
SOGI	Second Order Generalized Integrator
RMS	Root Mean Squared

THIS PAGE INTENTIONALLY LEFT BLANK

ACKNOWLEDGMENTS

There are many people in my life that I am thankful for:

To Marisa, the strongest person I know. I am so thankful to have you in my life. I could not have asked for a better wife and a better mother for our children.

To my three children, Alaina, Elizabeth, and Joanna. You are the reason for everything that I do, and I love you with all my heart.

To Dr. Giovanna Oriti and Dr. Alexander Julian for their help during this process: I especially thank them for listening to my ideas and helping to focus my efforts. Most of all, I thank them for allowing me to think on my own and for offering me the chance to pursue my own ideas.

To my parents, who always tried to teach me to be content, but at the same time, to pursue my dreams. I love you both.

THIS PAGE INTENTIONALLY LEFT BLANK

I. INTRODUCTION

A. MOTIVATION

Title 10 of the United States Code defines energy resilience as the ability to avoid, prepare for, minimize, adapt to, and recover from anticipated and unanticipated energy disruptions in order to ensure energy availability and reliability sufficient to provide for mission assurance and readiness, including task critical assets and other mission essential operations related to readiness, and to execute or rapidly reestablish mission essential requirements [1]. Figure 1 shows the breakdown of military installation power outages by cause.

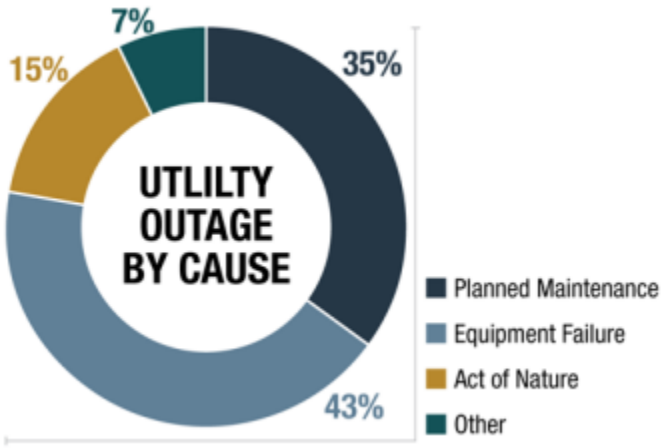

Figure 1. Utility Outages of Military Installations. Source: [1].

In FY 2017 Department of Defense (DoD) Components reported that there were approximately 1,205 power outages on military installations that lasted eight hours or longer, an increase from the previous year of 507 outages [1]. The DoD relies heavily on commercial power for its shore-based facilities and commercial power is susceptible to natural hazards, physical attacks, and cyber-attacks. These attacks could lead to degradation in the ability of the DoD to conduct critical missions including power projection, defense of the homeland, or operations directly supporting warfighting missions overseas [1]. According to [1], energy

resilience can be achieved in a variety of ways, including redundant power supplies, renewable power supplies, microgrid applications, and upgrading current infrastructure. The establishment of reliable microgrids would allow U.S. military bases to operate in conjunction with both domestic and foreign pre-existing electric main grid infrastructures but also act independently during a time of main grid failure. Energy reliability, energy security, and ultimately energy resilience can be achieved through the establishment and control of smart microgrids at key operating bases.

B. PREVIOUS WORK

Much research has been accomplished on the microgrid topology and its associated control structures. The majority of the research, thus far, has been to evaluate the overall functionality of the control structures associated with an Energy Management System (EMS) controlling a microgrid connection to and from the main grid. In [2], a comparison of the Phased Locked Loop (PLL) techniques for the design of the grid-connected inverter systems is performed and the author provides a good explanation of the prevalent PLL techniques used in grid connected inverters. This research is relevant because the connection techniques explored in this thesis are all derived from some variant of a PLL algorithm.

In [3], four different methods for generating the orthogonal signal were explored and tested extensively while [4] presents the simplest and least computationally expensive solution EMS. The grid Root Mean Square (RMS) voltage calculation used in [4] to determine the fault condition of the grid is computed in a clever way to minimize computation, time while at the same time maximizing accuracy. In [5] two dual second- order general integrators (DSOGI) were used in conjunction with a combination of overvoltage, under voltage, over frequency, and under frequency trip points to determine the EMS connection to the grid. This method proved to be very accurate but from a computational perspective was the costliest. The connection method presented in [5] was based on the research presented in [6], which described the multiple second-order generalized integrators (MSOGI) and their effectiveness under distorted grid conditions. It also presented methods for tuning the MSOGIs to different frequencies to achieve selective and adaptive filters working in parallel. Another EMS control strategy explored in this thesis was developed

using [7]. The simple dq rotating reference frame was implemented in simulation and compared to other strategies presented in [4]–[6].

This thesis presents a unique comparison of EMS control strategy techniques to IEEE Standard 1547-2018, which governs the interconnection and interoperability technical and test specifications and requirements for distributed energy resources [8]. To the author's knowledge, extensive research has not been completed in this area.

C. OBJECTIVE

This thesis had three objectives. First: Design, create, and verify a working Specialized Power Systems EMS model in Simulink similar to the laboratory EMS model designed, tested, and maintained by Dr. Alex Julian and Dr. Giovanna Oriti at the Naval Postgraduate School. Second: After the Specialized Power Systems model was tested and verified, use it to test different EMS grid disconnection strategies and compare their effectiveness. Third: Perform a comparison of the results from the simulation to the requirements presented in IEEE Standard 1547-2018.

D. THESIS ORGANIZATION

This thesis is organized in a manner that allows the reader to step through each stage of the model design and testing process. To fully understand the model used in this thesis the chapters are organized in sequential order according to when each phase of the design process occurred. Chapter I contains the introduction and Chapter II contains the background information relevant to the work presented in this thesis. Chapter III describes the physics-based model development process as well as a detailed description of the laboratory model used to verify the simulation model. Chapter IV describes the verification of the simulation model using laboratory data. This step is crucial in the engineering design process to ensure accurate simulation results for future simulations. Chapter V provides a detailed description of the different EMS control strategies evaluated in this thesis. Chapter VI includes the results of the simulation model testing of multiple EMS disconnection strategies along with a comparison of the results to IEEE Standard 1547-2018. Chapter VII contains the conclusion and recommendations for further research. The MATLAB code used to plot data and run any simulations is presented in the appendix.

THIS PAGE INTENTIONALLY LEFT BLANK

II. BACKGROUND

A. MICROGRID

The term microgrid can formally be defined as: “a group of interconnected loads and distributed energy resources within clearly defined electrical boundaries that act as a single controllable entity with respect to the grid. A microgrid can connect and disconnect from the grid allowing it to operate in both grid-connected or island mode” [9]. The main power grid overall design has remained essentially unchanged since its inception over a century ago. This lack of design change has led to many engineering problems such as a lack of control intelligence, actuation to individual loads, and integration of alternative or renewable generation sources or load technologies [10]. The modern electric grid is also aging. For example, more than 50% of the U.S. substation transformers are more than 35 years old. The age of the equipment coupled with outdated system layouts, outdated engineering, and obsolete problem characterization and solution approaches contribute to the reduced reliability and overall resiliency of the power grid [10]. The Department of Defense has a vested interest in the resiliency of the power grids used for vital operating equipment, with particular interest in forward operating bases.

The solution to the problem of the aging power grid is the integration of small, distributed generation sources. Interestingly, this was the solution proposed by Thomas Edison in the 1800s when Nicola Tesla proposed his ac grid technology [10]. The technology did not exist in the 1800s to fully implement Edison’s approach but now thanks to advances in power electronics his idea can be implemented in the form of microgrids that create local area power and energy systems (LAPES) to operate with, but are at the same time independently controlled from the grid [10].

Figure 2 shows the LAPES system connected with the grid at the Point of Common Coupling (PCC). The LAPES includes distributed energy resources (DER) or distributed resources (DR) such as internal combustion generators, photo voltaic cells, wind turbines, energy storage elements, and fuel cells as well as the control system required to interface with the grid. The purpose of the modern microgrid infrastructure is to provide reliable and

resilient electrical power using a combination of the conventional grid, renewable energy resources, storage elements, and a clever control structure.

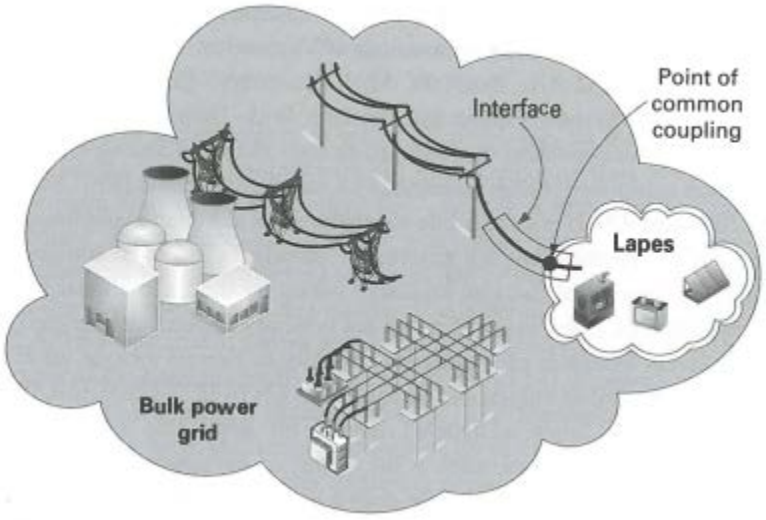

Figure 2. Grid Connected LAPES. Source: [10].

B. ISLANDING OR GRID CONNECTED

As discussed earlier a microgrid can operate in two modes; connected to the grid (grid-connected mode) or disconnected from the grid (islanding mode). The governing document for interconnection of a microgrid to a main power grid is IEEE Standard 1547-2018 which includes eight parts that individually cover different aspects of connecting a microgrid to a main grid in varying detail. This thesis focused on the portion of IEEE Standard 1547-2018 which covers the transient response time of a microgrid after a fault or disturbance is detected in the main grid.

Islanding is defined as "a condition in which a portion of a large power grid is able to operate separate from the rest due to the presence of local power generators" [10]. Four important definitions with regards to islanding of microgrids are defined in chapter eight of [8].

Unintentional Islanding: The DER energizes a portion of the area electrical power system (area EPS) not designed to operate in an islanding condition through the PCC which

is caused by inadvertent events that are typically initiated by a loss of area EPS or equipment failure [8], [11].

Intentional Islanding: "A planned electrical island that is capable of being energized by one or more Local EPSs. These (1) haves DER(s) and load, (2) have the ability to disconnect form and to parallel with the Area EPS, (3) include one or more Local EPS(s), and (4) are intentionally planned" [8]. Intentional islanding contains two categories: Scheduled intentional islands and unscheduled intentional islands.

Scheduled Intentional Islands: Formed through the DER operator or Area EPS manual action, facilities that deliver electric power to a load, manual action or other operating means that trigger the transition from being in parallel and synchronized with the Area EPS, to operation as an islanded system [8].

Unscheduled Intentional Islands: Islands formed autonomously from local detection of abnormal conditions at the interconnection(s) with the Area EPS, and then automatic relay action that triggers switching action to isolate the intentional island rapidly from the Area EPS [8].

The key difference between the unintentional island and intentional island is the intentional island is a scheduled or unscheduled energization of a planned portion of the local grid that is solely energized by a combination of DERs. In contrast to the unintentional island, which results when a breaker or other piece fault detecting equipment isolates a portion of the local grid, but at the PCC a DER is still energizing a portion of the local grid not isolated by the protective device. This situation is dangerous for a couple of reasons. 1) Damage to equipment could occur because the LAPES may not be in the correct control mode and therefor may not be regulating voltage and frequency of the unintentional island. 2) Damage to equipment or injury to personnel could occur because the cause of the protective device tripping is now nullified by the fact that the unintentional island is being energized by the DER of the LAPES [8], [11].

Figure 3 shows a neighboring portion of the grid that is not intended to become an island if a fault in the main grid occurs. In this situation power is being injected into the

main grid by the LAPES in grid-connected mode and therefore the LAPES is relying on the main grid for voltage and frequency control.

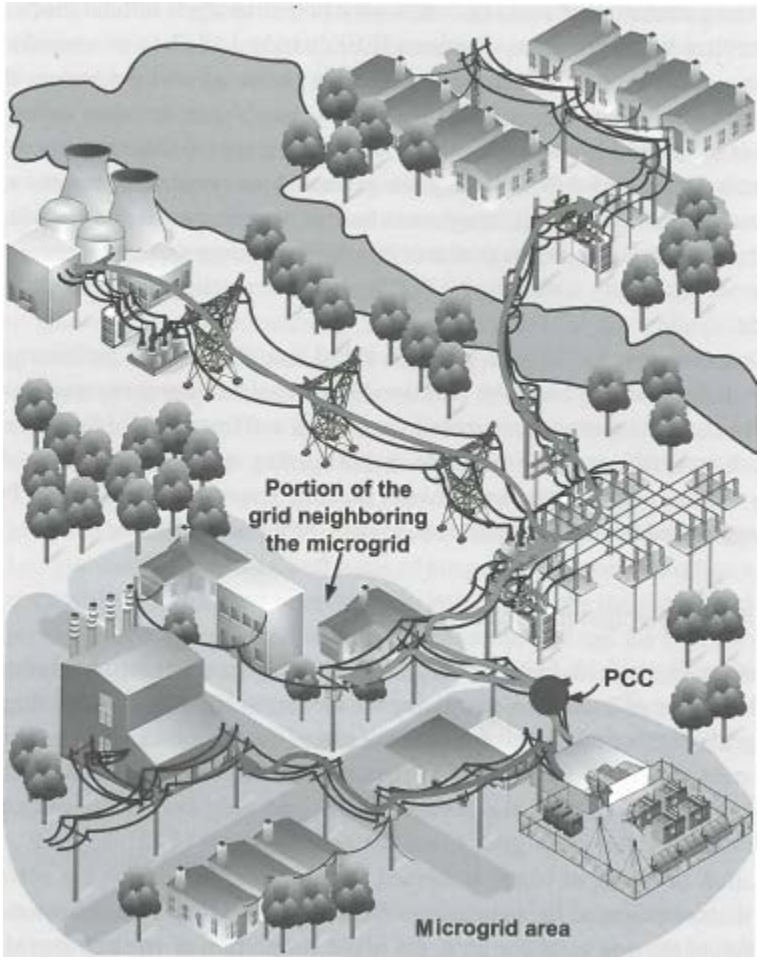

Figure 3. Microgrid Connected at PCC with Main Grid. Source: [10].

Figure 4 shows the creation of the unintentional island which is now being powered by a DER after the fault in the grid is detected and the acting protection device has tripped. To prevent damage to equipment and injury to personnel IEEE Standard 1547-2018 requires: “For an unintentional island in which the DER energizes a portion of the Area EPS through the PCC, the DER shall detect the island, cease to energize the Area EPS, and trip within 2 s of the formation of an island” [8].

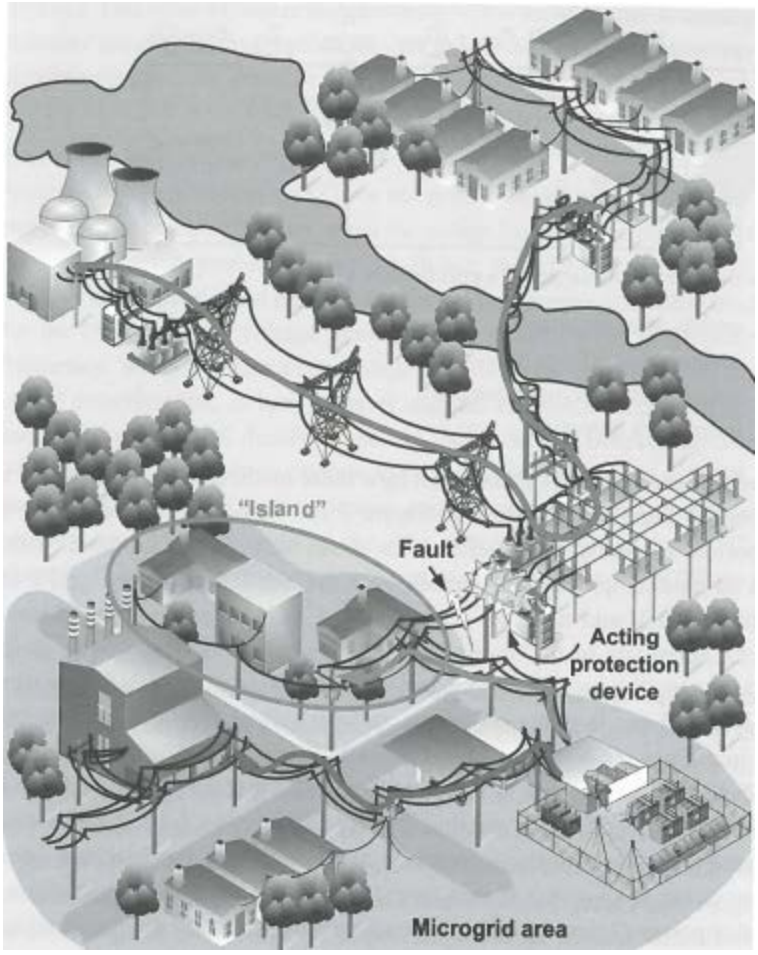

Figure 4. Creation of Unintentional Island after Fault in Grid. Source: [10].

C. TRANSITION-TO-ISLANDING MODE

The main focus of this thesis is the transition to Unscheduled Intentional Islands. IEEE Standard 1547-2018.4 explains: During a transition-to-island, a sufficient number of DER and DER of the correct type needs to be available to support the system voltage and frequency during the system disturbance or scheduled event that caused the island, for whatever time the Island Interconnection Device (IID) and protective relaying device takes to operate, to effect a successful transition [11]. These DER should be sufficient to dampen any transients produced in the island by this transition and act quickly enough to prevent protective relaying in the island from tripping-off islanded DER [11].

Figure 5 shows a DER island system with its own DER connected to an electric power system. According to IEEE Standard 1547-2018 the island system in this case would need to detect the fault and open B1 (Breaker 1) prior to B2 opening and securing power to the critical loads. The control and monitoring system would need to be fast enough to be able to prevent significant voltage or frequency fluctuations to the loads. For the purposes of this thesis all loads were presumed critical and the DER is an H-bridge inverter with a battery power supply [11].

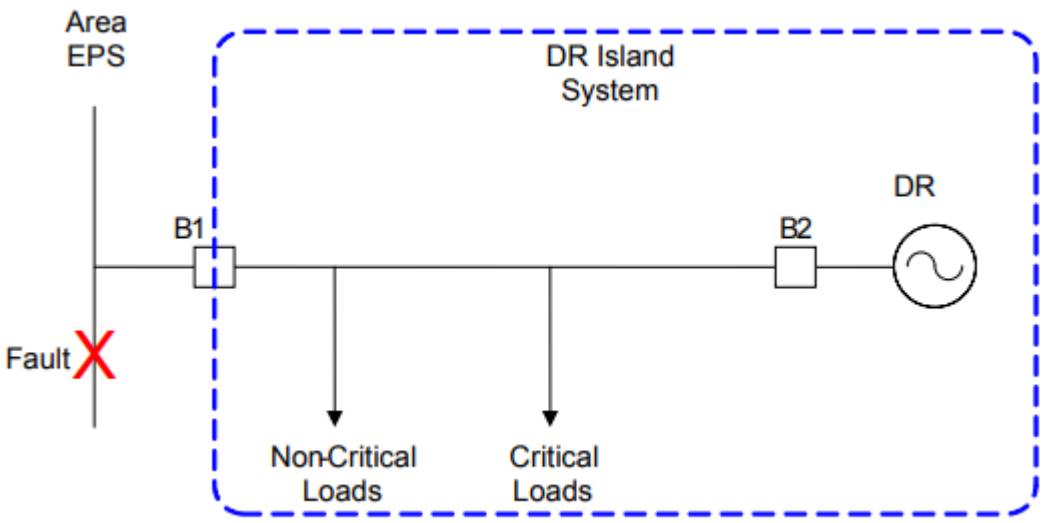

Figure 5. Intentional Island After Grid Fault. Source: [11].

1. "Shall Trip" Conditions

"Shall trip" conditions require transition to intentional island mode if the voltage disturbance in the Area EPS is above or below the thresholds shown in Table 1. One of the goals of this thesis was to examine the transition time from grid connected mode to islanding mode of operation after a fault in the grid was detected by the monitoring and control system. To examine this transition time IEEE Standard 1547-2018 section 8.2.4 and Clause 6 were used to develop the simulation scenarios. Section 8.2.4 of IEEE Standard 1547-2018 describes three conditions that requires an unscheduled transition to intentional island mode from grid connected mode. Of particular interest to this thesis is the second

condition in section 8.2.4 which states: “An intentional island may disconnect from the Area EPS and transition to intentional island mode for the following reason … If any of the trip conditions described in Clause 6 are met (i.e., where Clause 6 would allow or mandate tripping), the intentional island may transition to intentional island mode” [8].

In Table 1 clearing time is defined by IEEE Standard 1547-2018 as “the time between the start of an abnormal condition and the DER ceasing to energize the Area EPS” [8]. In this thesis the conditions defined in section 8.2.4 and Clause 6 of IEEE Standard 1547-2018 were applied with an H-bridge inverter replacing the DER and the main grid supply replacing the Area EPS. Category I Area EPS abnormal conditions is defined in IEEE Standard 1547-2018 and “is based on essential bulk power system (BPS) stability/ reliability needs and reasonably attainable by all DER technologies that are in common usage today” [8]. Category I conditions were chosen because they are the most restrictive and defined as common usage.

Table 1. Overvoltage and Under Voltage Tripping Times. Source: [8]

Shall trip—Category I				
Shall trip function	Default settings[a]		Ranges of allowable settings[b]	
	Voltage (p.u. of nominal voltage)	Clearing time (s)	Voltage (p.u. of nominal voltage)	Clearing time (s)
OV2	1.20	0.16	fixed at 1.20	fixed at 0.16
OV1	1.10	2.0	1.10–1.20	1.0–13.0
UV1	0.70	2.0	0.0–0.88	2.0–21.0
UV2	0.45	0.16	0.0–0.50	0.16–2.0

2. “Ride Through” Conditions

IEEE Standard 1547-2018 also mandates voltage and frequency “ride through” conditions. The purpose of the voltage and frequency ride through requirements are to minimize cycling of power equipment and loss of power to vital loads due to only minor disturbances in the main grid power supply [8].

Table 2 shows the voltage ride through requirements for category I systems. It can be observed that for a momentary voltage drop of approximately half of the nominal voltage the EMS should not trip and create an intentional island for a minimum of 0.16

seconds. These requirements are explored later in this thesis with regard to performance of vital operating equipment.

Table 2. Voltage Ride Through Requirements. Source: [8]

Voltage range (p.u.)	Operating mode/response	Minimum ride-through time (s) (design criteria)	Maximum response time (s) (design criteria)
$V > 1.20$	Cease to Energize[a]	N/A	0.16
$1.175 < V \leq 1.20$	Permissive Operation	0.2	N/A
$1.15 < V \leq 1.175$	Permissive Operation	0.5	N/A
$1.10 < V \leq 1.15$	Permissive Operation	1	N/A
$0.88 \leq V \leq 1.10$	Continuous Operation	Infinite	N/A
$0.70 \leq V < 0.88$	Mandatory Operation	Linear slope of 4 s/1 p.u. voltage starting at 0.7 s @ 0.7 p.u.: $T_{VRT} = 0.7\ \text{s} + \frac{4\ \text{s}}{1\ \text{p.u.}}(V - 0.7\ \text{p.u.})$	N/A
$0.50 \leq V < 0.70$	Permissive Operation	0.16	N/A
$V < 0.50$	Cease to Energize[a]	N/A	0.16

D. EMS DESCRIPTION

Figure 6 shows the EMS topology used for this thesis. It can be observed from Figure 6 that the H-bridge inverter is connected in parallel with the local loads and main utility grid through an LC filter. The DC bus power supply for the inverter is typically an energy storage device such as a battery accompanied by a buck/boost control system to regulate the DC bus voltage supply to the inverter Insulated-Gate Bipolar Transistor (IGBT) switches. The EMS facilitates two different operating modes, grid connected (current injection mode) and islanding (voltage control mode). In current injection mode the desired current injected by the H-bridge inverter is compared with the output current of the inverter through a Proportional Integral (PI) controller which in turn drives the gate signals to the IGBTs to control the current sent to the load from the inverter. In voltage control mode the inverter is disconnected from the main utility grid and controls the gate signals of the IGBTs through open loop pulse width modulation (PWM) unipolar voltage switching. As explained earlier, for the purposes of study in this thesis the conditions defined in section 8.2.4 and Clause 6 of IEEE Standard 1547-2018 were applied with an H-bridge inverter replacing the DER and the main grid supply replacing the Area EPS, as show in Figure 6. The main focus of study in this thesis is the control algorithms used to switch the EMS from grid connected to islanding mode of operation and their ability to

comply with IEEE Standard 1547-2018 voltage ride-through requirements. Each of the control algorithms received the same input, the PCC voltage, shown as V_{PCC} in Figure 6. To test the control algorithms a series of tests were conducted that involved disturbances in the main grid supply voltage of varying magnitude and duration during which, through a series of filters, reference frame transformations, and logic gates the control algorithms were required to make a determination to maintain connection with the main grid or transition to islanding control mode. If the EMS control algorithm determined that an islanding mode of operation was required, the breaker connecting the inverter to the main grid was opened and the inverter switch controlled mode from current injection to voltage control to maintain continuity of power to the load. Several EMS control algorithms were tested in this thesis to determine if one of them was able to comply with IEEE Standard 1547-2018 voltage ride-through requirements.

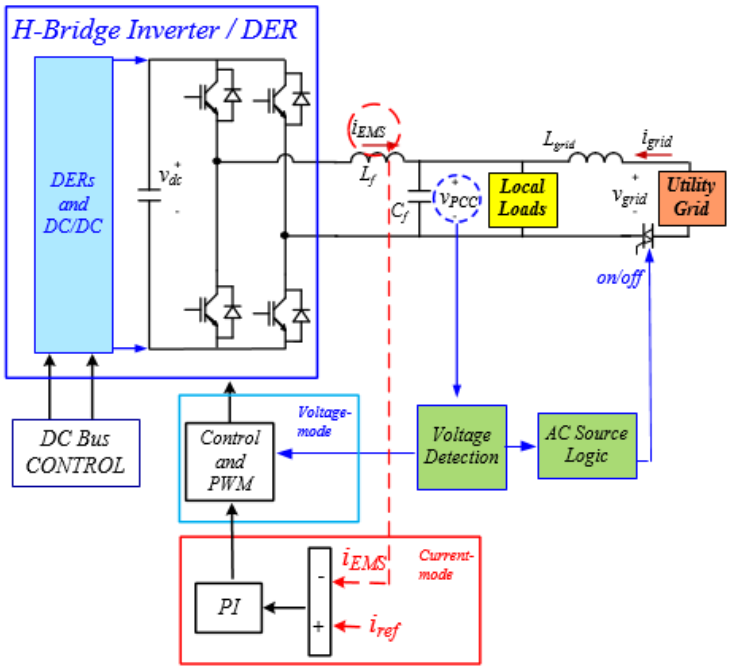

Figure 6. EMS Topology. Adapted from [3]

THIS PAGE INTENTIONALLY LEFT BLANK

III. MODEL DEVELOPMENT

A. INTRODUCTION

In this chapter the model development and verification process are explained. A large portion of research time was dedicated to developing a physics-based model of a preexisting physical system, shown in Figure 7, using Simcape electrical developed by MathWorks and Hydro-Quebec of Montreal [12].

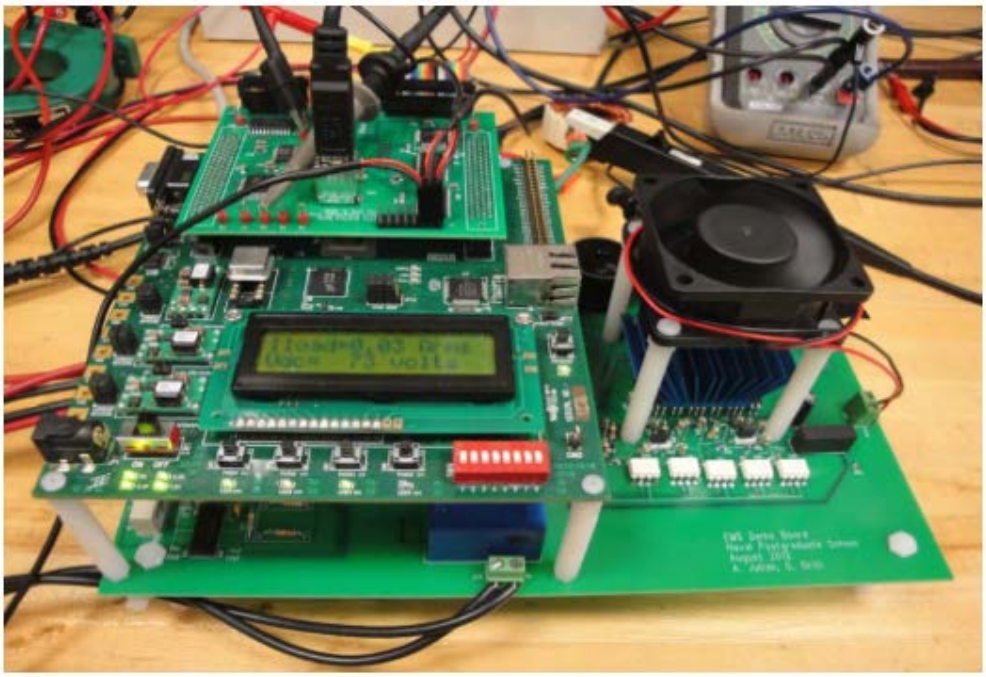

Figure 7. Laboratory Built EMS. Source: [13].

B. SIMSCAPE ELECTRICAL EXPLANATION

Simscape Electrical, formerly known as SimPowerSystems, is a powerful tool that can be used to model many different variations of physical systems. Simscape Electrical contains many different simulation tools, which include electromechanical actuation, hydraulic applications, smart grid modeling, electronic applications, and power grid applications. All these tools provide a means to the user to model a multitude of systems in the real world using physical components and physical quantities [12]. The components

inside of Simscape Electrical allow the user to analyze and design systems such as power generation systems conversion systems, transmission systems, and power consumption of an electrical grid [12].

Simscape Electrical functions under the operating umbrella of Simscape, the mathematical based modeling protocol. However, a key difference between Simulink and Simscape Electrical is that Simscape Electrical allows the user to model systems using physical components and in turn output physical values. For example, an inductor is modeled as a physical, real life inductor and a voltage measurement block could be used to obtain a measurement of the voltage across the inductor; in contrast to Simulink where the inductor would be modeled using the differential equation for the either the voltage across or current through the inductor. Simscape Electrical contains twelve different top-level libraries. Figure 8 shows an example of the structure of Simscape Electrical as it appears in Simulink.

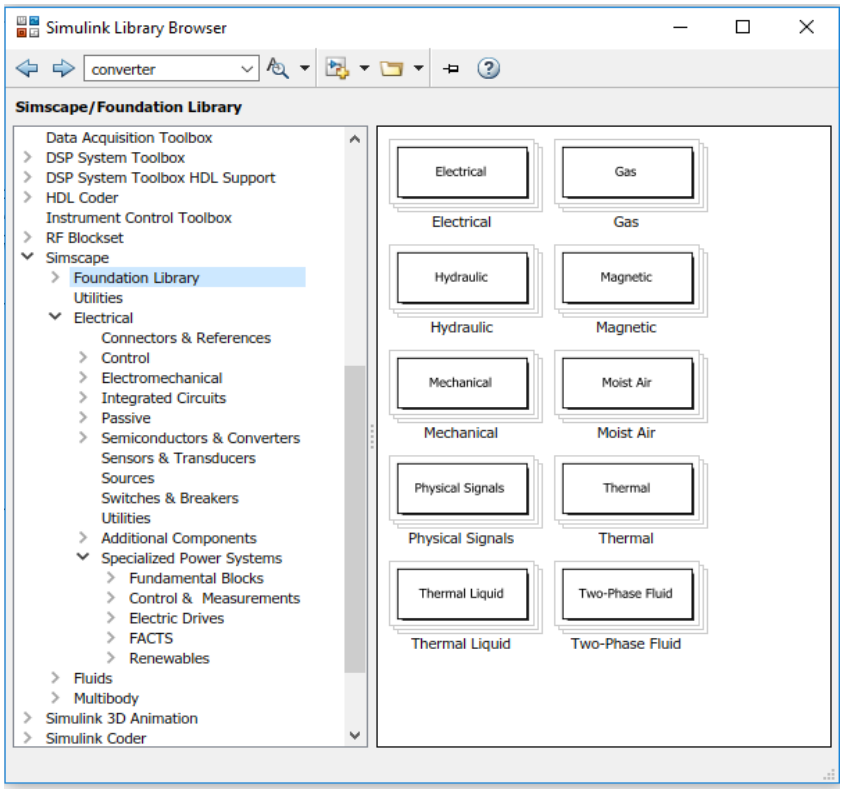

Figure 8. Simscape Electrical Topology. Source: [14].

These libraries allow the user to model mechatronic systems, analog circuit architectures, and single- and multi-phase electrical power systems [14]. All of the these libraries with the exception of Specialized Power Systems are designed to extend the Simscape Foundation domains and are fully compatible with Simscape technology [14].

The physics-based model created for this thesis was created in Specialized Power Systems whose library contains functional blocks, specific to model Power Systems [14]. These libraries allow the user to model typical power equipment such as transformers, electric machines and drives, and power electronics. Specialized Power Systems also contains control, measurement, and signal generation models that allow the user to model and test control algorithms [14], [15]. The "powergui" block, shown in Figure 9, in the Specialized Power Systems library allows the user to choose one of three simulation methods, continuous-time, discrete-time, or phasor to model the system and also provides functional analysis tools such as the Fast Fourier Transform analysis or the Hystereis Design Tool [15].

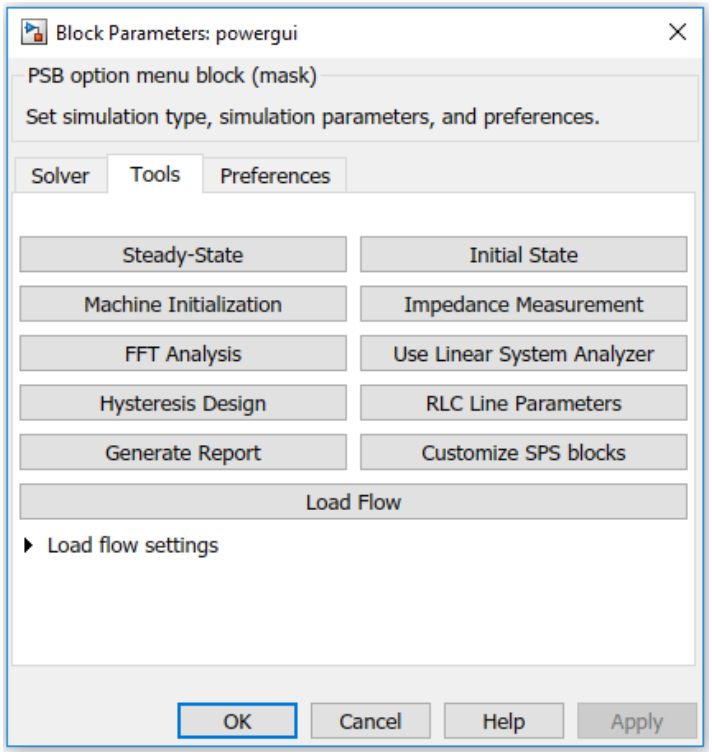

Figure 9. "powergui" Block Parameters. Source: [15].

Using the Specialized Power Systems library the functional blocks can be connected to Simulink blocks through either the Simulink signal input and output ports or measurement blocks from the Measurements sublibrary of the Fundamental Blocks Library [14].

C. MODEL DEVELOPMENT

The physics-based model development occurred in two steps. First, an H-bridge inverter was modeled (shown in Figure 6) using Specialized Power Systems components followed by integrating the H-bridge inverter into a simulation model of the EMS laboratory setup shown in Figure 7 using Specialized Power Systems.

1. H-Bridge Inverter Development

a. Inverter Theory

In this thesis a switch-mode unipolar Pulse-width-modulated inverter, shown in Figure 10, was used. A switch-mode dc-to-ac inverter is a dc-to-ac converter that converts DC power into sinusoidal ac voltage and normally operates in the dc-to-ac inverter mode of operation. The ability of the PWM inverter to be able to control the magnitude and frequency of the output waveform allows the inverter great flexibility in terms of application and also allows the EMS to reconnect to the power grid through the use of a PLL control system. The input dc voltage to the inverter is normally generated by using a battery and a buck / boost controller to obtain the desired dc bus voltage.

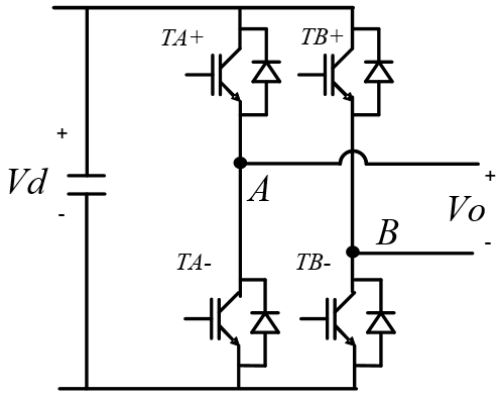

Figure 10. Basic H-Bridge Inverter. Adapted from [3].

To describe the PWM scheme a few key terms must be defined. The triangular waveform v_{tri} is oscillating at the switching frequency f_s which establishes the frequency at which the switches T_{A+}, T_{A-}, T_{B+}, and T_{B-} commutate [16]. The control signal $v_{control}$ is used to modulate the switch duty ratio and has a frequency of f_1 which also establishes the fundamental frequency, normally 60 Hz, of the inverter output [16]. The switches shown in Figure 10 are controlled by comparing v_{tri} with $v_{control}$ and $-v_{control}$ as shown in Figure 11.

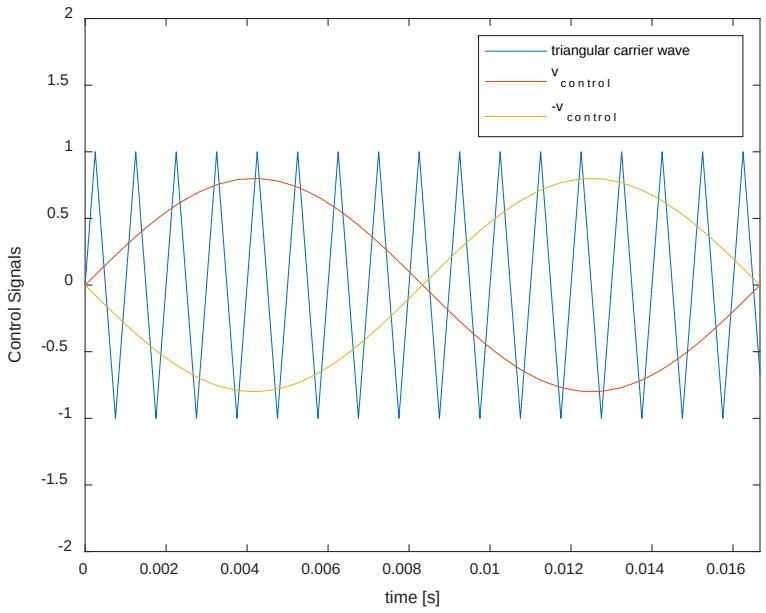

Figure 11. H-bridge Inverter Control Signals

Logical signals are generated to control the switches shown in Figure 10 by the following equations [16].

$$v_{control} > v_{tri} : \quad T_{A+} \text{ on} \tag{1}$$

$$v_{control} < v_{tri} : \quad T_{A-} \text{ on} \tag{2}$$

$$\left(-v_{control}\right) > v_{tri} : \quad T_{B+} \text{ on} \tag{3}$$

$$\left(-v_{control}\right) < v_{tri} : \quad T_{B-} \text{ on} \tag{4}$$

The switching of the IGBTs is determined by the logical signals produced by the output voltage shown in Figure 11. Figure 12 shows the simulated unfiltered unipolar voltage output of the inverter with a 200 Volt dc ideal source to control the DC bus input voltage to the inverter. The output voltage is then filtered through an LC filter to remove the higher order harmonics generated by the switching frequency of the inverter to produce the desired sinusoidal output voltage to the load.

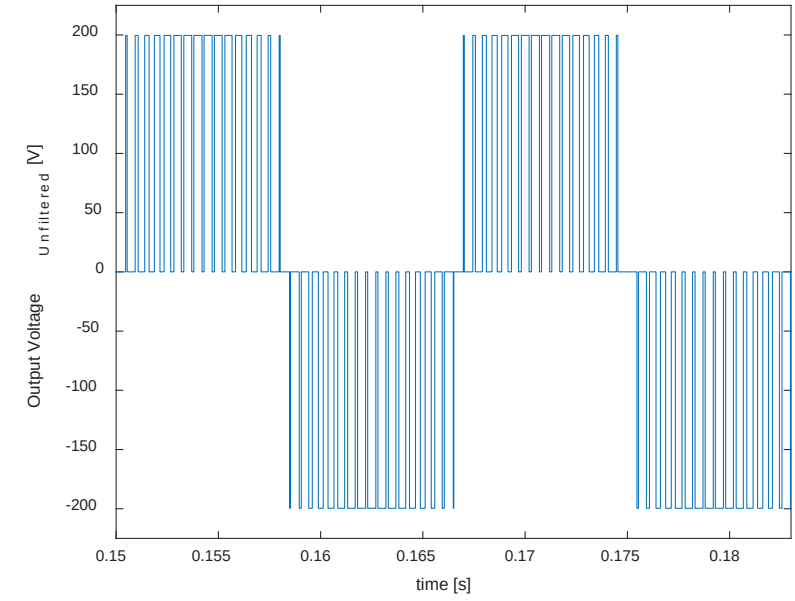

Figure 12. Unipolar Inverter Output Voltage (Unfiltered)

b. H-Bridge Inverter Design

The next step was to build an H-bridge inverter that modeled the laboratory setup shown in Figure 7. Figure 13 shows the model built using Specialized Power Systems functional blocks.

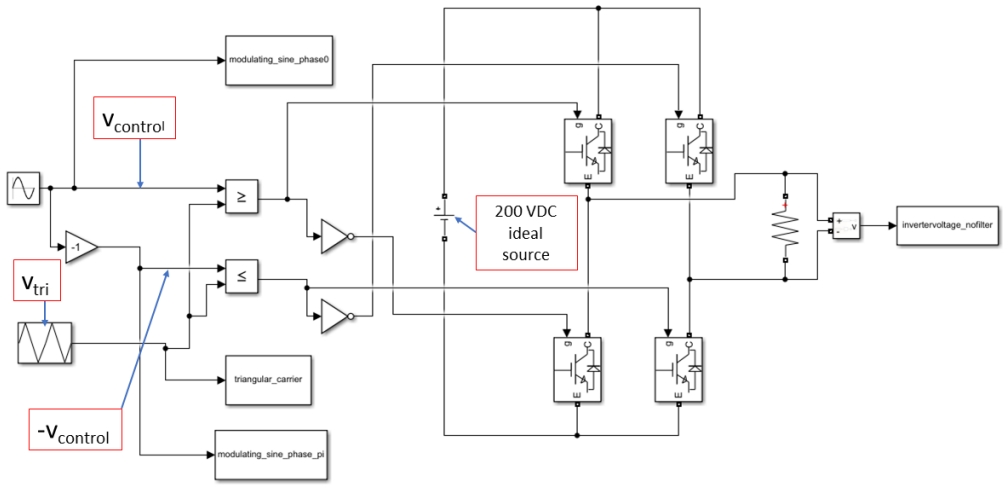

Figure 13. H-bridge Inverter Design (Specialized Power Systems)

The models main components include: a sinusoidal source, a triangle generator block, an ideal voltage source, and four IGBTs. The ideal sinusoidal source was set up to generate the $v_{control}$ and $-v_{control}$ parameters used in the comparator which was then used to generate the logical control signals for the IGBTs. To generate $v_{control}$ and $-v_{control}$ the sinusoidal source was configured with an amplitude of 0.8 and a frequency of $2\pi60$ rad/ sec. The amplitude of $v_{control}$ (0.8) controlled the amplitude of the output voltage of the inverter, the frequency of $v_{control}$ ($2\pi60$ rad/sec) controlled the output frequency of the inverter to the desired 60 Hz, and the gain of negative one was used to generate $-v_{control}$ as a 180-degree phase shift of $v_{control}$. The triangle generator block, set to 15000 Hz with an amplitude of 1, generated v_{tri} for use in the comparator blocks to generate, along with the sinusoidal source, the logical control signals for the IGBTs. The ideal dc voltage source was used in place of a buck / boost control structure to produce the DC bus voltage input to the inverter switches. The buck and boost control structure could however be implemented later into the model with little effort. The resistor in parallel with the voltage measurement block was set to 1 Ohm initially and used to provide some resistance in the circuit and to facilitate the use of the voltage measurement block. Finally, the IGBTs were initially set up with an internal resistance of 0.001 Ohm.

2. Laboratory Model Development

After a model of the H-bridge inverter was developed, a Specialized Power Systems model of the laboratory setup shown in Figure 7 was constructed. This model would later be validated using laboratory data and then used for subsequent testing. The laboratory model used in this thesis was constructed by Dr. Alex Julian and Dr. Giovanna Oriti and used in the IEEE transaction paper titled Power-Electronics-Based Energy Management System With Storage [4].

a. EMS Laboratory Description

The EMS setup described in [4] consists of an H-bridge inverter with a dc voltage source provided by six 12-Volt batteries connected in series to produce a 72-Volt output which was then boosted to approximately 210 Volts using a buck and boost stage [4]. Figure 14 shows the EMS architecture used in the laboratory setup.

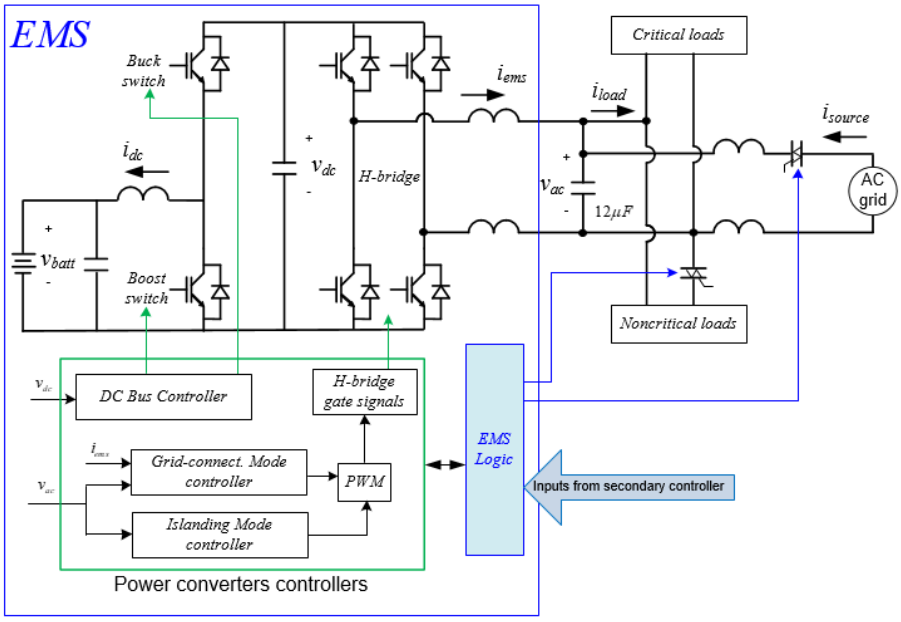

Figure 14. EMS Architecture (Laboratory). Source: [6].

The EMS functionality shown in Figure 14 was set up to accomplish the following three scenarios: 1) Peak shaving by tapping the energy storage system during high power

demand. 2) Islanding or stand-alone mode of operation when the main ac grid is no longer available. 3) Facilitate recharging of the battery using battery charging mode [4]. These three functionalities were integrated into the EMS control using an FPGA development board, a JTAG programming cable interface, Simulink software development tool, and the Xilinx System Generator Software [4].

Figure 15 shows the laboratory EMS logic flowchart which contains control logic built for the functionality of the three scenarios described in the preceding paragraph. However, the focus of this thesis was the islanding mode of operation and thus, only the RMS calculation, the Islanding mode algorithm and the Current Injection control algorithm are described here. The other control structures are described in detail in [4].

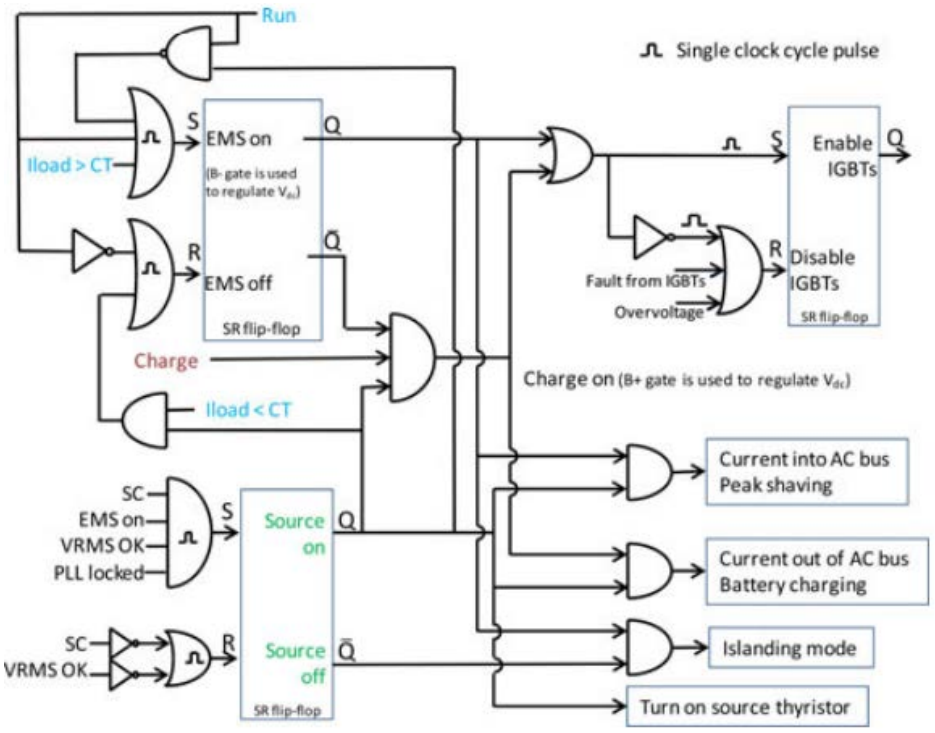

Figure 15. EMS Control Logic Flowchart (Laboratory). Source: [4].

(1) Estimated RMS calculation

The estimated RMS calculation in the laboratory EMS is one of the parameters used to determine the mode of operation of the EMS. The estimated RMS calculation provides input to VRMS OK inputs shown in Figure 16.

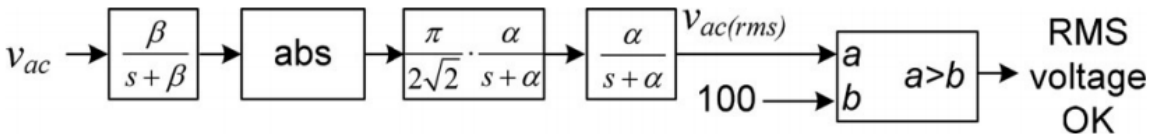

Figure 16. Estimated RMS Calculation (Laboratory). Source: [4].

Figure 16 shows the estimated RMS calculation developed in [4]. The estimated RMS calculation computed by the algorithm shown in Figure 16 determined the response time of the EMS switching from grid connected mode (current injection mode) to islanding mode (voltage control mode) of operation. The EMS mode switching time is discussed in detail in a later chapter of this thesis and only the RMS calculation algorithm is discussed here. To compute the estimated RMS value of the load voltage the v_{ac} is first filtered using a low pass filter with a corner frequency of $\beta = 700\pi$ radians per second [4]. Next, the absolute value is taken and then a low pass filter with corner frequency α is applied. In [4] the speed of response of the EMS was increased by adjusting the value of α from 20π to 60π radians per second and thus, a value of $\alpha = 60\pi$ radians per second was used for comparison in this thesis.

$$\frac{\pi}{2\sqrt{2}} avg\left(|V|\right) = \frac{\pi}{2\sqrt{2}} \frac{1}{\pi} \int_0^{\pi} V \sin(\theta) d\theta = \frac{\pi}{2\sqrt{2}} \frac{2V}{\pi} = V_{RMS} \tag{5}$$

Equation (5) shows how the gain value of $\pi/2*\sqrt{2}$ used to calculate the estimated RMS value yields the exact RMS value when v_{ac} is a sine wave and α is small [4]. To determine the state of the EMS the estimated RMS value was compared to 100 Volts. If the calculated RMS voltage is less than or equal to 100 Volts, the EMS assumes a grid

failure and switches to islanding mode of operation [4]. During this process a thyristor switch also opens to disconnect the non-critical loads from the EMS.

(2) EMS Control in Islanding Mode

The EMS in islanding mode of operation occurs when the ac grid is deenergized or when the EMS is disconnected from the grid [4].

Figure 17 shows the control algorithm for islanding mode of operation. When the EMS is in islanding mode of operation the control voltage v_{ac} is set to 110 Vrms and the electrical angle θ is obtained by integrating the angular frequency which is set to 60 Hz [4]. This signal is then used to drive the PWM H-bridge signals using open loop control [4].

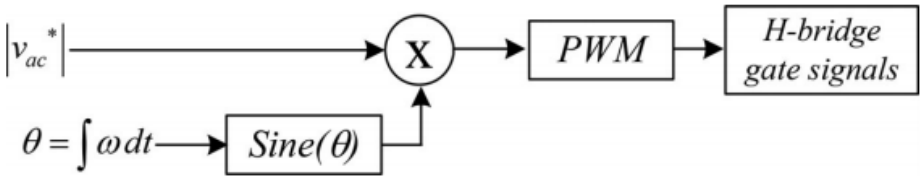

Figure 17. Control Algorithm for Islanding Mode. Source: [4].

(3) EMS Control in Current Injection Mode

The EMS can operate in two modes of current injection, battery charging and real or reactive power injection.

As mentioned earlier in this thesis only the current injection mode pertaining to real power injection was studied therefore only this functionality of the EMS is discussed here. In Figure 18 *I** is the desired control current to be injected into the system and *I* is the EMS current which is used in conjunction with the control current *I** to generate the error signal used in the PI controller to drive the PWM H-bridge signals. The δ is used to control the real or reactive power injected into the system but is typically set to zero to maintain the power factor at unity [4].

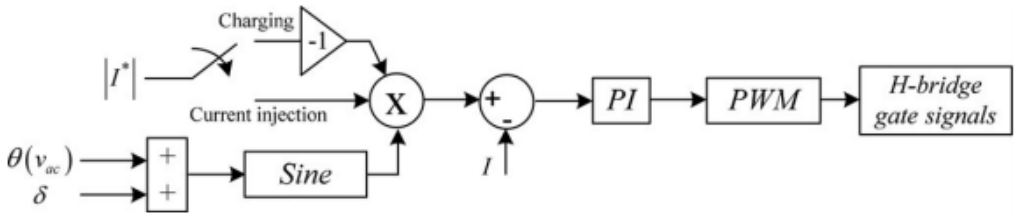

Figure 18. Control Algorithm for Current Injection. Source: [4].

b. EMS Model Description

A major goal of this thesis was to develop a simulated model of the laboratory setup using Specialized Power Systems embedded in Simulink. After the H-bridge Inverter was modeled using Specialized Power Systems the next step in the model development process was to integrate the H-bridge inverter with a load, the simulated grid, and the control structure for the IGBTs to create a more realistic model of the laboratory EMS. In this section the Specialized Power Systems Model implementation is described in detail. Each component is described as well as the differences between the laboratory model and the simulation.

Figure 19 shows the complete Specialized Power Systems Model of the laboratory EMS. The Current Controller, IGBT Control Selector, Breaker Simulation, Grid Simulation, and RMS Calculation are described in the following sections. The load portion of the model will be described in the Model Verification section.

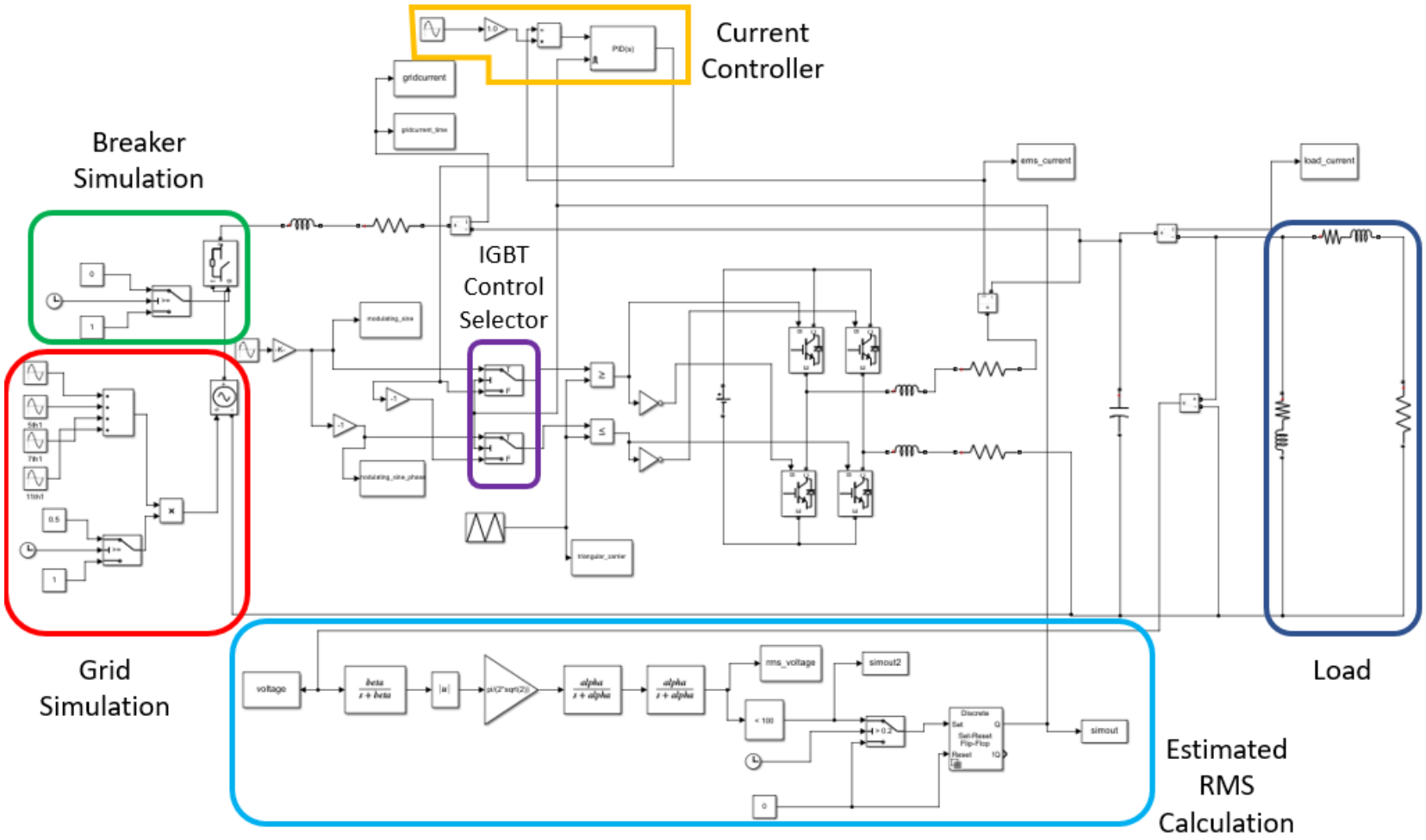

Figure 19. EMS Model

(1) Current Controller

The current controller shown in Figure 20 was implemented using a sine wave block with an amplitude of one followed by a gain block which was used to control the desired current injection magnitude (reference value). The other input to the subtraction block originates from a Specialized Power Systems Current Measurement block measuring the current output of the H-bridge inverter. The error between the control and measured current is then fed into the Proportional Integral Derivative (PID) controller which was implemented with a Proportional Gain (P) of 0.06 and an Integral Gain (I) of 5000/8. The PID controller was also implemented with an external level reset which was triggered when the model was used to simulate a reconnection to the main grid after operating in islanding mode. Without the external reset the PID would continuously accumulate error while the EMS was in islanding mode. This accumulated error could then cause a large current spike when the EMS was resynchronized with the grid. Finally, the output of the PID controller control signal is used for comparison against v_{tri} to generate the logical control signals for the IGBTs.

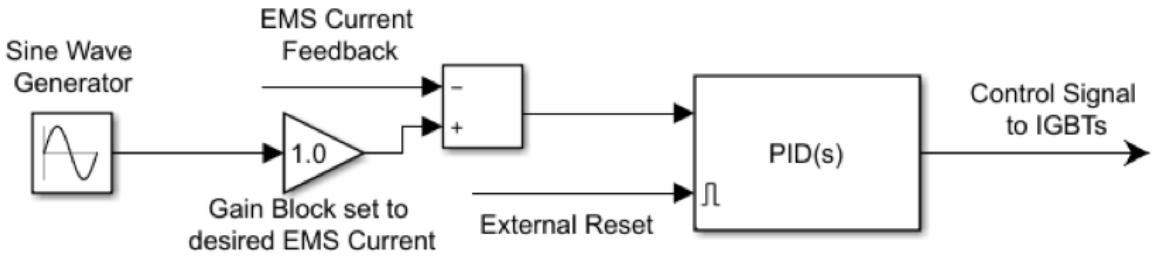

Figure 20. Current Controller (Model)

(2) IGBT Control Selector

Figure 21 shows the selector for the control signal used in the comparators to generate the logical control signals for the IGBTs. These switches are what allows the model to switch between voltage control mode (islanding mode of operation) and current injection mode (grid connected mode of operation). The driving signal for the switch comes from the estimated RMS voltage calculation portion of the model. This value will be a one

or a zero depending on the operating mode of the EMS. The switch will pass the control signal from the current controller when the estimated RMS value is above the threshold (grid connected mode) (control input = 0) and will pass the voltage control signal when the system is in islanding mode (control input = 1).

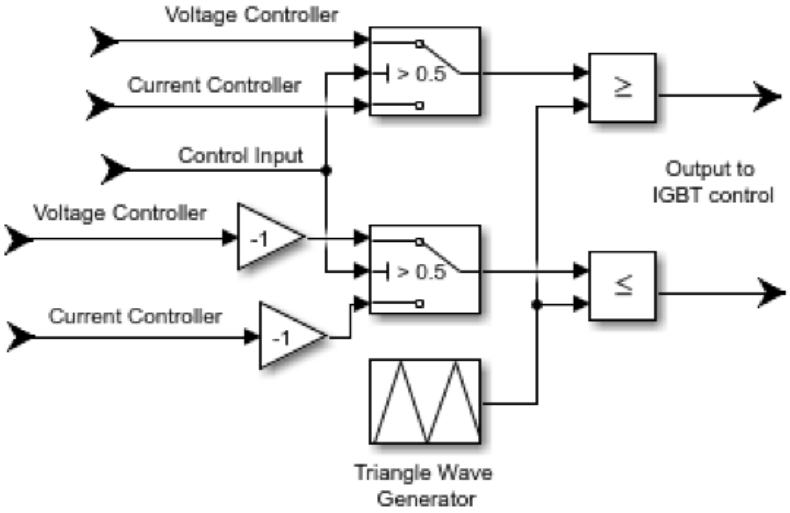

Figure 21. IGBT Control Selector

(3) Breaker Simulation

Figure 22 shows the breaker simulation portion of the model. An ideal switch, which is designed to be controlled with a binary 1 or 0, 1 being closed and 0 being open, was used in this portion of the model development. The control of the ideal switch was accomplished by using the Simulink switch located to the left of the ideal switch shown in Figure 22. This allowed the ideal switch to be opened at a predetermined time chosen by the user. In the scenario depicted in Figure 22 at the start of the simulation the breaker would initially be in the closed position, then, at 0.5 seconds into the simulation the switch would pass a zero instead of a one, thereby opening the breaker. The model was constructed in this manner to mimic the laboratory setup which replicated a total loss of grid voltage by opening the grid feeder breaker at a time chosen by the user.

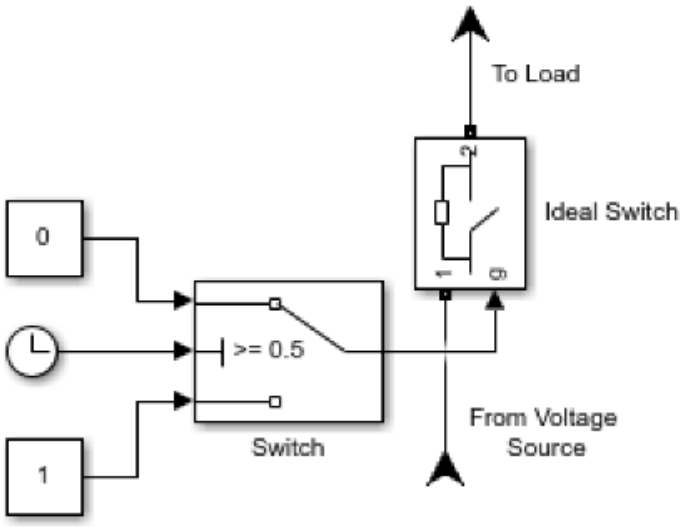

Figure 22. Breaker Simulation

(4) Grid Simulation

Figure 23 shows the model setup for the grid simulation. The grid simulation was accomplished by using four sine wave generators coupled with a summing block. The uppermost Sine Wave block was set to an amplitude of $110*\sqrt{2}$, a frequency of $2\pi 60$ rad/ sec, and a phase of 0 radians. The subsequent three blocks where used to simulate the harmonics that existed in the voltage being supplied by the local power company. The 5^{th}, 7^{th}, and 11^{th} harmonics were chosen considering previous work conducted by Dr. Alex Julian using the laboratory setup described in this thesis [3]. The switch block at the bottom of Figure 23 provided a method to simulate a disturbance in the grid voltage at a predetermined time by setting the upper constant block to any normalized value of the grid voltage. As depicted in Figure 23 a grid voltage disturbance of 0.5 of the nominal grid voltage would occur at the time the user inputs into the switch. Finally, the Controlled Voltage Source shown on the right in Figure 23 allows the user to convert from a Simulink block mathematical value to a Specialized Power Systems physical value of voltage. Using this configuration allows the user flexibility to simulate any amplitude, frequency, and phase values for the grid voltage.

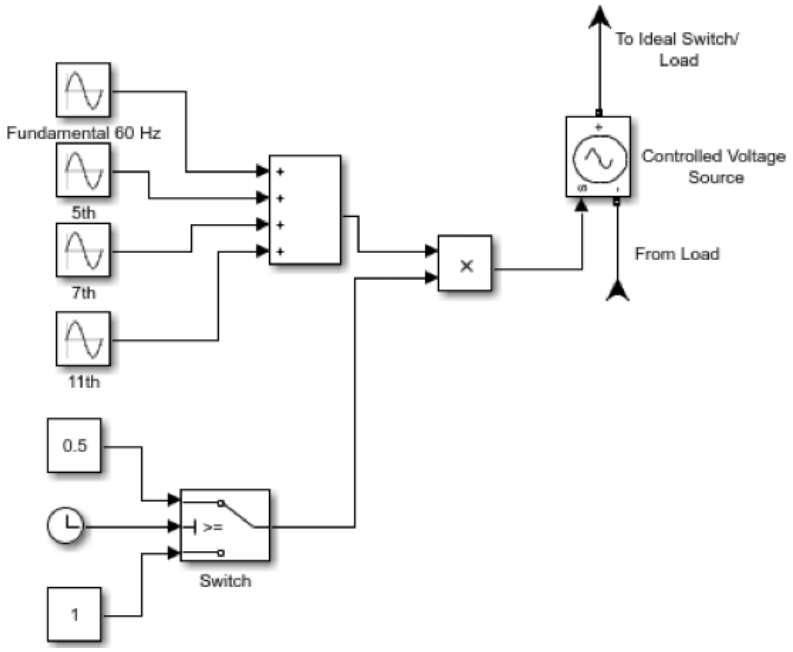

Figure 23. Grid Simulation

(5) Estimated RMS Calculation

Figure 24 shows the estimated RMS algorithm portion of the simulation. This calculation is described in detail in the laboratory EMS section of this thesis and thus only the model implementation is covered here. The PCC voltage on the left side of Figure 24 is provided by a voltage measurement block shown in Figure 19. The output of the algorithm provides the control input to the IGBT selector switches shown in Figure 21 as "control input." The switch and Set-Reset Flip-Flop were only used for to ensure that the logical "trip" values were passed at the correct time. The simulation and the laboratory EMS differ in the fact that the simulation starts from a zero-voltage condition and the laboratory EMS is already in a steady state condition when the feeder breaker is tripped. The Simulink switch is set to 0.2 seconds and allows time for the estimated RMS voltage to rise to a steady-state value above 100 Volts. The Set-Reset Flip-Flop ensures that after the EMS switches to islanding mode (voltage control mode) and the value of the RMS voltage returns to above 100 Volts the IGBT control selector switches shown in Figure 21 do not switch back to the current control mode input.

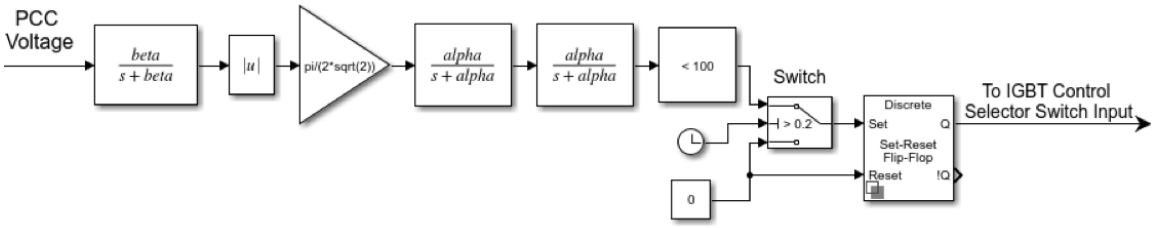

Figure 24. Estimated RMS Algorithm

The model described in this section was used to verify the functionality of simulation when compared to laboratory data. It was then modified as described later in this thesis to facilitate testing other EMS control algorithms.

IV. MODEL VERIFICATION

A. INTRODUCTION

An important part of the engineering process is to complete a verification of a simulation model created to mimic a real world system. This important validation ensures that the results from the EMS model were accurate when testing different islanding control methods. In this section the method used to validate the EMS model created using Specialized Power Systems is described in detail.

B. EMS MODEL VERIFICATION

To complete the verification of the EMS model a test scenario was developed to be used for both the laboratory prototype EMS and the EMS model. Data acquired from the laboratory prototype was then compared to the data obtained from the EMS model simulation.

1. EMS Model Verification Organization

a. Load Selection

The first step in the verification process was to decide on the load that would be used for testing purposes. A linear load was chosen because the focus of this test was the verification of the simulation model and a non-linear load may have yielded more ambiguity in the data obtained; possibly masking the data required to prove the validity of the model. The linear load chosen was not a purely resistive load because a more realistic load with greater dynamic response was desired to ensure the model was working correctly. The load component of the EMS laboratory setup is shown in Figure 25.

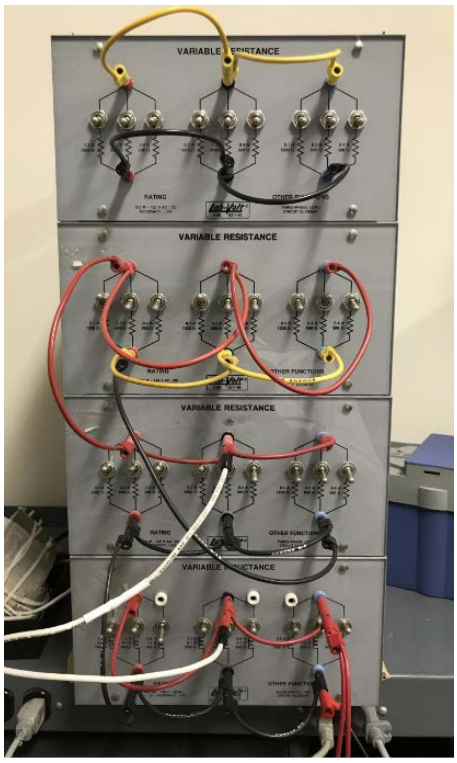

Figure 25. EMS Laboratory Load Selection

Using the LabVolt variable load selector a combination of a resistive and inductive load was selected. Figure 26 shows the load chosen for the model verification test.

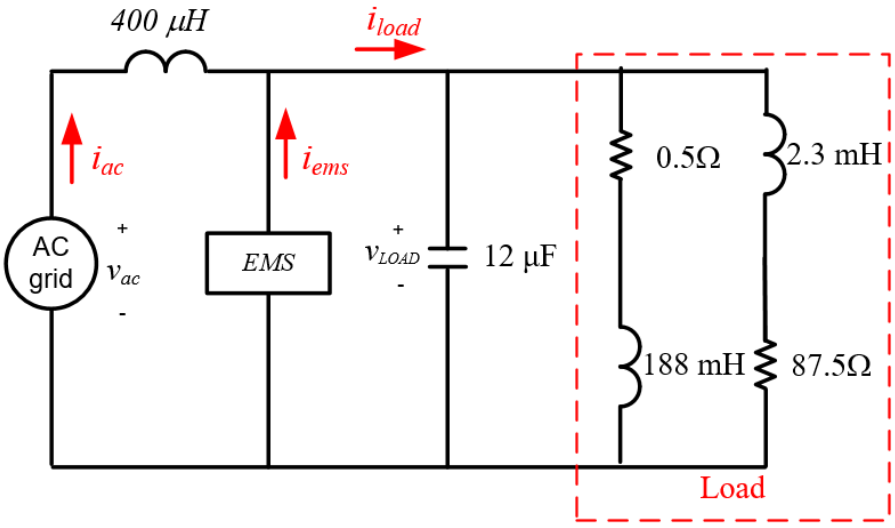

Figure 26. Model Verification Load. Adapted from [3].

b. Model Verification Test Scenario

To begin the test, the EMS in the laboratory was connected to the load described in the previous section and then commanded to inject one amp of current in phase with the input voltage. The grid voltage was supplied from the wall outlet at approximately 110 Volts RMS and a frequency of 60 Hz. The next step was to simulate a complete loss of the grid voltage and allow the EMS to assume all of the load. This was accomplished by opening a feeder breaker between the wall outlet and the EMS and allowing the EMS to then switch from current injection mode (grid connected) to voltage control mode (islanding mode) and supply the load with 110 Volts RMS at a frequency of 60 Hz.

To complete the verification process the EMS model was setup to perform the same functionality as the EMS in the laboratory described in the EMS Laboratory Description section. As explained in the Grid Simulation section of this thesis the grid was simulated to include voltage components at the fundamental frequency of 60 Hz and also components at the 5^{th}, 7^{th} and 11^{th} harmonics. To ensure that the results obtained from the EMS model could be accurately compared to the lab results these frequency components were included in this portion but are not necessarily required for further testing scenarios. The simulation of the total loss of the grid voltage was accomplished by opening the ideal switch shown in Figure 22.

2. Model Verification Results

To complete the model verification three key parameters of the EMS were evaluated; grid current, EMS current, and load voltage. Each of these parameters were chosen for a specific verification purpose. The EMS laboratory data was extracted as a csv file data type and imported into MATLAB using the csvread command and the data from the EMS model simulation and the EMS laboratory were then plotted over the same time period [17].

The grid current was chosen for two reasons. 1) To provide data to ensure that the grid current produced in the simulation model was accurately modeling the harmonic frequencies that are present in the grid supplied voltage in the laboratory EMS. 2) To ensure that the response of the ideal switch in the simulation was accurately modeling the response of the breaker opening in the laboratory EMS.

The EMS current was chosen for two reasons. 1) To ensure that the EMS model simulation was initially injecting the proper current. 2) To verify that the EMS assumed all of the load current after the EMS switched control modes.

The load voltage was chosen to be able to verify that the EMS model effectively switched from current injection mode (grid connected) to voltage control mode (islanding mode).

a. Grid / Source Current

Figure 27 shows the comparison between the simulation grid current and the grid current supplied to the laboratory EMS by the local power company just before and after the feeder breaker and ideal switch are opened. The voltage harmonics injected into the simulation model the harmonics supplied by the power company very well and the ideal switch appears to accurately model the breaker response.

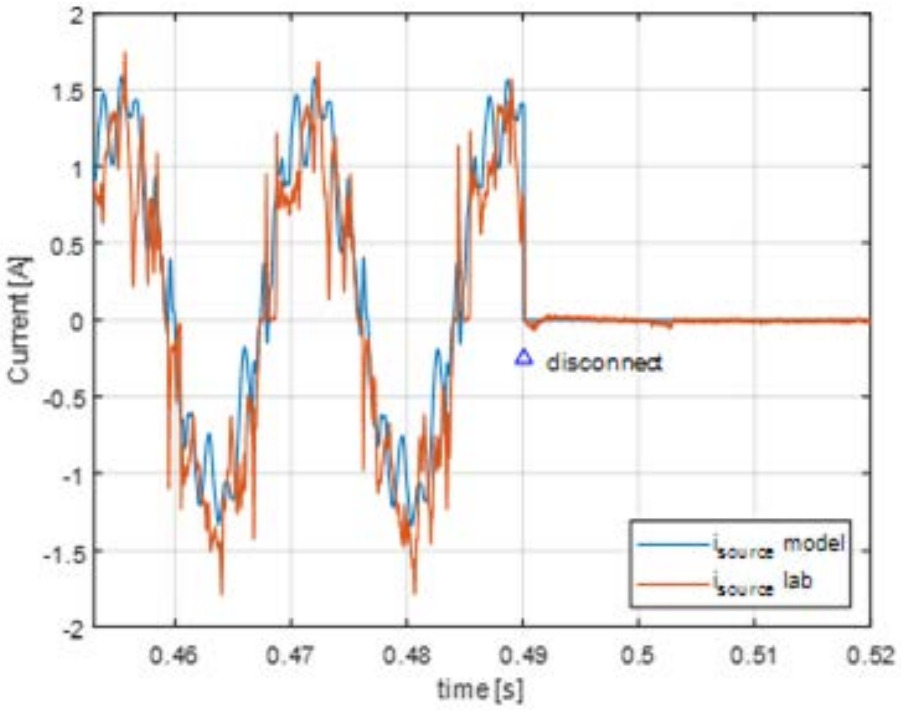

Figure 27. Laboratory EMS and Simulation Grid Current Comparison

b. EMS Current

Figure 28 shows the EMS current of the Laboratory EMS and the EMS Model. The purpose of this comparison was to show that the simulation accurately modeled the 1 A of injection current while operating in current injection mode (grid connected) and then also accurately modeled the response of the system when a grid failure was detected and the EMS switched to voltage control mode (islanding mode). As mentioned in the Load Selection section of this thesis a simple resistive only load was not used because it was desired to have a load that would provide some dynamic response while at the same time maintaining linear properties. Figure 28 shows the breaker and ideal switch opening at approximately 0.49 seconds, the EMS switching from grid connected to islanding mode after the estimated RMS voltage falls below 100 Volts, and the subsequent rise and decay in ems current towards a steady state value, caused by the time constant of the resistive inductive (RL) load. It is also noted that the current becomes much smoother once the EMS is supplying all of the load current because the harmonics of the grid voltage are no longer present. Figure 28 clearly shows that the EMS model very accurately models the response of the laboratory EMS including the time delay associated with calculating the estimated RMS value of voltage when switching modes of operation.

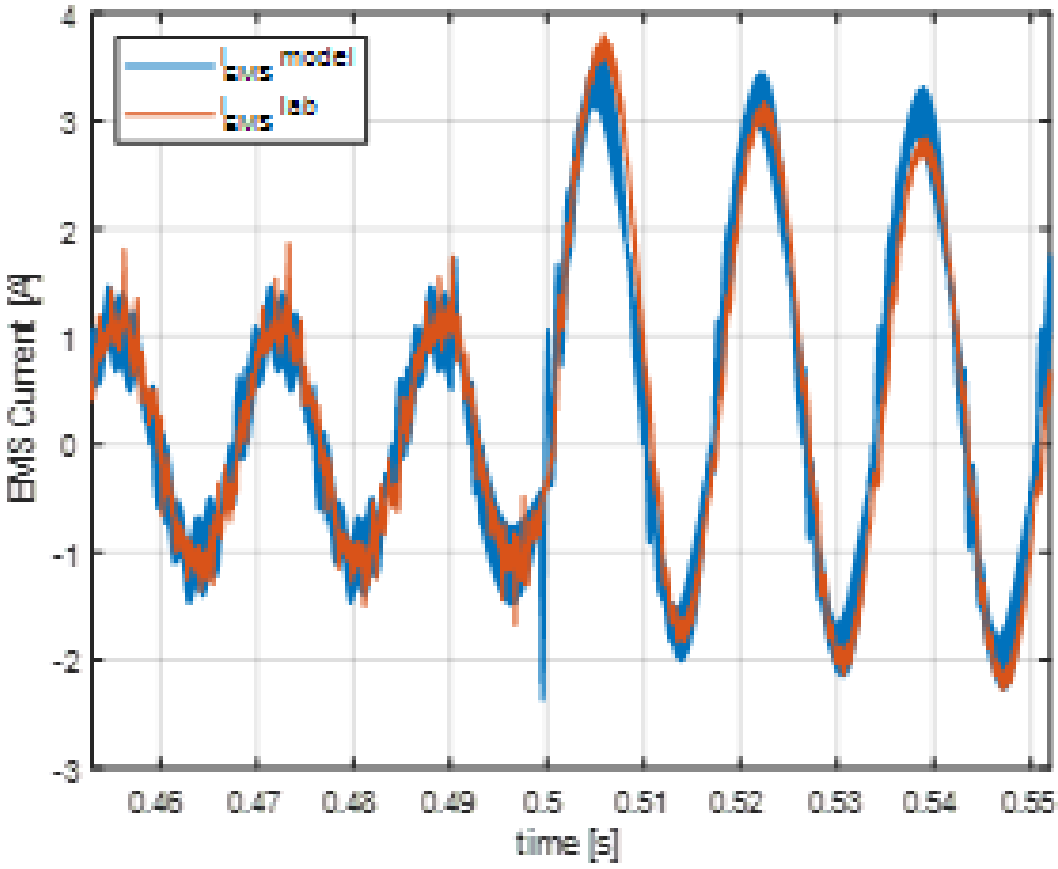

Figure 28. Laboratory EMS and Simulation EMS Current Comparison

c. Load Voltage

Figure 29 shows the load voltage just before and after opening the feeder breaker and ideal switch at approximately 0.49 seconds. While in current injection mode prior to the breaker opening the simulation model closely replicates the input load voltage supplied by the local power company. After the breaker opens and the EMS switches to voltage control mode the EMS model closely replicates the response of the laboratory EMS during the transient and steady state portions.

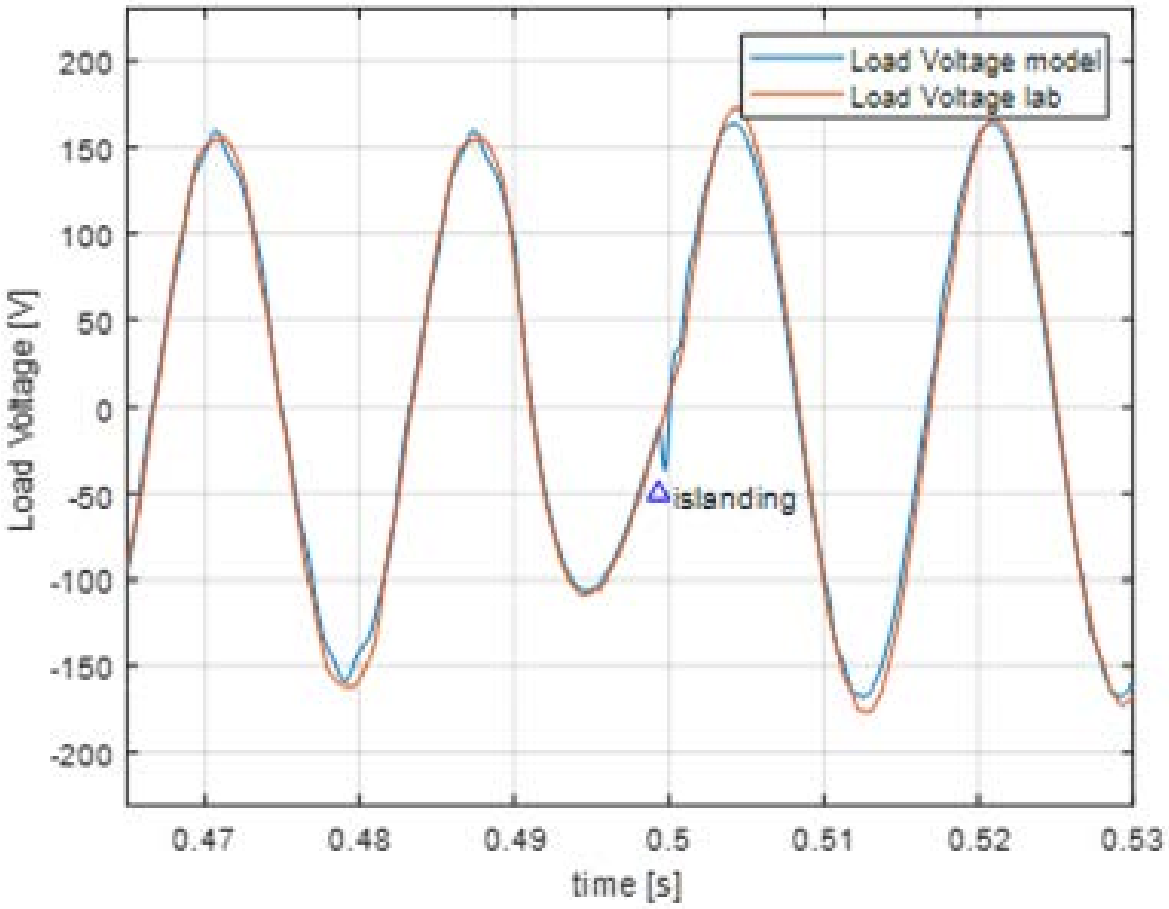

Figure 29. Laboratory EMS and Simulation Load Voltage Comparison

3. Conclusion

In the engineering process a working model is vital tool for use in testing system responses. The EMS model verification using actual laboratory data was a critical step in the model development process. With the simulation model verified using laboratory data it could now be modified to perform testing on other methods of grid disconnection.

THIS PAGE INTENTIONALLY LEFT BLANK

V. EMS CONTROL DISCONNECTION METHODS

A. INTRODUCTION

In this section the methods used for disconnection from the main grid are described in detail. Each of the disconnection techniques uses a different algorithm to either filter or transform reference frames of the voltage at the PCC. To facilitate comparison with IEEE Standard 1547-2018 the EMS model used in the verification process was altered to allow for testing of two abnormal voltage operating conditions; an under voltage condition and an overvoltage condition.

Figure 30 shows the grid voltage fault configuration that was added to the EMS model to allow for the under voltage and overvoltage conditions to be implemented in the EMS model. The UV/OV constant value in conjunction with the switch and clock allowed the grid voltage to be reduced or increased to any voltage value shown in Table 2 at a predetermined time.

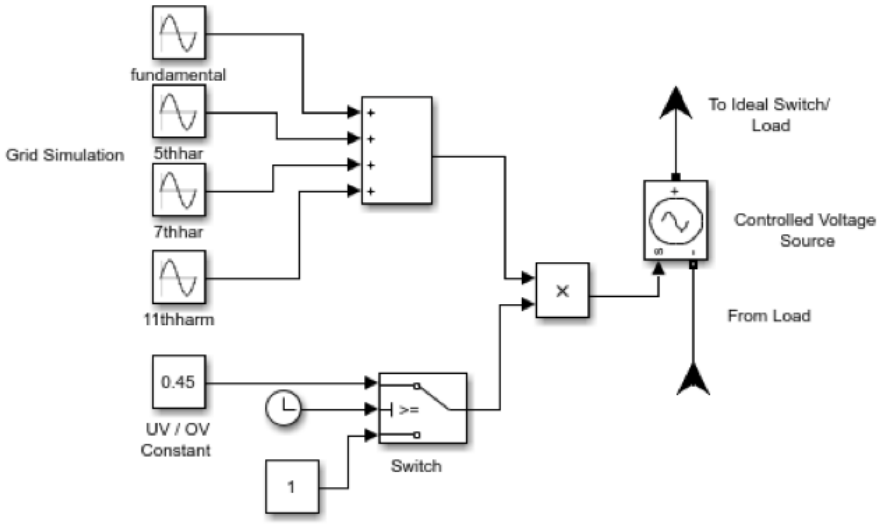

Figure 30. Grid Voltage Fault Model Configuration

An RMS calculation block from the Specialized Power Systems Measurements library was also added to each model described in this section to facilitate comparison of the voltage at

the PCC to required vital load voltages. This RMS value of the PCC voltage was later compared to experimentally determined computer shutdown voltages and also provided a consistent method of comparing each disconnection method with the others.

B. PEAK DETECTION METHOD

The peak detection method used for disconnection was described in detail in the Laboratory Model Development Section earlier in this thesis. Figure 16 shows the estimated RMS calculation used in the laboratory EMS and Figure 24 shows the estimated RMS calculation used in the EMS model.

The EMS model used for testing the peak detection method was the same model used in the Model Verification section of this thesis with the addition of the grid fault model configuration shown in Figure 30 and the overvoltage (OV) and under voltage (UV) comparators shown in Figure 31. The addition of the overvoltage and under voltage comparator blocks ensured the EMS model could accommodate both a grid fault involving an overvoltage and under voltage condition. When the peak detection algorithm determined that an islanding condition was required by comparing the estimated voltage to the OV and UV set points the output signal was generated to open the grid feeder breaker (logical 0), shown in Figure 22, and switch control mode of the inverter from current injection to voltage control by outputting a logical 1 to the IGBT control input shown in Figure 21. This action would isolate the inverter from the grid and place it in voltage control mode (islanding mode) operation.

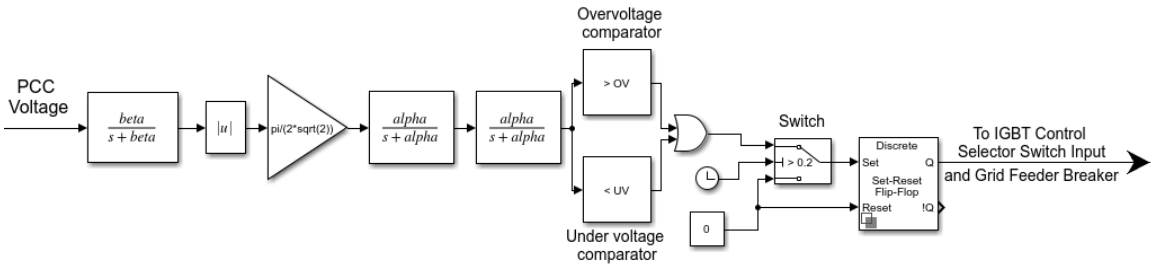

Figure 31. Estimated RMS Calculation (OV and UV)

C. DQ REFERENCE FRAME METHOD

1. DQ Reference Frame Theory

The direct-quadrature (dq) reference frame, also known as the synchronous reference frame has been used in many modern day electrical applications. In the dq reference frame or rotating reference frame ac values become dc values. Because the PI controller is widely used in the engineering industry this feature of the dq reference frame makes it very desirable for industry wide applications. In this thesis the direct component (d) of the dq reference frame output was normalized using the peak value of the sinusoidal grid voltage input (120 * √2 Volts) and then compared as a per unit value to voltage values listed in Table 2. This comparison was then used to determine the operating mode of the EMS. Equation (6) shows the transformation equation from the α β reference frame to the dq reference frame. Normally, the dq reference frame is used for 3 phase systems that have been transformed into the α β reference frame; however, for this thesis and other single-phase systems, the orthogonal β component is generated using the α voltage vector.

$$\begin{bmatrix} v_d \\ v_q \end{bmatrix} = \begin{bmatrix} \cos(\theta) & \sin(\theta) \\ -\sin(\theta) & \cos(\theta) \end{bmatrix} \begin{bmatrix} v_\alpha \\ v_\beta \end{bmatrix} \tag{6}$$

2. Orthogonal Signal Generation

Four different methods for orthogonal signal generation, Quarter Cycle Delay Method, the Differentiation Method, the Second Order Generalized Integrator (SOGI) Method, and the All Pass Filter Method are explored in [3]. In this thesis the SOGI method for orthogonal signal generation was used because the author of [3] determined that the SOGI was the method least effected by noise and harmonics.

The Generalized Integrator (GI) is the base of proportional-resonant controllers and has also been used for an adaptive filter based structure called the SOGI.

Figure 32 shows the SOGI Adaptive Filter block diagram. The input to the SOGI is the PCC voltage (v) and the output is the filtered direct component (v') and the filtered quadrature component (qv'). The gain (k) controls the bandwidth for both the band pass filter for the direct

component v' and the low-pass filter for the quadrature component qv' [6]. An important property of the SOGI shown in Figure 32 is that the omega' is not the input frequency of the system but the resonance frequency of the filter. This feature of the SOGI will play an important role in the disconnection method discussed in the next section.

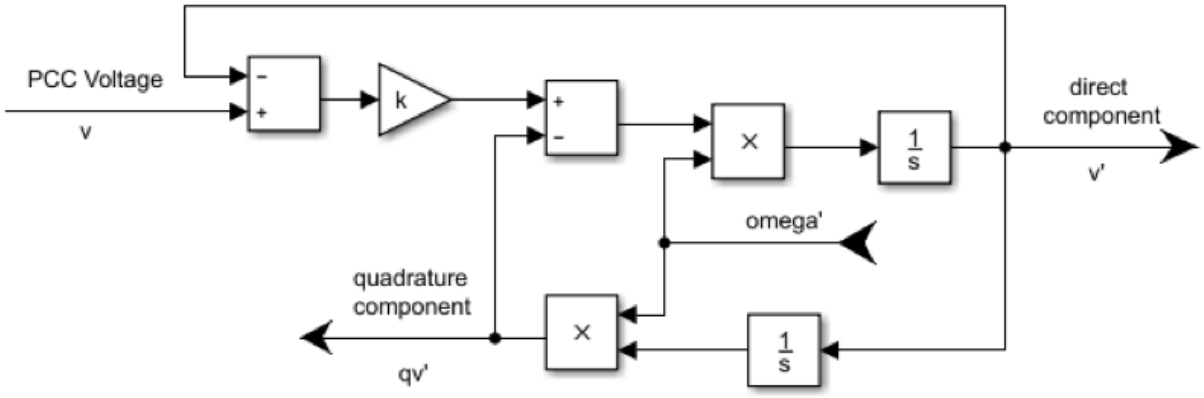

Figure 32. SOGI Adaptive Filter Block Diagram. Adapted from [6]

$$D(s) = \frac{v'}{v}(s) = \frac{k\omega' s}{s^2 + k\omega' s + \omega'^2} \tag{7}$$

$$Q(s) = \frac{qv'}{v}(s) = \frac{k\omega'^2}{s^2 + k\omega' s + \omega'^2} \tag{8}$$

Equation 7 and Equation 8 show the transfer functions for the adaptive filter shown in Figure 32 for the direct (D) and the quadrature component (Q) respectively [6].

Figure 33 shows the Bode diagrams for the adaptive SOGI filter where the gain k effects only the bandwidth of the filter and is independent of the resonance frequency ω'. The quadrature component Q(s) shown in Figure 33 confirms that the output signal (qv') shown in Figure 32 is always generated with 0 dB attenuation and -90 degree phase shift at the resonance frequency of the filter [6].

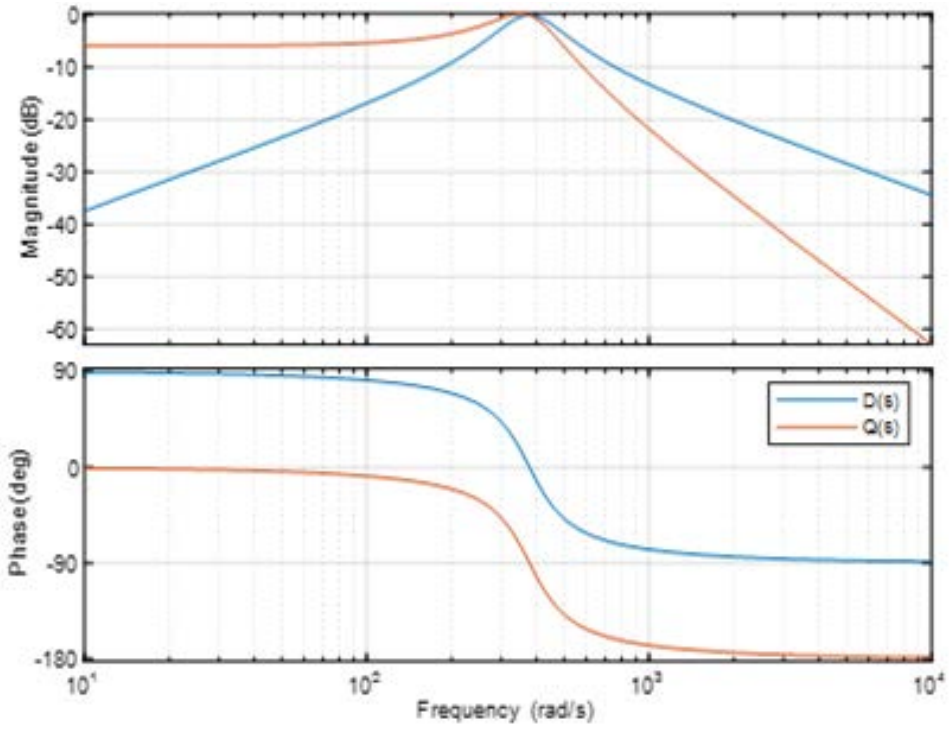

Figure 33. Bode Diagram SOGI Adaptive Filter

Figure 34 shows the generated components from the SOGI adaptive filter. To provide an example of how the generated direct and quadrature components are filtered versions of the input to the SOGI, the input voltage (v) shown in Figure 34 included harmonics at the 5^{th}, 7^{th}, and 11^{th}. Figure 34 shows that the filtered direct component (D(s)) is the same magnitude as the input voltage with fewer harmonics and the quadrature component (Q(s)) is the same magnitude as the input voltage (v) but phase shifted by 90 degrees and with fewer harmonics.

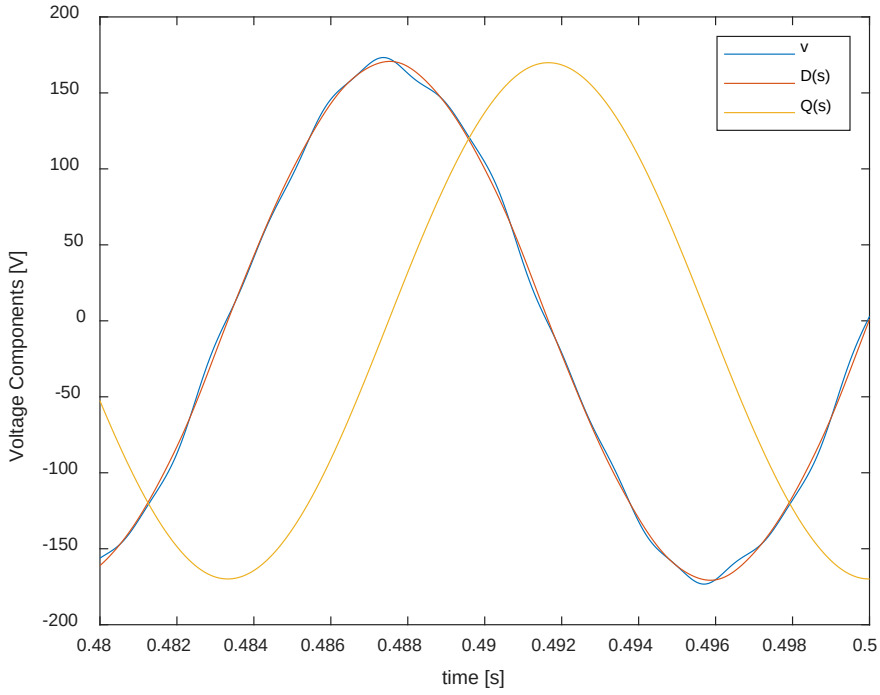

Figure 34. SOGI Adaptive Filter Output

3. DQ Reference Frame Implementation

To implement the dq reference frame disconnection method into simulation the αβ0 to dq0 Specialized Power Systems block was used and is shown in Figure 35.

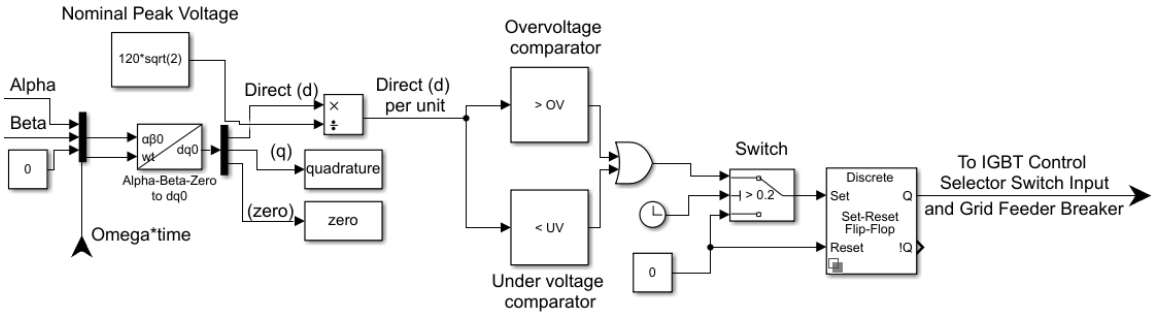

Figure 35. αβ0 to dq0 Implementation

Figure 35 shows the implementation of the dq0 method in the EMS model. The input to the αβ0 to dq0 block are the outputs of the SOGI shown in Figure 32, alpha = v',

beta = qv', and zero = 0. The direct component (d) output of the αβ0 to dq0 block was normalized by the nominal peak value of the grid voltage (120*√2 Volts) and compared to an OV and UV set point for disconnection (islanding) determination. The islanding execution of the inverter occurs in the same manner as described in the peak detection method.

D. MULTIPLE SOGI METHOD (MSOGI METHOD)

The multiple SOGI frequency locked loop (MSOGI-FLL, MSOGI in this thesis) method in detail are described in [6]. This control structure contained three major components; the SOGI as discussed in the dq reference frame section, a frequency locked loop (FLL), and a harmonics decoupling network (HDN). The FLL and HDN are explained in detail below [6].

1. Frequency Locked Loop

A FLL is a synchronization system that generates an output signal at the same frequency of the reference signal through the use of a feedback loop and controller.

In the MSOGI adaptive filter an FLL was implemented to allow for adaptation to varying input frequencies.

The FLL pictured in Figure 36 tunes the resonance frequency of the SOGI filter to the input voltage frequency. The FLL contains a gain normalization parameter along with the actual gain parameter (Γ). This configuration allows the FLL gain parameter to set the dynamics of the frequency estimation and the gain normalization parameter to linearize the response [6]. The feed-forward frequency value (ω_f) presets the detected frequency around its nominal value allowing the residual error controlled by the PI controller to be reduced [18].

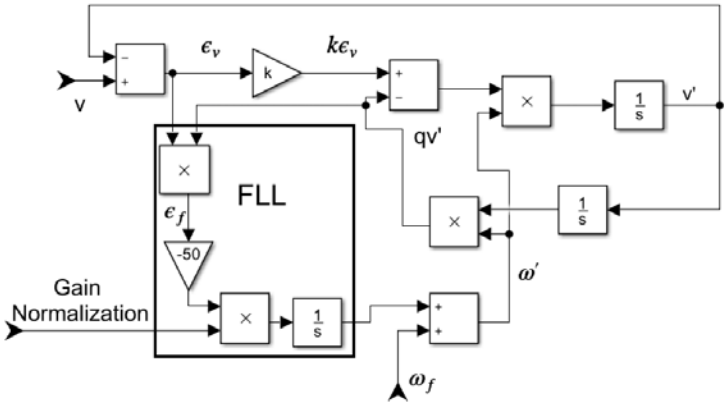

Figure 36. SOGI FLL. Adapted from [6].

$$t_{s(FLL)} \approx \frac{5}{\Gamma} \tag{9}$$

Equation 9 shows the approximate settling time of the linearized FLL [6]. For a gain of 50 the approximate settling time is 0.1 seconds calculated using Equation 9.

Figure 37 shows the estimated frequency (ω') calculation response time of the FLL with a decrease in frequency from 60 Hz to 40 Hz. The simulated data corresponds very well with the estimated settling time calculated using Equation 9.

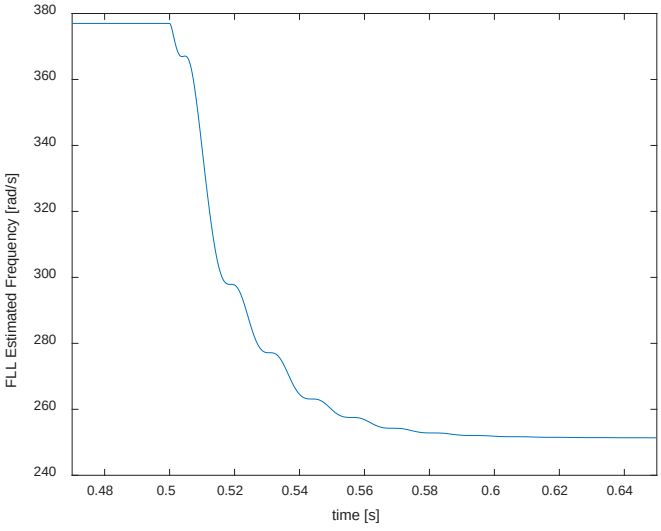

Figure 37. FLL Frequency Estimate Response Time. Adapted from [6].

$$E(s) = \frac{\varepsilon_v}{v}(s) = \frac{s^2 + \omega'^2}{s^2 + k\omega' s + \omega'^2} \tag{10}$$

Equation 10 shows the transfer function relating v and ε_v. presented in Figure 36 [6].

Figure 38 shows the bode plot for the phase of qv' and ε_v. It can be observed from Figure 38 that when the input frequency (ω) is less than the detected (estimated) frequency ω', qv', and ε_v are in phase. When the input frequency is greater than the estimated frequency qv' and ε_v are in counter phase [6]. These properties of the FLL allow the frequency error term (ε_f) to be developed shown in Equation 11 [6].

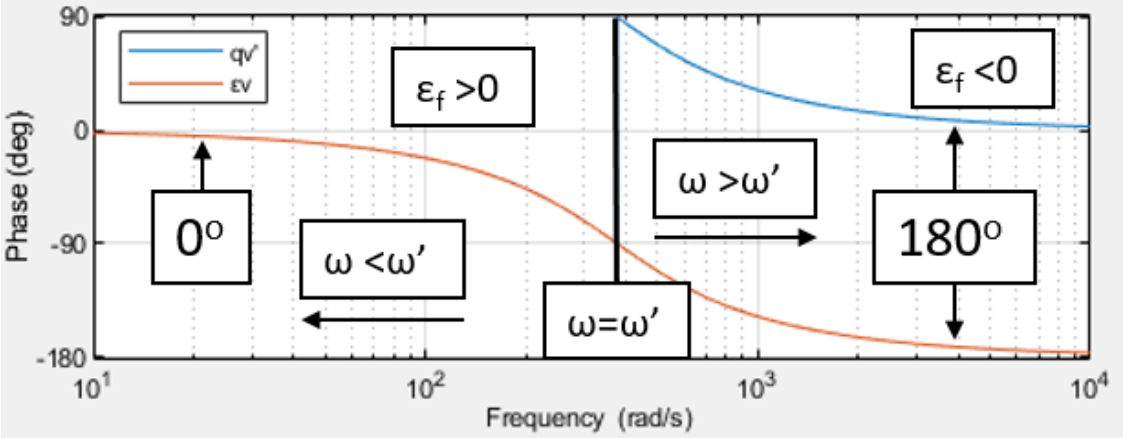

Figure 38. Bode Phase Diagram FLL. Adapted from [6].

$$\varepsilon_f(\,frequency\ error) = qv' * \varepsilon_v \tag{11}$$

Table 3 shows that when the input frequency is less than the estimated frequency an average positive value of the frequency error is generated and vice versa for an estimated frequency lower than the input frequency. When the estimated frequency is locked onto the input frequency the error term is zero. A negative gain (Γ) is used to ensure that the controller remains stable and drives the frequency error to zero [6].

Table 3. FLL Frequency Error Summary. Adapted from [6].

	$\omega < \omega'$	**$\omega > \omega'$**	**$\omega = \omega'$**
qv' and ε_v	In phase	Counter Phase	
Average Frequency Error (ε_f)	Positive	Negative	Zero

Figure 39 shows the response of the FLL for two scenarios. Figure 39 (a) and (c) show the values for input voltage (v_{in}), qv', and ε_v and ε_f respectively for an instantaneous decrease in frequency at time t = 0.5 s from 60 to 40 Hz and Figure 39 (b) and (d) show the values for input voltage (v_{in}), qv', and ε_v and ε_f respectively for an instantaneous increase in frequency at time t = 0.5 s from 60 to 80 Hz. Using Equation 11 and Figure 39 (a) and (b) it can be shown that initially the frequency error is zero because the voltage error is equal to zero. From Figure 39 (a) and (c) it can be observed that after the decrease in frequency occurs qv' and the voltage error are in phase with one another generating a positive frequency error shown in Figure 39 (c). The positive frequency error coupled with the negative gain in the FLL drives the detected frequency to the input frequency when the input frequency is lower than the detected frequency. From Figure 39 (b) and (d) it can be observed that after the increase in frequency occurs qv' and the voltage error are in counter phase with one another. Because qv' is positive while ε_v is negative and vice versa the average error shown Figure 39 (d) is negative. The negative frequency error coupled with the negative gain in the FLL drives the detected frequency to the input frequency when the input frequency is higher than the detected frequency.

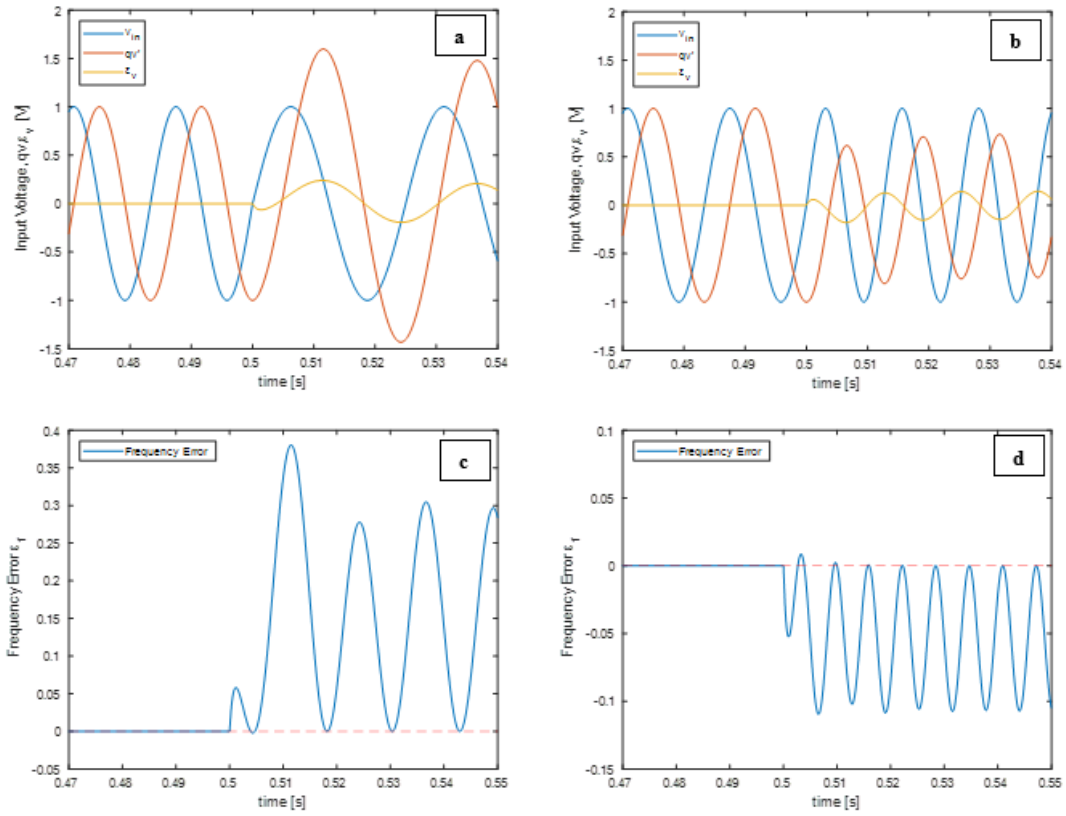

(a) vin, qv', and $\varepsilon_{v;}$ (b) vin, qv', and ε_v; (c) ε_f (Frequency Error); (d) ε_f (Frequency Error)

Figure 39. FLL Frequency Error Response

2. Harmonics Decoupling Network (HDN)

The adaptive SOGI filter presented earlier provides some filtering capability for harmonics in the input voltage to the system. However, observing the Bode plots shown in Figure 33 the filter will have a decreased performance with harmonics close to the resonance frequency of the SOGI [6]. To counter this effect, the gain (k) of the filter could be adjusted to a lower value but this would cause a decrease in the response time of the system. A solution to this problem is to introduce the HDN, shown in Figure 40, into the system [6].

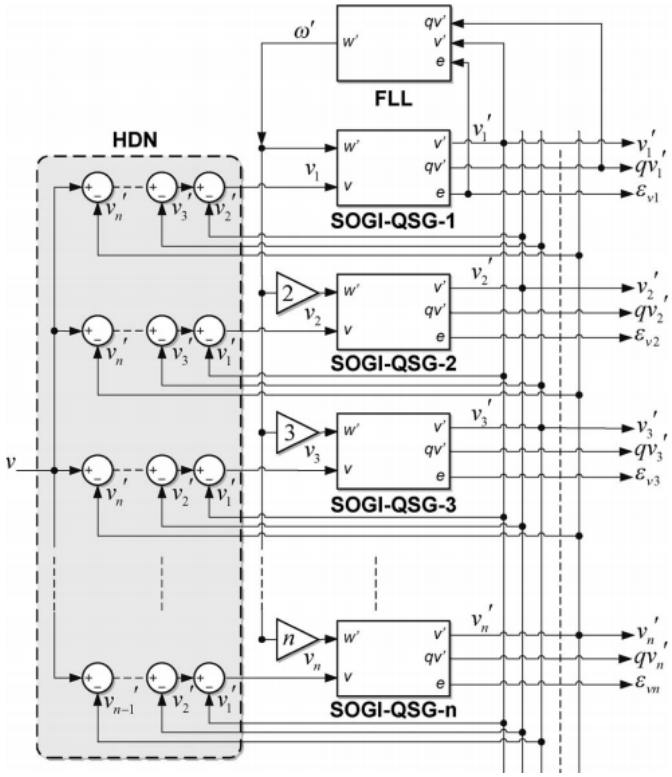

Figure 40. Multiple SOGI Adaptive Filter HDN. Source: [6]

The HDN shown in Figure 40 provides a cross-feedback network that greatly improves the filtering capability of the MSOGI by allowing each SOGI tuned at its respective frequency to provide an input to the other SOGIs. The Bode plots of the SOGI adaptive filter shown in Figure 33 shows that the SOGI direct (D(s)) component tuned at a specific frequency is a filtered version of the input with no change in the phase angle and 0dB attenuation at the resonance frequency [6].

To verify the operation of the HDN a simulation was setup using the same harmonics that were used in the verification portion of this thesis. The input voltage (v) shown in Figure 40 included harmonics at the 5^{th}, 7^{th}, and 11^{th} of the fundamental of 60 Hz. Figure 41 (a) shows the fundamental input frequency of 60 Hz in blue and the output of the SOGI filter tuned at 60 Hz in dashed red. The output of the SOGI filter closely matches the fundamental frequency input. The subsequent plots of Figure 41, (b) – (d) show their respective harmonic components along with the output of the SOGI filters tuned

at their particular frequencies. Because each of the individual frequency components is then fed back into the other SOGI blocks through the HDN the output of each SOGI filter v'_n (shown in Figure 40), where n is equal to 5,7,and 11, is only the frequency component associated with that particular SOGI filter. It can be observed from each of these plots that each of the SOGI filters tuned at their respective frequencies allows the HDN to filter out and remove the harmonic components present in the input signal and thereby produces an output more representative of only the fundamental component of the voltage input. Figure 41 shows that the harmonic input shown in blue very closely matches the output each SOGI filter, shown in dashed red, tuned at the corresponding frequency.

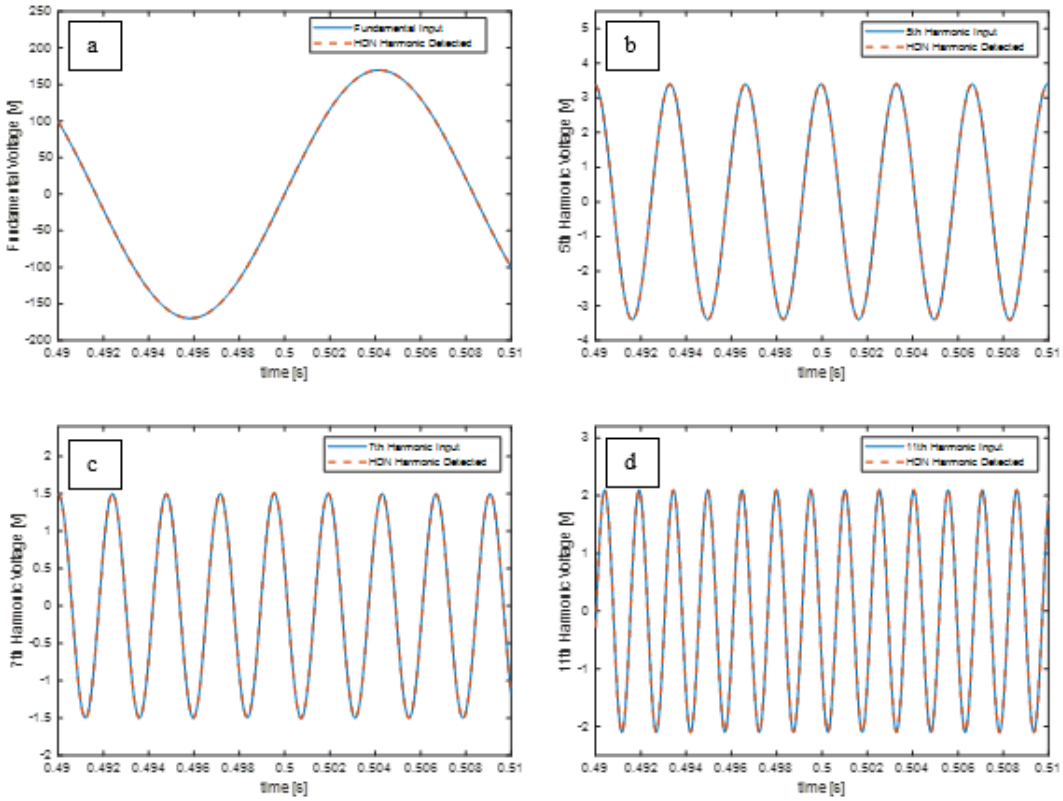

(a) Fundamental Frequency; (b) 5th Harmonic; (c) 7th Harmonic; (d) 11th Harmonic

Figure 41. HDN Frequency Detection Verification

3. Threshold Implementation

Equation 12 was used to provide a method to compare the voltage output of the MSOGI with the voltage values shown in Table 2 [6].

$$\left|v'\right| = \sqrt{(v')^2 + (qv')^2} \tag{12}$$

Where v' and qv' are the output of the SOGI tuned at the fundamental frequency shown in Figure 40. Because the HDN provides a highly filtered v' output and the quadrature component generated by the SOGI is based on this output the corresponding magnitude of v' is also highly filtered. By using the magnitude of the output of the SOGI the threshold comparison can be accomplished using a constant value; a feature that will be shown in a later section of this thesis to be of great importance.

VI. RESULTS

In this section the results of the simulations are discussed and divided into three main subsections; computer shutdown voltage test, clearing time response, and IEEE Standard 1547-2018 comparison.

For clarity, a few terms are explained as follows:

1. Disconnection Parameter: This term describes the parameter used to determine the operating state of the EMS (grid-connected or islanding mode of operation). Each method described in this section relied on a different disconnection parameter. This disconnection parameter is the signal that is compared with the voltages shown in Table 2 and if the conditions are met subsequently causes the grid feeder breaker to open and the inverter to switch control mode from current injection to voltage control.

Peak Detection Method – The estimated RMS value calculated by the algorithm shown in Figure 24.

DQ Method – The normalized direct (d) output of the dq Specialized Power Systems block shown in Figure 35. This value was normalized using the peak value of the input voltage (120 *√2 Volts).

MSOGI Method – The normalized threshold value described by Equation 12. This value was normalized using the peak value of the input voltage (120 *√2 Volts).

Extended MSOGI Method – This method uses the same threshold value as the MSOGI method shown in Equation 12. This method, which will be described in detail later, is essentially an extension of the MSOGI method with more SOGI filters added to the HDN to filter out harmonics generated by non-linear loads.

True RMS Method – The normalized output of the Specialized Power Systems RMS block. Rather than the estimated RMS value used in the peak detection method, this method uses a true RMS value of the PCC voltage to compare to the

voltage values shown in Table 2. This value was normalized using the RMS value of the input voltage (120 V RMS).

2. PCC / Load Voltage: The PCC is defined by IEEE Standard 1547-2018 as "The point of connection between the Area EPS and the Local EPS" [8]. For the thesis simulations this is the point where the H-bridge inverter and the simulated grid voltage intersect. This point is also common to where the load voltage is measured. Therefore, in this section the PCC voltage is synonymous with the load voltage and is used interchangeably.

3. Fault / Disturbance: IEEE Standard 1547-2018 defines the "disturbance period" as "The range of time during which the *applicable voltage* or system frequency is outside the *continuous operation* region" [8]. In this section of the thesis the term "fault" is shown in some of the figures and used synonymously with "disturbance" as defined by the IEEE Standard [8].

A. COMPUTER SHUTDOWN VOLTAGE TEST

The computer shutdown voltage test was developed to determine if a computer without an Uninterrupted Power Supply would shut down if the grid voltage was maintained within the requirements of IEEE Standard 1547-2018.

Figure 42 shows the laboratory setup for testing the shutdown voltage for different computers. The laboratory test setup consisted of a Variac connected to the 120 Volt 60 Hz grid supply, a Fluke voltmeter, a power strip, and the computer used for testing. The power strip was used only to provide a common point of coupling for the output of the Variac and the Fluke voltmeter.

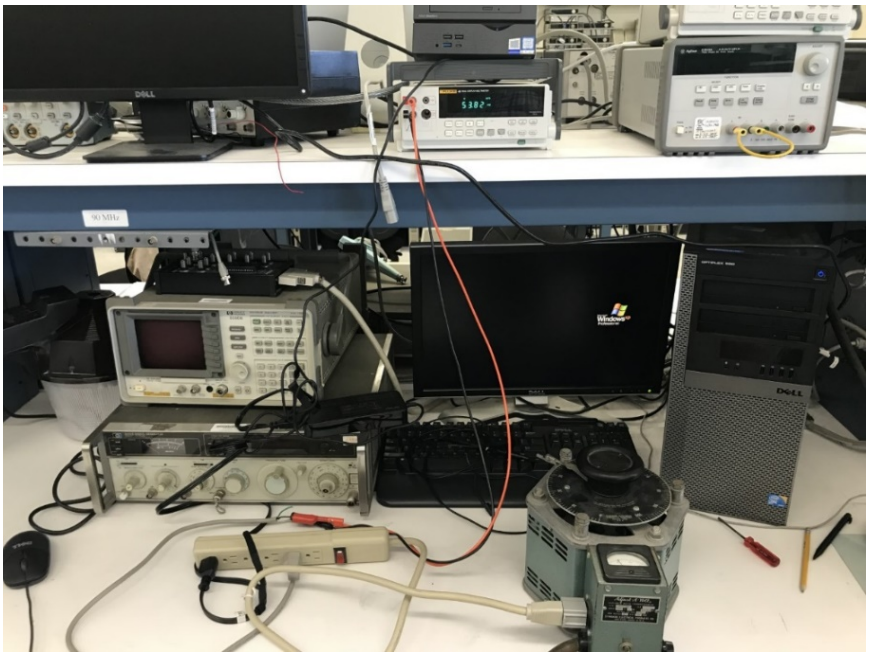

Figure 42. Computer Voltage Shutdown Voltage Test Setup

Three different computers were chosen for the test; an Asus VC66, a Dell Optiplex 755, and a Dell Optiplex 9020. Two Dell computers were chosen because the DoD uses Dell products extensively throughout its network. Both of the Dell computers were equipped with internal power supplies. Due to its size, the Asus required an external power supply.

To perform the test three steps were used: 1) The power strip was plugged into the output of the Variac and the output voltage of the Variac was adjusted to approximately 120 Volts RMS as read on the Fluke voltmeter. 2) The computer being tested was plugged into the power strip, powered on, and allowed sufficient time to boot up. 3) The computer input voltage was lowered by lowering the Variac output voltage until the power light on the computer went out. During the last step the computer shutdown voltage was recorded as the value visible on the Fluke voltmeter. Table 4 summarizes the results of the test.

Table 4. Computer Shutdown Voltages

Computer Model	**Shutdown Voltage [V_{RMS}]**
Asus VC66	53.83
Dell Optiplex 755	32.49
Dell Optiplex 9020	67.08

The values shown in Table 4 were obtained under ideal operating conditions for a computer. The laboratory where this test was conducted is maintained at a temperature suited for electronic equipment and the computers were not performing any arduous computations at the time the test was conducted. The operating environment for computers, especially in military applications, may not be under ideal conditions. The operating environment as well as computational load may increase the shutdown voltages shown in Table 4 making them more susceptible to grid voltage disturbances.

Table 5 shows a summary of the voltage ride-through requirements from Table 14 of IEEE Standard 1547-2018 for a Category I system used for this test. It can be observed that if the voltage falls between 0.50 and 0.70 (p.u.) (60 V_{RMS} and 84 V_{RMS} for 120 V_{RMS} input) of the nominal voltage at the PCC the EMS must not isolate the intentional island from the main grid supply for a minimum of 0.16 seconds. In the computer voltage shutdown test the 60 Volts (0.5 p.u.) calculated from Table 5 is less than the 67.08 Volts shutdown voltage of the Dell Optiplex 9020. This shows that a computer connected to a EMS maintained EPS may shutdown during grid voltage fluctuations allowed by IEEE Standard 1547-2018.

Table 5. Summary of Table 14 of IEEE Standard 1547-2018. Source: [8]

Voltage range (p.u)	**Operating mode/ response**	**Minimum ride-through time (s)**	**Maximum response time (s)**
$0.50 \leq V < 0.70$	Permissive Operation	0.16	N/A

In this experiment only shutdown voltages for computers were tested. In some situations, the microgrid may be part of an area that contains a hospital or communications center. This hospital or communications center may be reliant on the EMS to switch to

islanding mode quickly enough to prevent shut down of vital equipment. Ideally, the EMS would be allowed to switch to islanding mode during a situation that might cause a disruption to vital equipment such as computers and other electronic equipment. As shown from this experiment the IEEE Standard as written may cause a loss of vital equipment to due grid fluctuations that require a voltage ride-through period.

B. COMPLETE VOLTAGE LOSS TEST

The complete voltage loss test is the first fault condition scenario used for testing the EMS clearing time response of the three disconnection methods described in the EMS Control Disconnection Methods section. Similar to the model verification test, this test was conducted by opening the grid feeder breaker at a predetermined time to remove the source voltage. The set points shown in Table 2 for operating mode of "cease to energize" (0.50 and 1.20 p.u) were used to set the trip condition for each disconnection method. Each disconnection method was tested with and without harmonics in the source voltage and at varying times in the source voltage cycle. For comparison purposes the Specialized Power Systems RMS block was added to each simulation model and provided a consistent method of comparing each disconnection method with the others.

The tests described in this section were all conducted from a steady state condition with the EMS injecting approximately 1 Amp of real current into the load. All minimum and maximum values of current and voltage shown in the figures are measured in absolute values.

1. Peak Detection Method

The first disconnection method tested was the peak detection method. Figure 43 shows the peak detection disconnection method with no harmonics and the fault occurring at a peak of the voltage cycle.

Figure 43 (e) shows the lower threshold value set to 60 Volts in accordance with Table 2 of IEEE Standard 1547-2018. It can be observed from Figure 43 (a) that the clearing time of 0.0224 seconds is greater than one period of the source voltage. This causes the voltage transient shown in Figure 43 (b) which causes the RMS load voltage, shown in Figure 43 (f), to decrease to a value of approximately 55 Volts. Comparing this voltage to the values of

computer shutdown voltages shown in Table 4; the 55 Volts RMS after the fault insertion was lower than the Dell Optiplex 9020 shutdown voltage and very close to the Asus VC66 shutdown voltage. Figure 43 (e) and (f) show the Load Current and EMS Current transients respectively. These transients subside and reach a steady state value after approximately 0.186 seconds. This transient would be nullified with a more resistive load as the value of the time constant of the circuit lowers and the time to reach steady state is lessened.

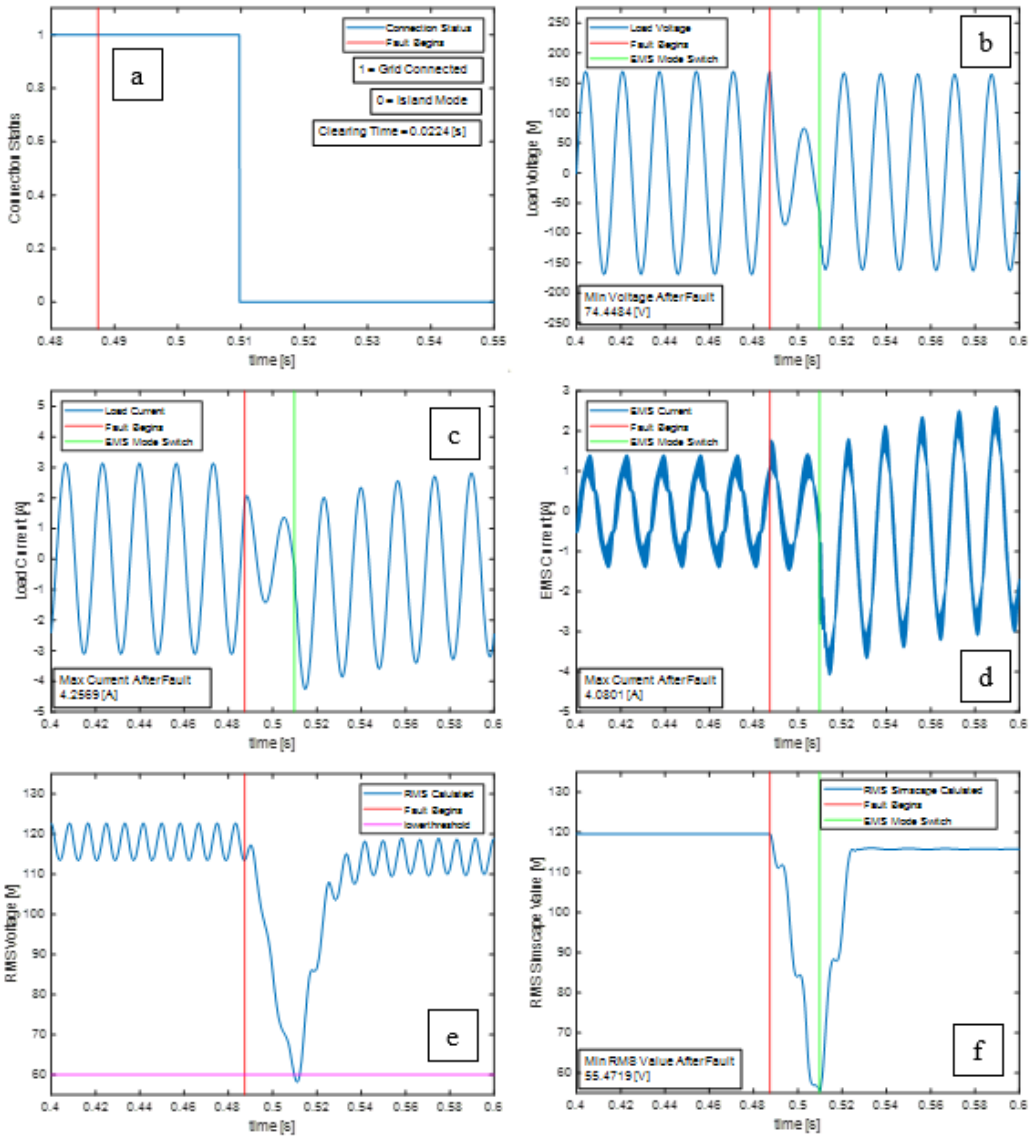

(a) Connection Status; (b) Load Voltage; (c) Load Current; (d) EMS Current; (e) Peak Detection Disconnection Parameter; (f) RMS Block Calculation

Figure 43. Peak Detection Method (No Harmonics) (Peak Cycle)

Figure 44 shows the peak detection method with harmonics in the source voltage and the fault occurring at a peak in the voltage cycle. Comparing Figure 43 and Figure 44 it can be observed that the addition of harmonics has little effect on the transient response of the system. This is due in part to the low pass filter integrated into the estimated RMS voltage calculation algorithm used to determine the EMS connection status.

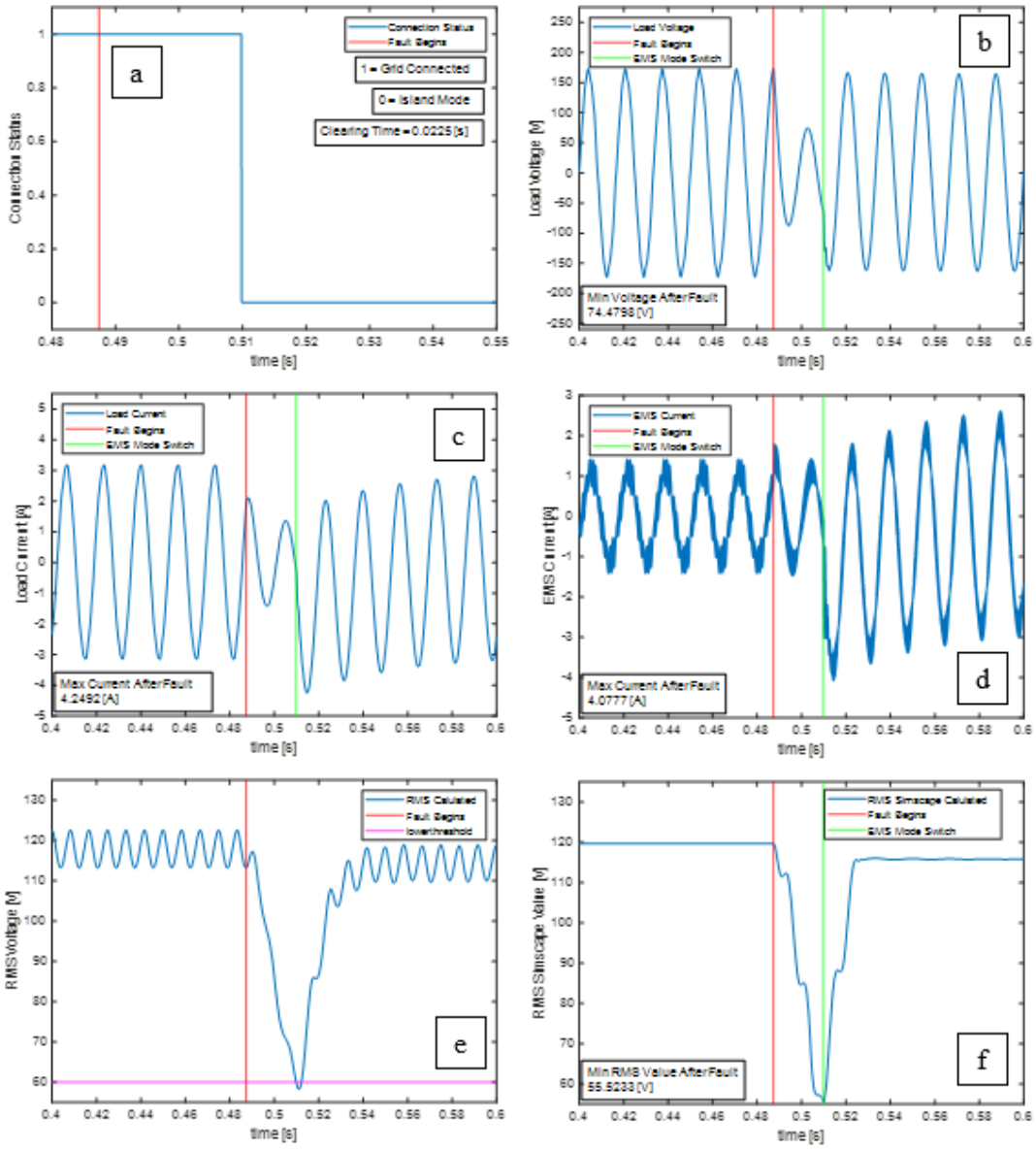

(a) Connection Status; (b) Load Voltage; (c) Load Current; (d) EMS Current; (e) Peak Detection Disconnection Parameter; (f) RMS Block Calculation

Figure 44. Peak Detection Method (Harmonics) (Peak Cycle)

Figure 45 shows the peak detection method with harmonics in the source voltage and the fault occurring at the zero value in the voltage cycle. Comparing Figure 44 and Figure 45 the change in the time in the voltage cycle that the fault occurs has little effect on the transient response of the system with the exception of the increase in the clearing time of 0.0032 seconds. However, the clearing time for all three scenarios tested are well within the clearing time of 0.16 seconds required by IEEE Standard 1547-2018

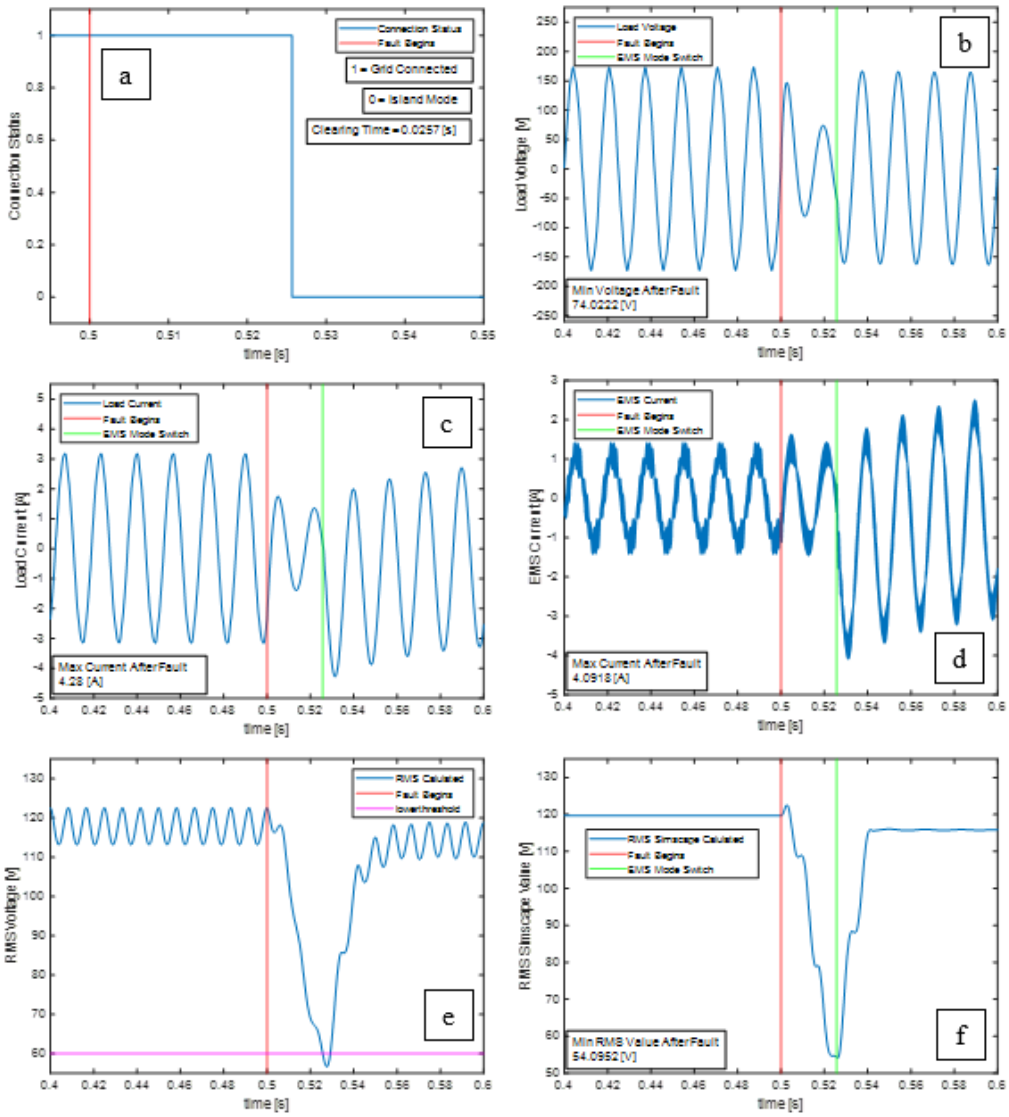

(a) Connection Status; (b) Load Voltage; (c) Load Current; (d) EMS Current; (e) Peak Detection Disconnection Parameter; (f) RMS Block Calculation

Figure 45. Peak Detection Method (Harmonics) (Zero Cycle)

2. DQ Method

The next disconnection method tested was the dq method which has the benefit of transforming ac values directly into dc values.

Figure 46 shows the dq disconnection method with no harmonics in the source voltage and the fault occurring at a peak in the source voltage cycle. Figure 46 (a) shows a decrease in the clearing time of 0.0144 seconds when compared to the peak detection method. Figure 46 (b) shows that because the clearing time occurs in less than one-half of the period of the voltage cycle the RMS value of the load voltage, shown in Figure 46 (e), only decreases to approximately 98 Volts. This is important because it ensures that the load voltage will be maintained high enough to prevent all three computers that were tested in the computer shutdown test from shutting down. Figure 46 (b), (c), and (d) show a larger transient on the load voltage, load current, and EMS current respectively when compared to the peak detection method. This larger transient is most likely produced by the respective voltage and current values remaining at larger values, caused by the faster clearing time response of the dq disconnection method.

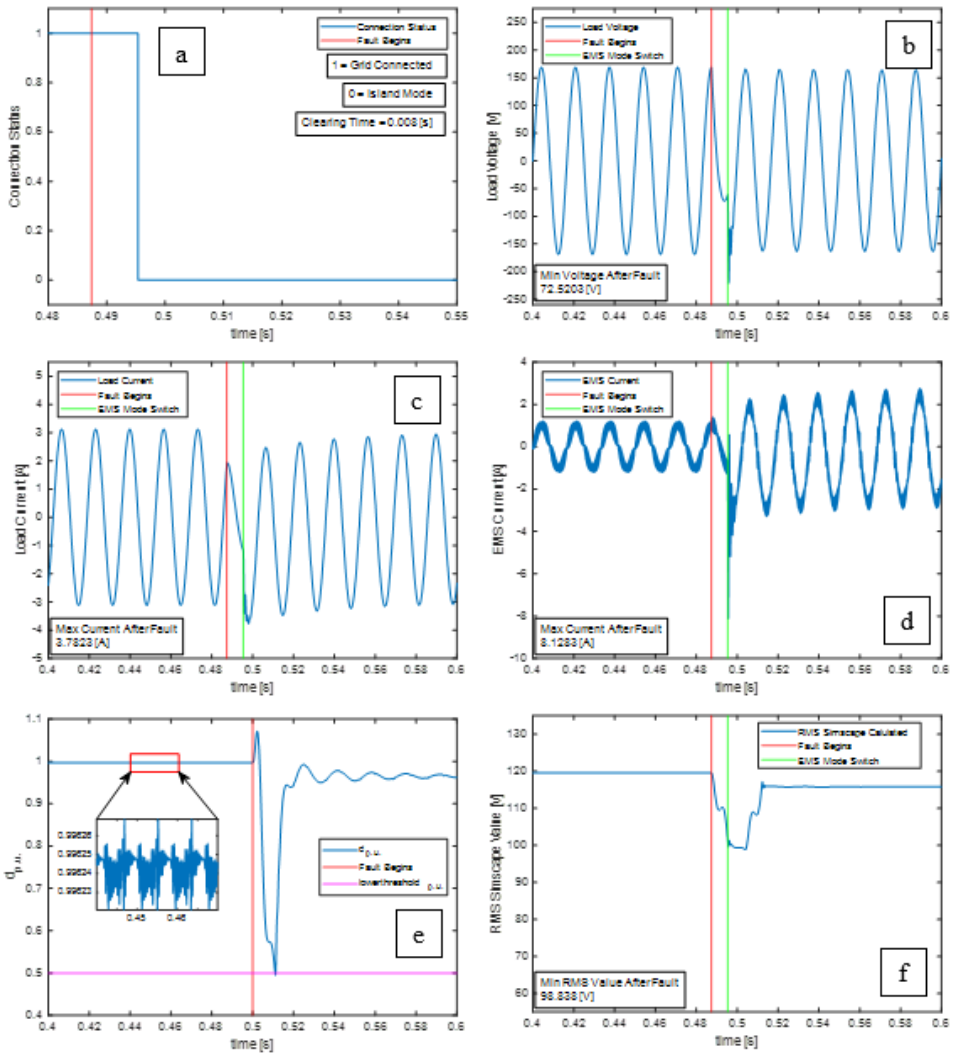

Connection Status; (b) Load Voltage; (c) Load Current; (d) EMS Current; (e) DQ Disconnection Parameter; (f) RMS Block Calculation

Figure 46. DQ Disconnection Method (No Harmonics) (Peak Cycle)

Figure 47 (a) shows the dq disconnection method with harmonics in the source voltage and the fault occurring during a peak in the source voltage cycle. Comparing Figure 46 and Figure 47 the addition of harmonics in the source voltage has little effect on the transient of the system after the fault occurs with one important exception, the calculated direct component (d) value. Comparing Figure 46 (e) and Figure 47 (e) it can be observed that the fluctuations in the calculated direct component (d) used to determine the disconnect signal increase as harmonics are added to the source voltage.

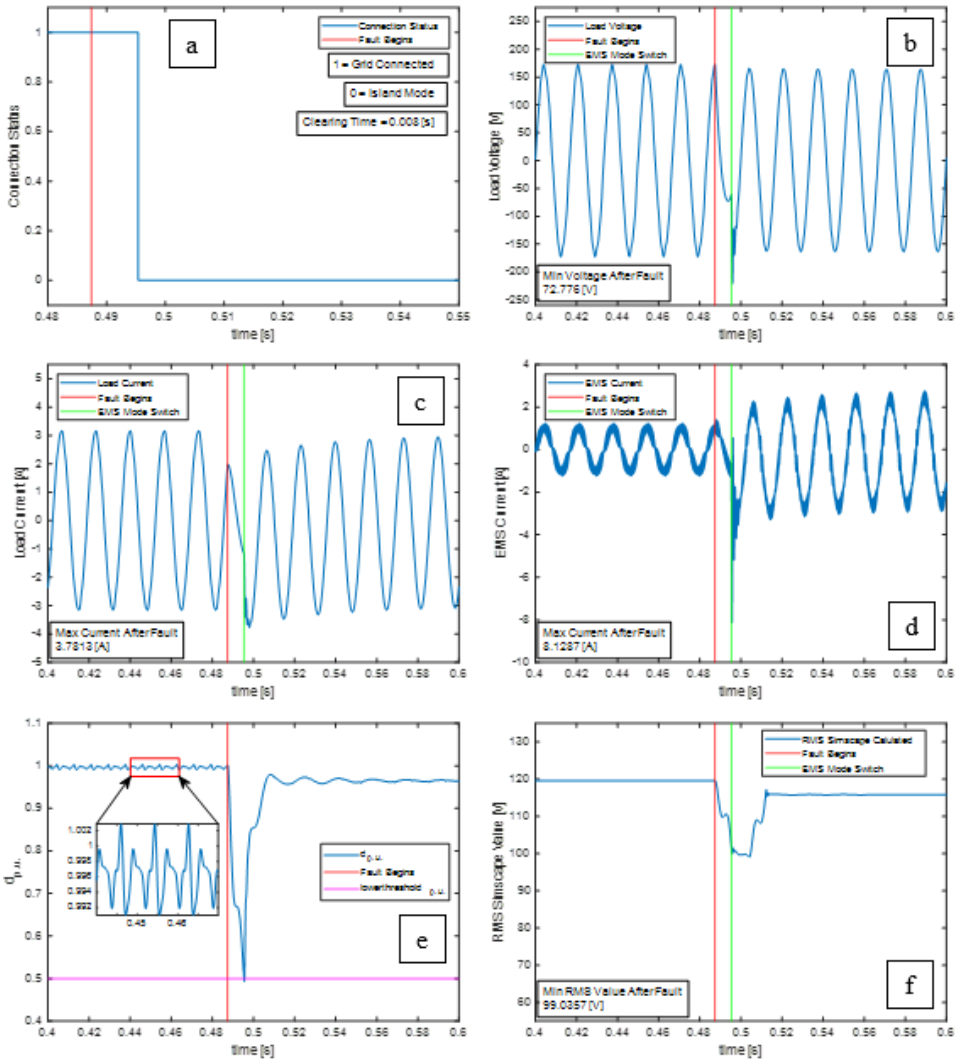

(a) Connection Status; (b) Load Voltage; (c) Load Current; (d) EMS Current; (e) DQ Disconnection Parameter; (f) RMS Block Calculation

Figure 47. DQ Disconnect Method (Harmonics) (Peak Cycle)

Figure 48 shows the dq disconnection method with harmonics in the source voltage and the fault occurring during a zero point in the source voltage cycle. Figure 48 (a) shows a slight increase of 0.003 seconds in the clearing time when compared to Figure 47 (a). The slight increase in clearing time yields a smaller transient in load voltage, load current, and EMS current shown in Figure 48 (b), (c), and (d) respectively when compared to the case when the fault occurred at the peak of the voltage cycle. This same behavior was observed when comparing the peak detection method with no harmonics in the source voltage and

the dq disconnection method with no harmonics in the source voltage. Therefore, the transient that occurs after the fault is dependent on the voltage and current values when the EMS switches control modes. For example, if the voltage and current values are lower when the EMS switches control modes the clearing time is longer and the voltage and current transients are less severe.

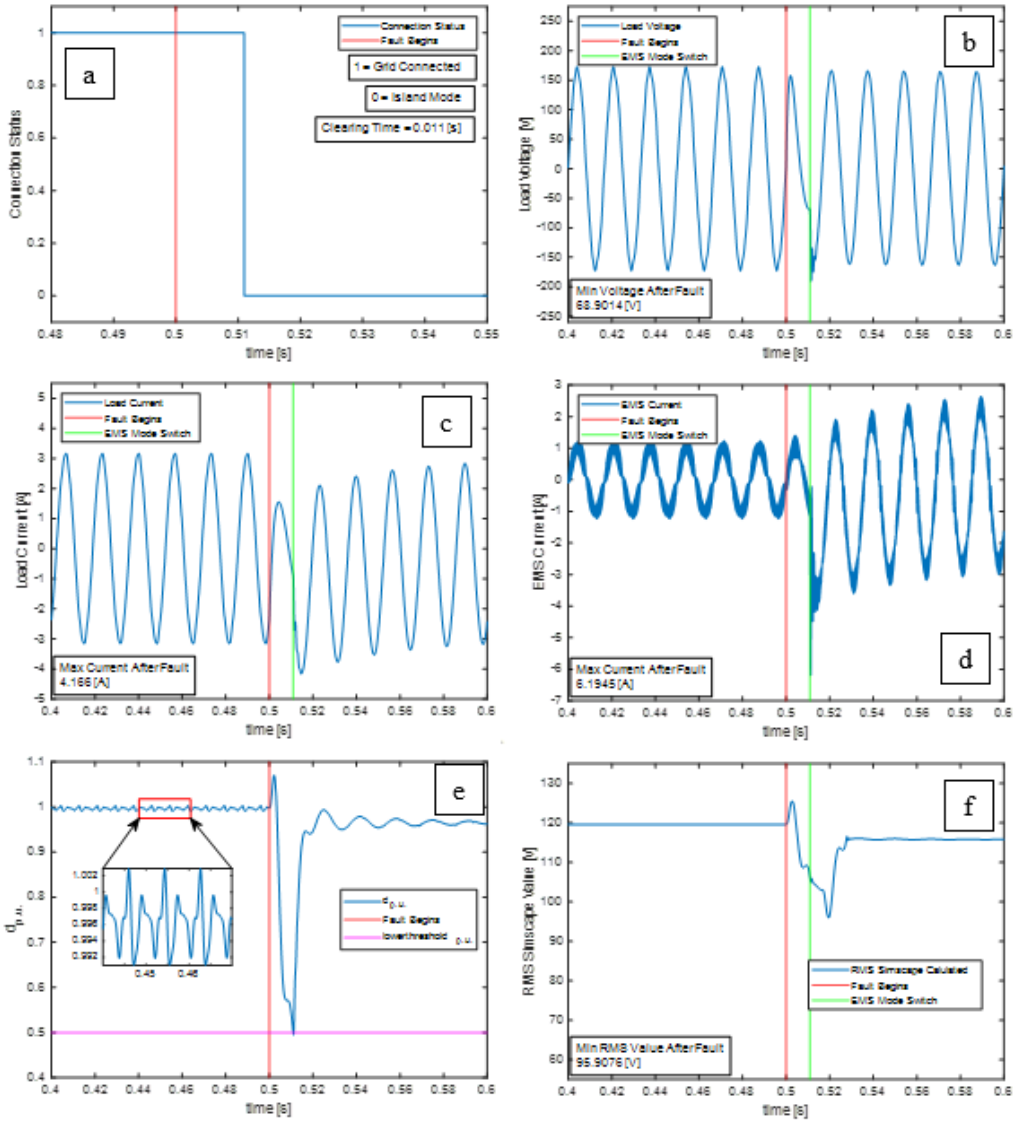

(a) Connection Status; (b) Load Voltage; (c) Load Current; (d) EMS Current; (e) DQ Disconnection Parameter; (f) RMS Block Calculation

Figure 48. DQ Disconnection Method (Harmonics) (Zero Cycle)

3. MSOGI Method

The MSOGI method was the last method tested. An important benefit to the MSOGI method topology is its inherent ability to filter out specific harmonic components in the source voltage to create a smoother estimated dc voltage of the input that can used in the EMS disconnection assessment.

Figure 49 shows the MSOGI disconnection method with no harmonics in the source voltage and the fault occurring during a peak in the source voltage. The results of this test are similar to the results of the dq disconnection method shown in Figure 46. The clearing time for each method is similar with the dq method being slightly shorter (approximately 0.002 seconds) than the MSOGI method. Because the clearing times are similar and the fault occurs at the same time in the source voltage cycle the transients for the load voltage, load current, and EMS current also yield similar results.

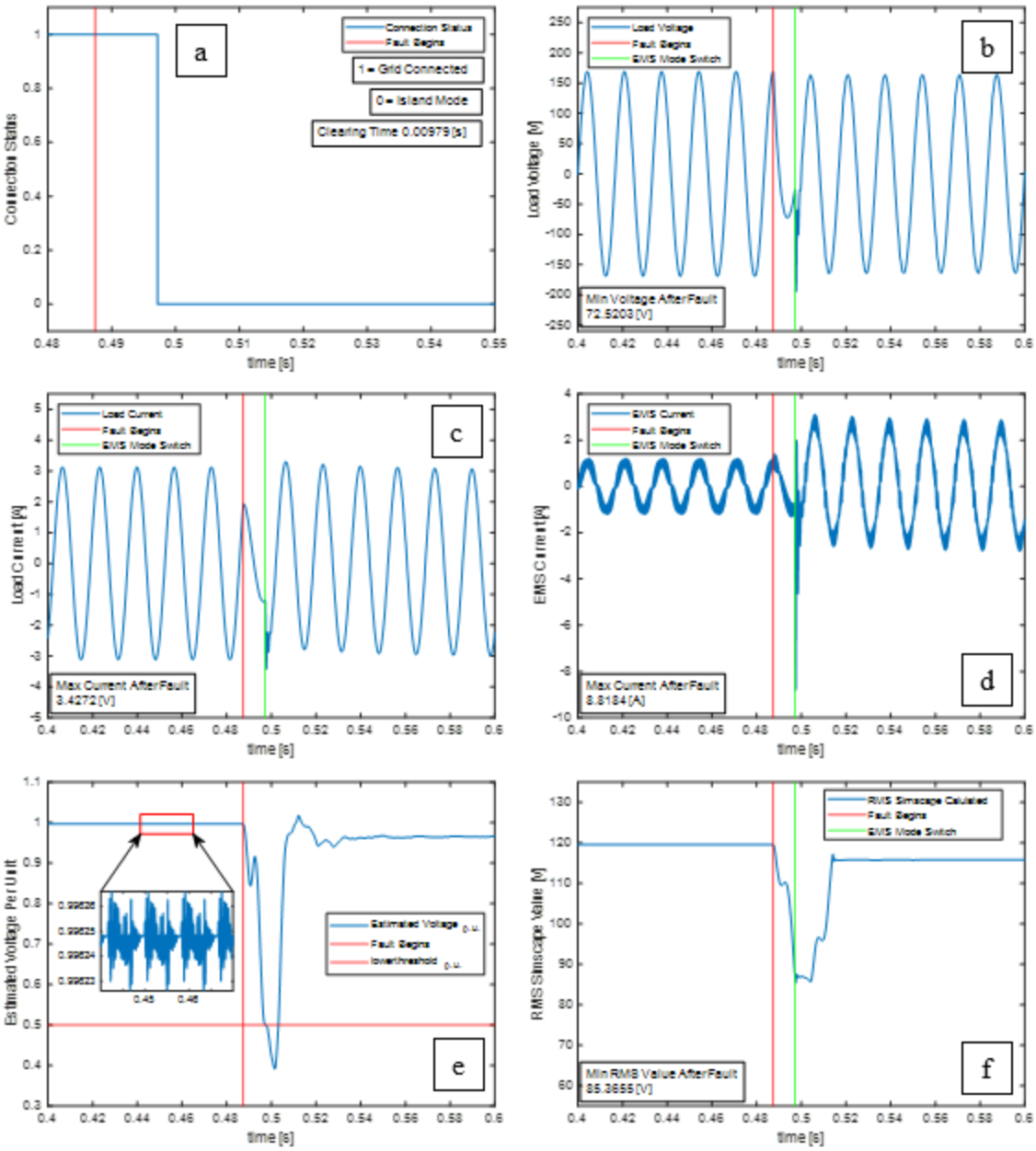

(a) Connection Status; (b) Load Voltage; (c) Load Current; (d) EMS Current; (e) MSOGI Disconnection Parameter; (f) RMS Block Calculation

Figure 49. MSOGI Disconnection Method (No Harmonics) (Peak Cycle)

Figure 50 shows the MSOGI disconnection method with harmonics in the source voltage and the fault occurring at a peak in the source voltage cycle. It can be observed from Figure 50 (c) and (d) that unlike the previous tests the load current and EMS current

both increase to an initial higher positive value instead of a more negative value and then proceed to their respective steady state values following the transient. It can be observed from Figure 43 through Figure 48 (c) and (d) that in each of these cases the EMS switched control mode when the load current and the EMS current were in the negative portion of their respective cycles. Figure 50 (c) and (d) show the opposite condition where both the load current and EMS current are in a positive portion of their respective cycles when the EMS switches control mode. Thus yielding an opposite effect in the transient response of the system as previously observed.

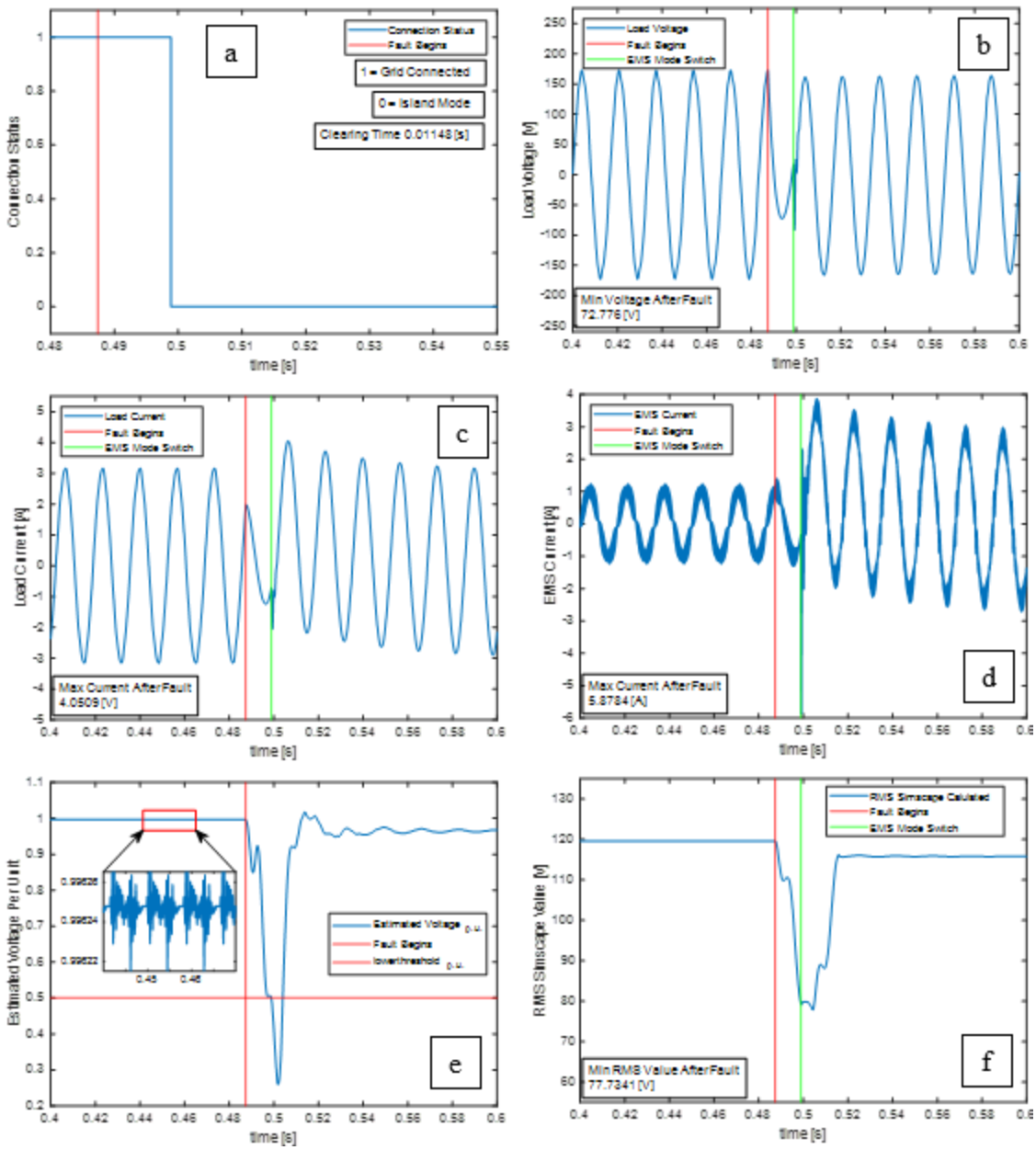

(a) Connection Status; (b) Load Voltage; (c) Load Current; (d) EMS Current; (e) MSOGI Disconnection Parameter; (f) RMS Block Calculation

Figure 50. MSOGI Disconnection Method (Harmonics) (Peak Cycle)

It is important to note that the addition of harmonics to the source voltage has little effect on the disconnection calculation value shown in Figure 50 (e) when compared to the dq disconnection method. It can be observed from Figure 46 (e) and Figure 47 (e) subplots

that when harmonics were introduced into the source voltage the fluctuations in the direct component (d) per unit voltage used for the disconnection determination increased from 0.006% to 1.2% of the per unit voltage; in contrast to the MSOGI disconnection method in which the estimated voltage per unit fluctuations remained essentially constant.

Figure 51 shows the MSOGI disconnection method with harmonics in the source voltage and the fault occurring during a zero point in the source voltage cycle. It can be observed from Figure 50 and Figure 51 that the change in the fault time has little effect on the response of the system with the exception of the load current and EMS current transient orientation. Figure 51 (c) and (d) show the EMS switching control modes during a negative portion of the load current and EMS current cycle; thus, causing a similar transient response as previously observed in Figure 43 thru Figure 49.

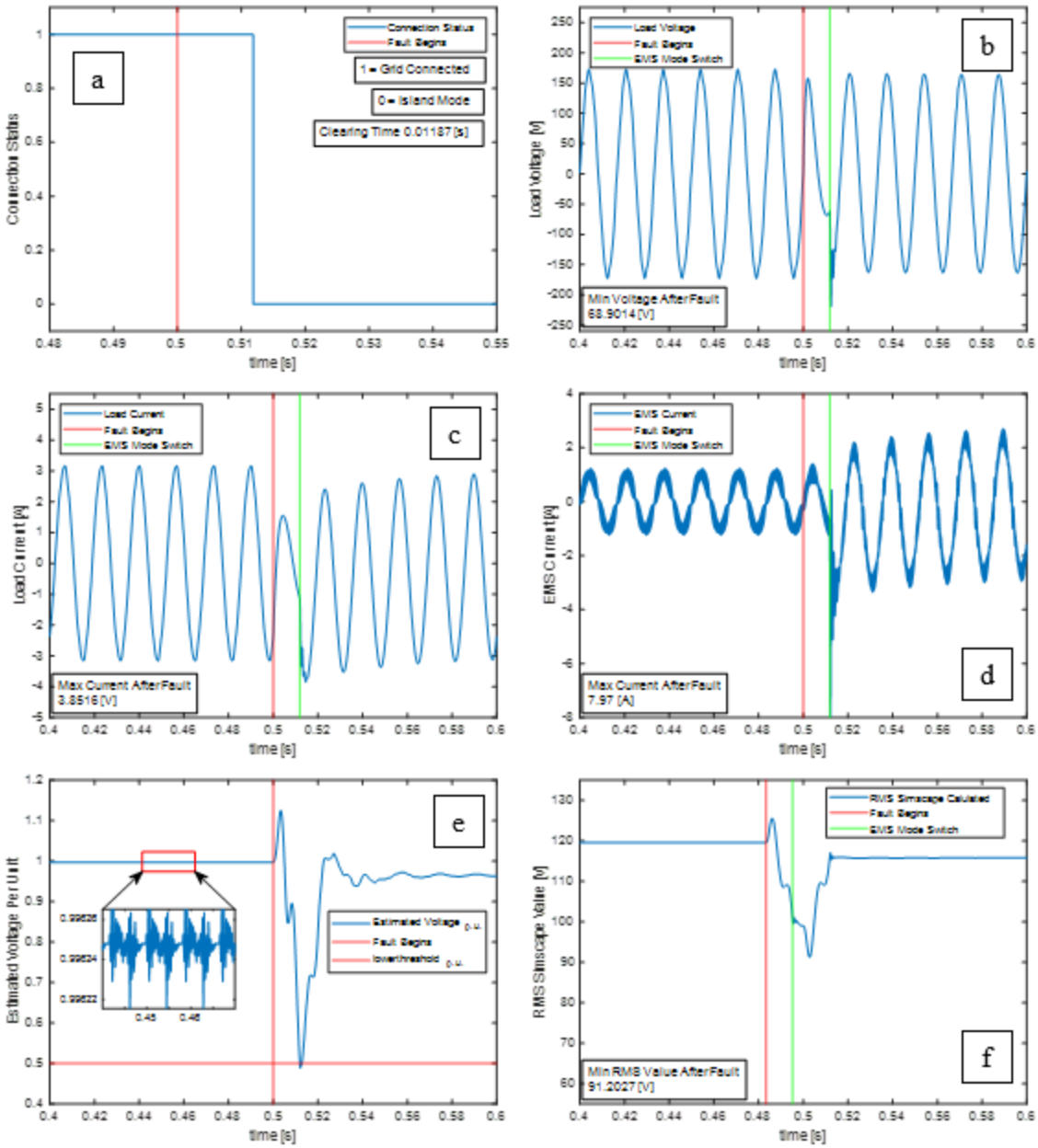

(a) Connection Status; (b) Load Voltage; (c) Load Current; (d) EMS Current; (e) MSOGI Disconnection Parameter; (f) RMS Block Calculation

Figure 51. MSOGI Disconnection Method (Harmonics) (Zero Cycle)

The complete voltage loss test showed some key differences in the response of the systems when using the different disconnection methods. The following observations are worth noting: 1) The peak detection method did not yield a fast enough clearing time to

prevent a possible computer shutdown. Note: All the clearing times could be reduced if the lower threshold value was increased but this would not be compliant with IEEE Standard 1547-2018. 2) The harmonics inserted in the source voltage had a more significant effect on the fluctuations in the disconnection parameter in the dq disconnection method compared to the MSOGI method. 3) The transient response and peak voltages and currents after the fault occurred were affected by how long the system took to respond to the fault condition.

C. EMS DISCONNECTION PARAMETER TEST

The ultimate goal of this thesis was to determine if one of the disconnection control methods could be used as an EMS control structure while adhering to IEEE Standard 1547-2018 requirements. To further test the different disconnection methods a test was implemented to see the effects on the disconnection parameter specifically when harmonics were introduced into the source voltage and the linear load was replaced by a non-linear load. The non-linear load, shown in Figure 52, used in the simulation is a representation of a common single-phase diode bridge rectifier.

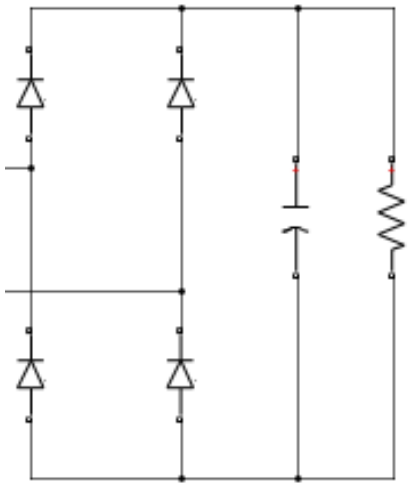

Figure 52. Common Diode Bridge Rectifier. Adapted from [4]

This test specifically explored the peak to peak value of the disconnection parameter under steady state conditions prior to a fault occurring. To explore the effect of harmonics and non-linear loads on the disconnection parameter each disconnection method: peak detection, dq, and MSOGI was tested using three different scenarios:

1. No harmonics in the grid voltage and a linear load.
2. Harmonics in the grid voltage and a non-linear load.
3. Harmonics in the grid voltage and a non-linear load.

For comparison purposes the peak detection disconnection parameter was normalized to 120 Volts RMS.

1. Peak Detection Method

Figure 53 shows the peak detection method disconnection parameter test. It can be observed from Figure 53 that the pk-pk value of the disconnection parameter remains relatively unaffected by the introduction of harmonics in the grid voltage and the non-linear load. However, noting the values in Table 2 the relatively large pk-pk values in the peak detection method disconnection parameter would not be suitable for accurate calculations adhering to the voltage ride-through requirements set forth in IEEE Standard 1547-2018. For example, if a voltage disturbance occurred in the grid supply voltage causing the voltage to lower to approximately 0.70 Volts (p.u.) the fluctuation in the peak detection disconnection parameter of approximately 0.077 would generate a pk-pk range in the disconnection parameter of approximately 0.623 to 0.777. It can be observed from Table 2 that this fluctuation would place the disconnection parameter in two different categories which may cause an islanding condition prior to the required voltage ride-though time. An additional issue explored in the next section of this thesis is that large fluctuations in the peak detection disconnection parameter may also cause an immediate inadvertent islanding of the microgrid prior to the specified voltage ride-through times shown in Table 2 if the fluctuation of the disconnection parameter rises above 1.20 (p.u.) or falls below 0.50 (p.u.).

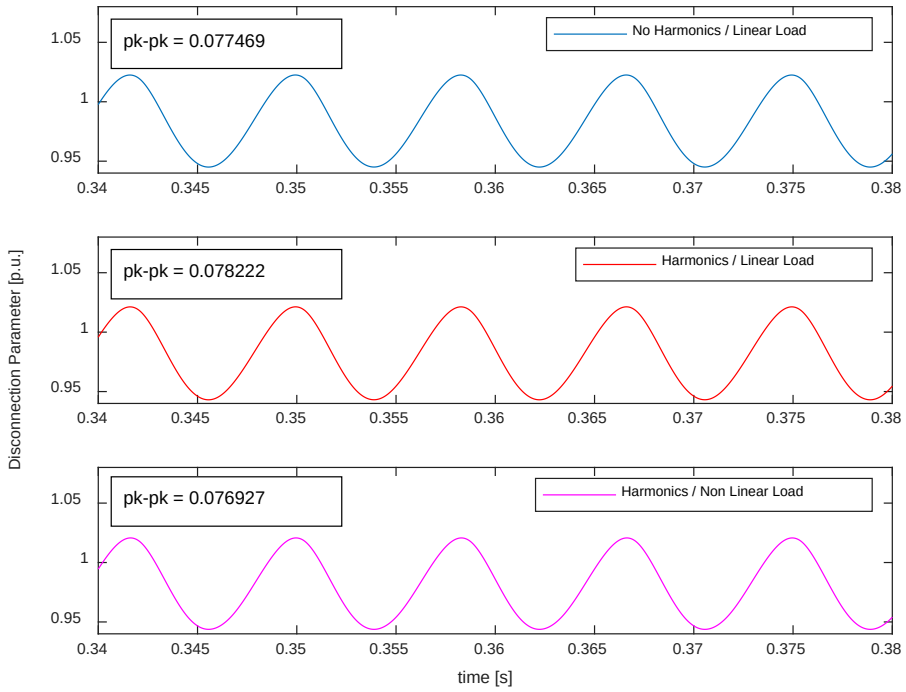

Figure 53. Disconnection Parameter Test (Peak Detection Method)

2. DQ Method

Figure 54 shows the dq method disconnection parameter test. It can be observed from Figure 54 that as the harmonics in grid voltage are added and a non-linear load replaces the linear load the pk-pk value of the disconnection parameter increases but the maximum pk-pk value remains relatively low when compared to the peak detection disconnection parameter. To compare the two methods, if a disturbance in the grid voltage similar to the one described in the previous section occurred the fluctuation in the dq disconnection parameter of approximately 0.017 would generate a pk-pk range in the disconnection parameter of approximately 0.683 to 0.717. While this fluctuation may still cause a premature islanding condition the range of values where this might occur is much lower than when compared to the peak detection method.

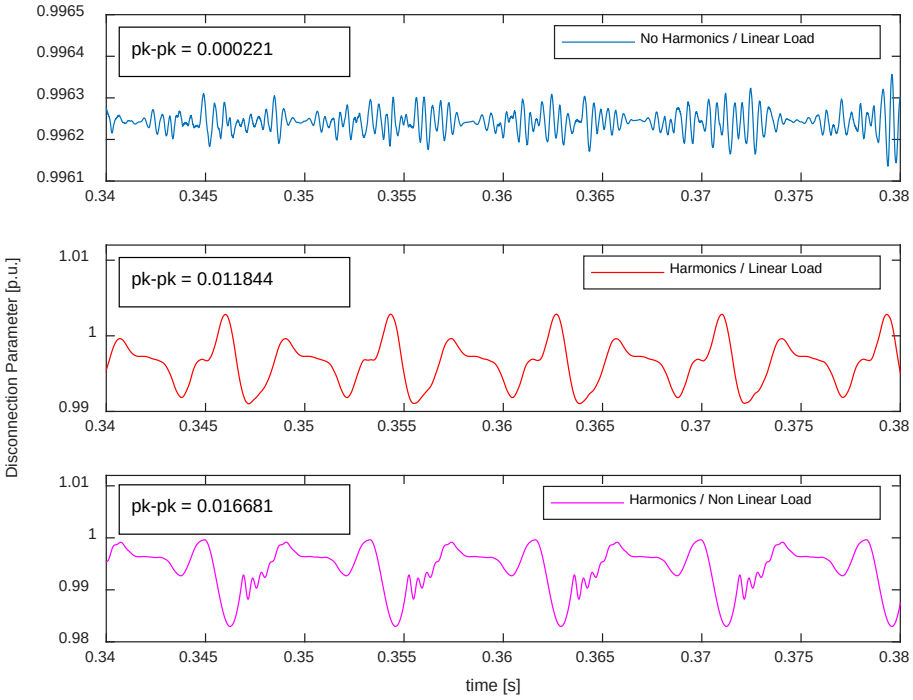

Figure 54. Disconnection Parameter Test (dq Method)

3. MSOGI Method

Figure 55 shows the MSOGI method disconnection parameter test. It can be observed from Figure 55 that the introduction of harmonics in the grid voltage and a non-linear load generates a maximum pk-pk value in the disconnection parameter of approximately 0.0086, approximately half of the pk-pk value of the dq disconnection parameter. This lower pk-pk value occurs because of the filtering capability of the MSOGI method. While the dq method has some inherent filtering capability due to the quadrature component being generated by the use of a SOGI block; the multiple SOGI blocks, combined with the HDN, tuned at specific experimentally determined harmonic values of the grid voltage allows for a much smoother output in the disconnection parameter.

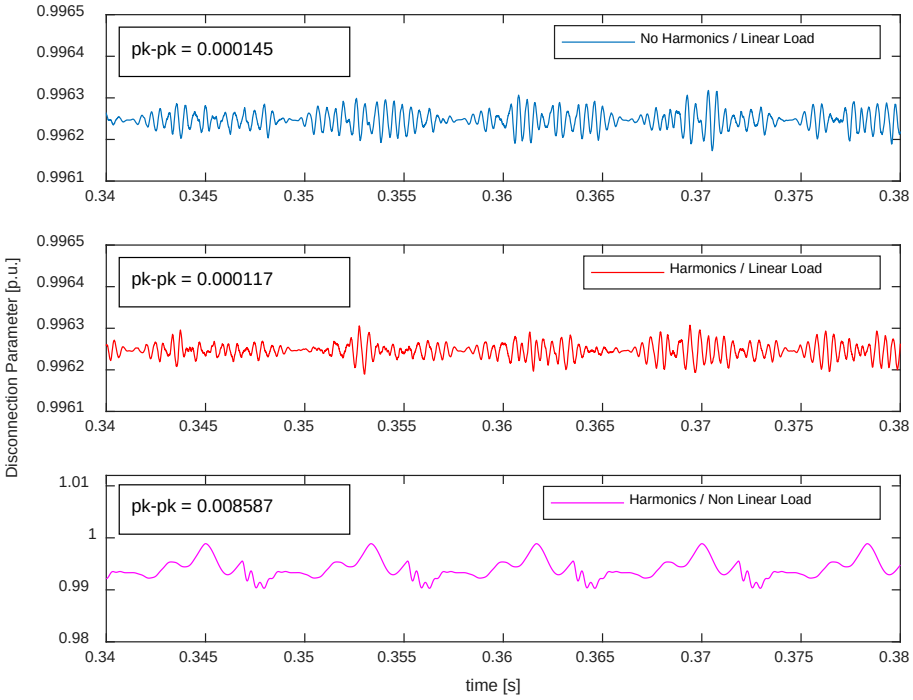

Figure 55. Disconnection Parameter Test (SOGI Method)

Comparing the three methods during steady state conditions is an important test because it helps to show the viability of each method adhering to IEEE Standard 1547-2018 requirements under real world conditions with harmonics present in the grid voltage and the more prevalent non-linear loads. The disconnection parameter test shown in this section proved that the peak detection method is not a viable option to ensure adherence to IEEE Standard 1547-2018 voltage ride-through requirements. However, the dq method and MSOGI method proved to be viable options with the MSOGI method yielding the more accurate results.

D. EMS DISCONNECTION PARAMETER DISTURBANCE TEST

In the previous section each disconnection method was tested during steady state conditions. Another important feature of each disconnection method is its transient performance during a grid voltage disturbance. To explore each method's transient response a disconnection parameter disturbance test was developed. This test was

conducted by simulating a voltage disturbance (fault setting) in the grid voltage and then observing the disconnection parameter transient response. Voltage disturbances of 1.19, termed “Rise” in the figures following, and 0.51, termed “Fall” in the figures following, were chosen because they represent the most extreme condition up to 0.01 volts per unit of a mandatory islanding condition that the microgrid would be required to respond to under normal operating conditions. It is important to note three key aspects of the transient response in the figures following: 1) The time it takes for the disconnection parameter to reach the disturbance value. 2) The oscillation of the disconnection parameter once it reaches the disturbance value. 3) Whether an immediate islanding condition would result from the transient or steady state response of the disconnection parameter. In the figures that follow a slight difference may be noted between the fault setting (disturbance value) and the disconnection parameter steady state value. This variation is caused by a combination of the simulation including a 0.4 Ohm resistor in series with the grid supply voltage source and the voltage being monitored at the PCC. The 0.4 Ohm resistor causes a small voltage drop, whose value depends on the magnitude of the grid current. Because the voltage input to the disconnection algorithms is the PCC voltage and not the grid voltage the disconnection parameter steady value in the figures is slightly lower than the fault setting. This however, would be an accurate representation of a real world microgrid design because IEEE Standard 1547-2018 requires the PCC voltage to be the voltage parameter used for islanding determination [8].

Each of the tests were simulated with the “Rise” and “Fall” disturbances occurring at 0.5 seconds and only the worst case scenario of harmonics in the grid voltage and a non-linear load were tested. Also, to ensure that the tests were conducted under the same conditions the FLL in the MSOGI method was bypassed and a constant value of $2\pi 60$ rad /sec was used in the simulation.

1. Peak Detection Method

Figure 56 shows the results of the disconnection parameter test using the peak detection method. It can be observed from Figure 56 that in both the rise and fall cases the disconnection parameter oscillates around the disturbance value so much that it would

cause an immediate islanding condition and not satisfy the required 0.2 second ride-through time shown in Table 2.

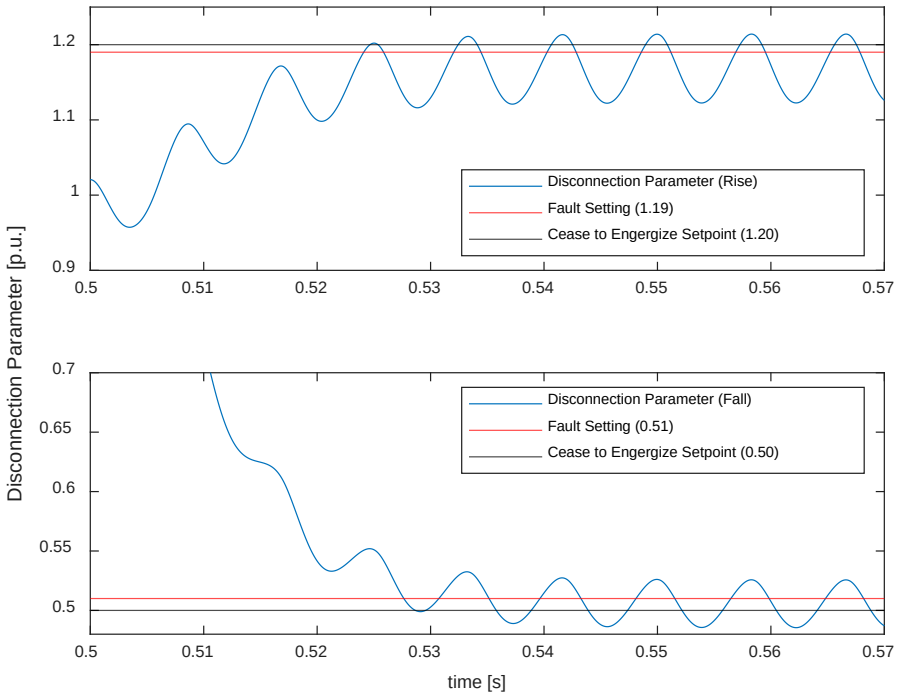

Figure 56. Disconnection Parameter Disturbance Test (Peak Detection Method)

2. DQ Method

Figure 57 shows the results of the disconnection parameter test using the dq method. It can be observed from Figure 57 that in both cases the disconnection parameter reaches the disturbance value after approximately 0.015 seconds and the transient does not result in an immediate islanding condition. To achieve this response, the gain value in the orthogonal signal generator SOGI block shown in Equation 8 and Equation 9 was adjusted to $\sqrt{2}/1.2$. In the voltage rise case the oscillations in the disconnection parameter caused the disconnection parameter to dip into the 1.15 to 1.175 per unit category shown in Table 2 which could result in a longer minimum ride-through time calculation.

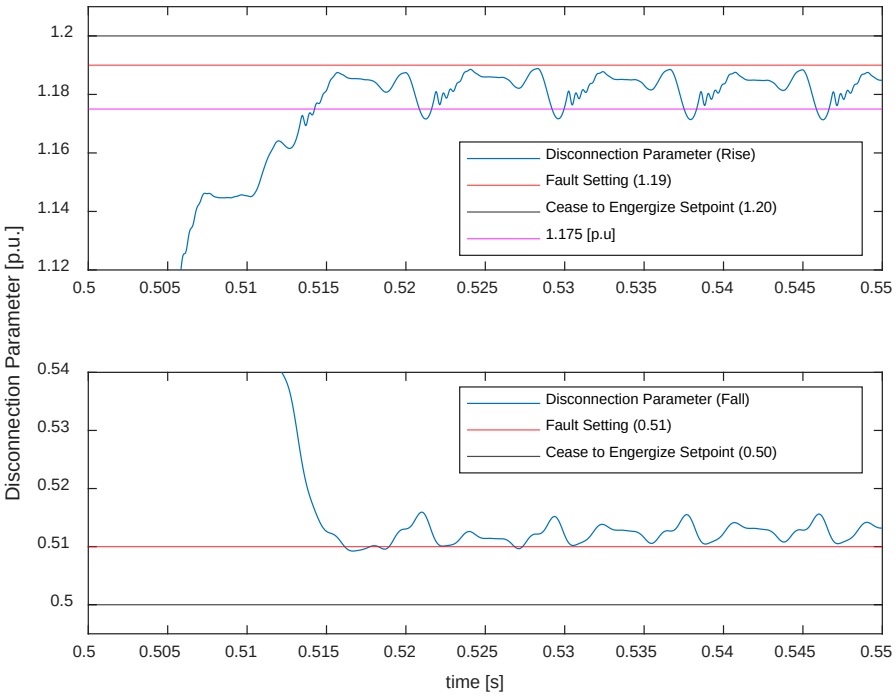

Figure 57. Disconnection Parameter Disturbance Test (dq Method)

3. SOGI Method

Figure 58 shows the results of the disconnection parameter test using the MSOGI method. To achieve this transient response, the gain value shown in Equation 7 and Equation 8 for each SOGI block was adjusted to $\sqrt{2}/1.45$. In each case the disconnection parameter reaches the disturbance value approximately 0.02 seconds after the fault occurs and an immediate islanding condition does not occur. The lower plot in Figure 58 shows that the steady state disconnection parameter value has almost no fluctuations even with harmonics in the source voltage and a non-linear load. The upper plot shows that the disconnection parameter oscillations have decreased when compared to the dq method but are still prevalent. In this scenario these oscillations have no effect on the system response regarding ride-through time requirements but if a different value of the voltage disturbance was chosen these oscillations may cause the system to not be in compliance with the IEEE Standard.

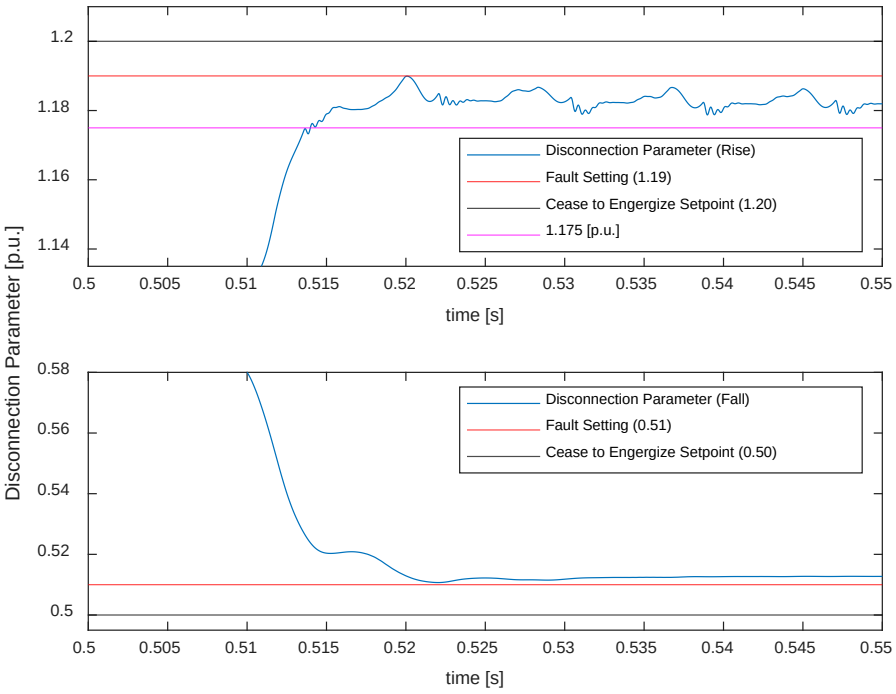

Figure 58. Disconnection Parameter Disturbance Test (MSOGI Method)

E. ADDITIONAL METHODS

To combat the fluctuations in the disconnection parameter shown during the disconnection parameter disturbance test, two additional methods were developed. The first was an extension of the MSOGI method described previously. This method, called the extended MSOGI method, added additional SOGI filters tuned at specific harmonic frequencies components that were generated by the non-linear load. The second was a true RMS application which was implemented using the RMS block in the Specialized Power Systems library in Simulink.

1. Extended MSOGI Method

a. Extended MSOGI Method Development

To implement the extended MSOGI method additional tuned SOGI filters were added to the original SOGI model developed for testing the SOGI method. The original

SOGI and HDN filter network used in the MSOGI method of this thesis included SOGI filters tuned at the experimentally determined grid harmonic values of the 5^{th}, 7^{th}, and 11^{th}. The addition of the single-phase diode bridge rectifier introduces additional harmonics to the voltage at the PCC which were not accounted for in the original MSOGI method. To determine which additional SOGI filters would be required an idealized diode rectifier circuit was used.

Figure 59 shows the idealized diode bridge rectifier circuit used to determine the SOGI filters required for the extended MSOGI method. The load (capacitor and resistor) shown in Figure 52 were replaced by a current source i_d. To determine the additional harmonics the Fourier analysis of i_s was performed and the fundamental and harmonic components were determined to have the following rms values in the idealized case shown in Figure 59. [16]

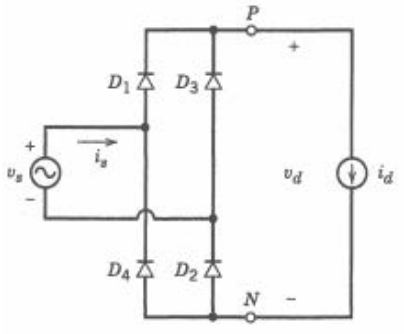

Figure 59. Idealized Diode Bridge Rectifier. Source: [16]

$$I_{s1} = \frac{2}{\pi}\sqrt{2}I_d \tag{13}$$

$$I_{sh} = \begin{cases} 0 & \text{for even values of h} \\ \frac{I_{s1}}{h} & \text{for odd values of h} \end{cases} \tag{14}$$

Equation 13 and Equation 14 show the values of the fundamental component and harmonic components normalized to the rms value of the fundamental frequency component [16].

Figure 60 shows the graphical representation of Equation 13 and Equation 14 with the associated magnitudes of the harmonic components normalized to the fundamental frequency magnitude. It can be observed from Figure 60 that the additional harmonic components of the 3rd, 9th, and 13th need to be accounted for once the non-linear load was added to the simulation. To account for these additional harmonics the topology of Figure 40 was used and the additional SOGI adaptive filters were added and tuned at the 3rd, 9th, and 13th harmonics.

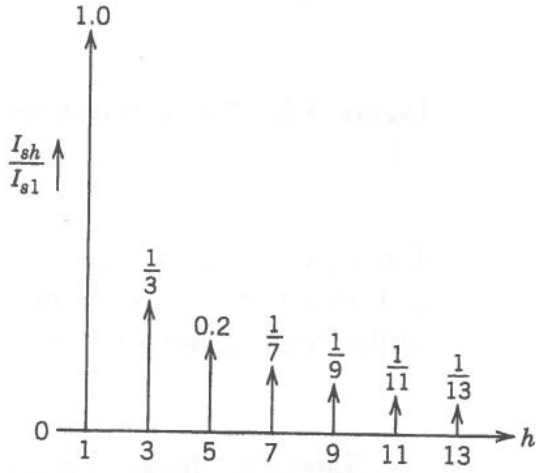

Figure 60. Harmonic Components of i_s. Source: [16]

b. Extended MSOGI Method Results

Figure 61 shows the results of the extended MSOGI method. The lower plot of Figure 61 displays the disconnection parameter zoomed in. It can be observed from this plot that the value of the pk-pk fluctuations, approximately 0.0015, in the steady state disconnection parameter are much smaller when compared to the previous MSOGI method shown in Figure 58. Of note, the gain value shown in Equation 7 and Equation 8 for each SOGI block was adjusted to $\sqrt{2}/2.8$ to achieve the best balance between speed and accuracy during the transient. This gain value minimized the overshoot of the disconnection parameter during the transient but at the same time increased the time it took for the disconnection parameter took to reach the disturbance value by approximately 0.02 seconds when compared to the MSOGI method shown in Figure 58. The "Fall" disturbance

was not shown here because the results were similar to the results shown in Figure 58 with only a slight difference between the disturbance value and the disconnection parameter value.

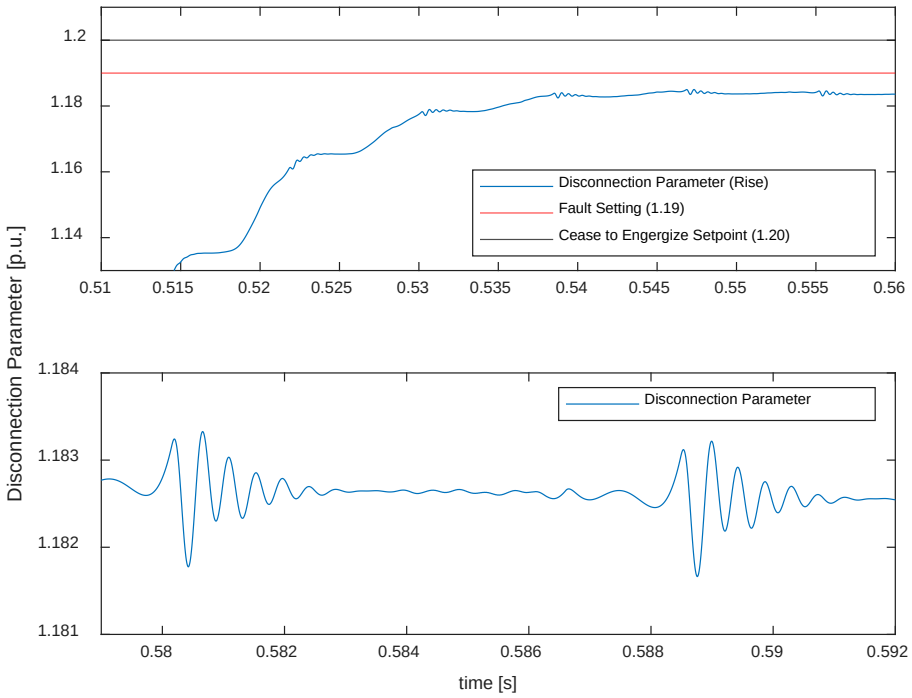

Figure 61. Disconnection Parameter Disturbance Test (Ext. MSOGI)

2. True RMS Method

The last disconnection method explored was the true RMS method using the Specialized Power Systems RMS block which calculates the true RMS value of the signal. Even with the harmonics in the grid voltage and a non-linear load, because the true RMS value is an average value it inertly filters out the fluctuations in the voltage value seen at the PCC.

Figure 62 shows the results of the true RMS method disconnection parameter disturbance test. It can be observed from Figure 62 that the steady-state disconnection parameter has no fluctuation and the transient time to reach the disturbance value is similar

to the time seen in the MSOGI method and dq method previously shown. However, a key difference is the overshoot that occurs in the “Rise” disturbance at approximately 0.02 seconds after the disturbance. This overshoot could cause an immediate islanding condition if the disturbance value was close enough to the immediate islanding set point in Table 2 and must be accounted for if implementing this method as a control technique.

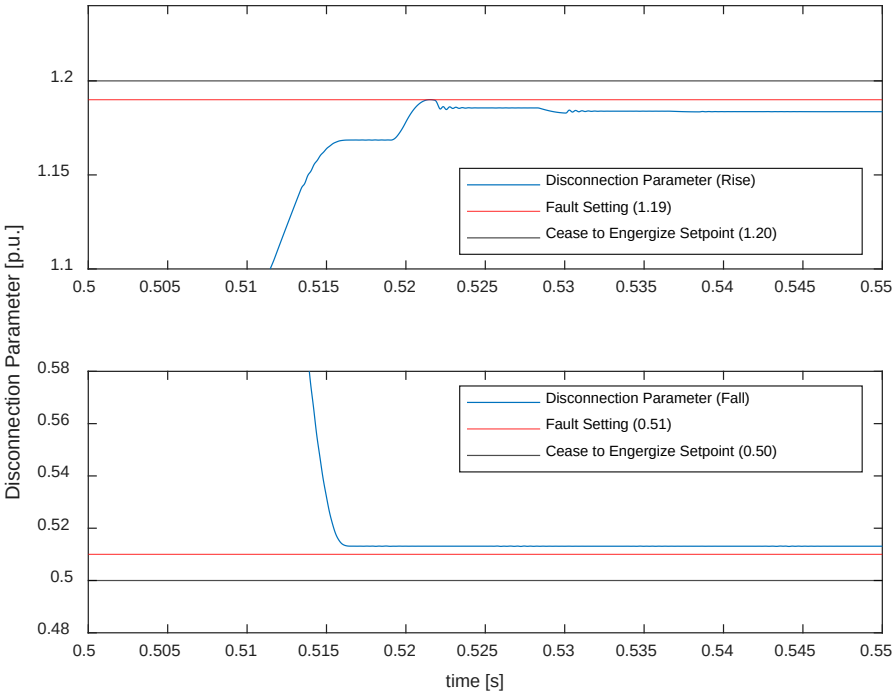

Figure 62. Disconnection Parameter Disturbance Test (True RMS)

Because of their performance in the disconnection parameter disturbance test the extended MSOGI method and true RMS method were chosen to be implemented in a simulation that would test their ability to adhere to IEEE Standard 1547-2018 voltage ride-through requirements. The key to adhering to the IEEE Standard is the accuracy of the control method and not necessarily the speed at which it reacts to disturbances in the grid voltage.

F. IEEE STANDARD 1547-2018 IMPLEMENTATION

The ultimate goal of this thesis was to find a viable option to be used as a control structure in a microgrid that would adhere to IEEE Standard 1547-2018 ride-through requirements. Ride-through is defined by IEEE Standard 1547-2018 as the "ability to withstand voltage or frequency disturbances inside defined limits and to continue operating as specified" [8]. Because diode rectifier circuits are becoming more prevalent in common electric devices a suitable control structure must be able to cope with the voltage fluctuations inherent in the grid voltage caused by these non-linear loads. To test the control structures used in these applications a Specialized Power Systems model was developed to facilitate testing different control topologies as well as a synchronization system for reconnection to grid. To implement this EMS model two major changes were made to the EMS model used in previous testing. These two changes are explained in the next section.

1. Changes to Simulation

a. IEEE 1547-2018 Standard Test Algorithm

Figure 63 shows the algorithm developed to test the IEEE Standard 1547-2018 voltage ride-through requirements shown in Table 2. The input to the algorithm is the normalized disconnection parameter calculated by the extended MSOGI and true RMS algorithms. In the comparator blocks the disconnection parameter is then compared to each of the values listed in Table 2 and a logical TRUE value is then generated at the output of the comparator blocks if the required condition exists. The On/Off Delay block shown in Figure 63 then stores this value for the time set by the user and then outputs the value if the value is still true after the time set by the user has expired [19]. In this application each of the On/Off Delay blocks were set to the required ride-through times per Table 2. The Set-Reset Flip-Flop block was used to store the correct value until the trip signal was required. If the algorithm determined that a disturbance in the grid voltage required an islanding condition of the microgrid, in accordance with Table 2, the trip signal was fed into the IGBT control selector, labeled "Control Input" in Figure 21, to switch the control mode of the inverter from current injection to voltage control and also into the grid feeder breaker control shown in Figure 22 to isolate the inverter from the grid. The top two On/

Off Delay blocks were added and set to 0.05 seconds to help prevent erroneous immediate islanding conditions by requiring the immediate islanding condition to exist for more than 0.05 seconds before actuating a trip signal.

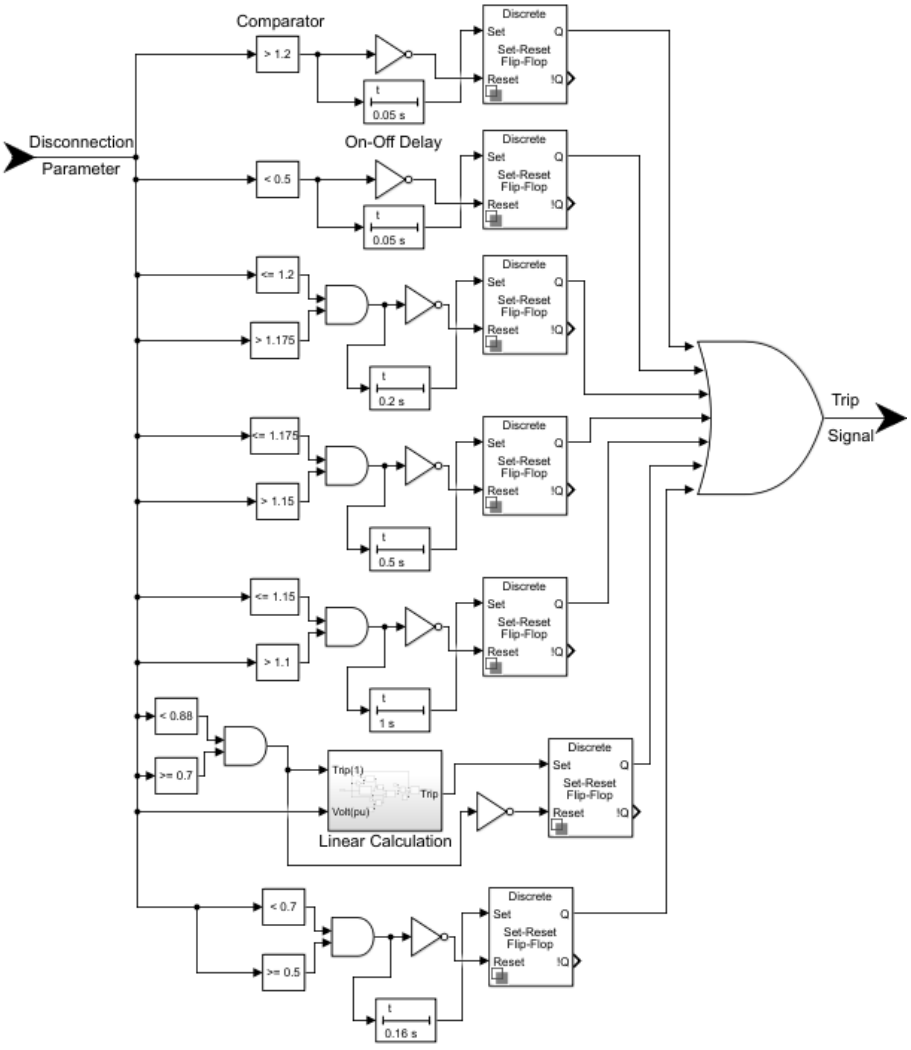

Figure 63. Simulink Standard Implementation Algorithm

Equation 15 shows the linear calculation from Table 2 to calculate the required voltage ride-through time in the voltage range from $0.70 \leq V < 0.88$ where "T_{VRT}" is the Total Voltage Ride Through Time and "V" is the disconnection parameter [8].

Figure 64 shows the details of the linear calculation algorithm used to develop the trip signal for the values between 0.70 and 0.88 shown in Table 2. In this range of values, a linear calculation of ride-through time had to be completed to comply with the standard. To comply with IEEE Standard 1547-2018, the linear calculation algorithm must accommodate two conditions:

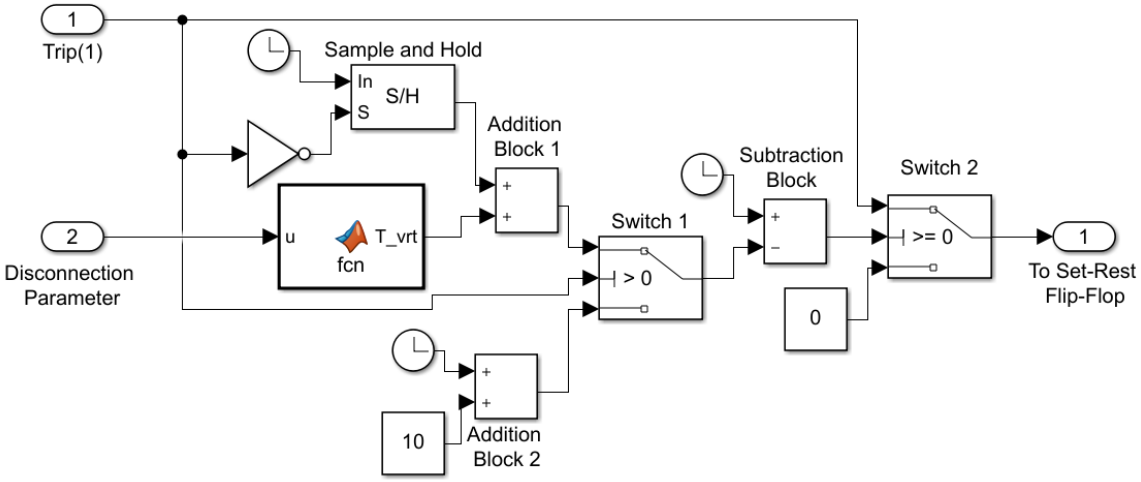

Figure 64. Linear Calculation Algorithm

$$T_{VRT} = 0.7s + \frac{4s}{1p.u.}(V - 0.7\,p.u.) \tag{15}$$

1) The disconnection parameter is not in the 0.70 to 0.88 voltage range. In this case the linear calculation block must not generate a trip signal.

2) The disconnection parameter is in the 0.70 to 0.88 voltage range. In this case the linear calculation block must generate a trip signal and wait the required ride-through time that results from the calculation shown by Equation 15 and if the disconnection parameter is still in the 0.70 to 0.88 voltage range the linear calculation algorithm must output a trip signal. If the disconnection parameter is no longer in the voltage range after the required ride-through time has surpassed the trip signal must not be generated, i.e., the grid voltage has been restored.

The two conditions are explained as follows:

Condition 1) In Figure 64 the “Trip(1)” signal is the output of the comparator blocks in the range of 0.70 to 0.88 shown in Figure 63. If this signal is a logical 0, i.e., the disconnection parameter is not in the 0.70 to 0.88 range “Switch 1” will pass the (clock value + 10) from “addition block 2” to the “subtraction block” which will subtract the “clock” value resulting in a value of negative 10 being fed into “Switch 2.” “Switch 2” will then pass a (logical 0) to the “Set-Reset Flip-Flop” which will maintain the trip signal input to the OR gate shown in Figure 63 a logical 0.

Condition 2) In Figure 64 the “Trip(1)” signal is a logical 1, i.e., the disconnection parameter value is in the 0.70 to 0.88 range. In this case the logical 1 from the comparator blocks shown in Figure 63 is passed to the “sample and hold block” through a NOT gate. The “sample and hold block” holds the “clock” value corresponding to the time the disconnection parameter entered the 0.70 to 0.88 voltage range. This value is then added to the ride-through time calculated by Equation 15 in “addition block 1.” This output of “addition block 1” is then passed by “switch 1” to the “subtraction block” which then subtracts this value from the current “clock” value. The output of the “subtraction block” will remain negative and will pass a logical zero until the ride-through time calculated by Equation 15 is met; at which point the output of the “subtraction block” is greater than zero and “switch 2” passes the logical 1 from the “Trip(1)” signal. This then causes a logical 1 to be fed to the “Set-Reset Flip-Flop” which transmits this value to the OR gate in Figure 63, ultimately generating a trip signal. If the disconnection parameter departs from the 0.70 to 0.88 voltage range during this process the “Trip(1)” signal will revert to a logical 0 and the situation described in condition 1 will occur and no trip signal will be generated.

b. Synchronization Topology

To fully complete the model a grid synchronization method was implemented.

Figure 65 shows the grid synchronization method algorithm. To synchronize the grid voltage with the PCC voltage the RMS value of the difference between the two voltage values is fed into a PID controller where $K_P = 0.2$, $K_I = 0$, and $K_D = 0$. The output of the PID controller is fed into a saturation block to limit the value of the H-bridge inverter control voltage frequency to no less than 59 Hz to ensure the synchronization algorithm

does not violate IEEE Standard 1547-2018 frequency standards. The output of the saturation block then adjusts the input frequency parameter of the H-bridge inverter $v_{control}$ signal and therefore adjusts the frequency of the output voltage of the H-bridge inverter. With the frequency of the inverter voltage (PCC voltage) (59 Hz) lower than the frequency of the grid voltage (60 Hz) the phase angle of the two voltages will ultimately synchronize with one another. The amount it takes for the synchronization to occur will depend on the phase difference between the two voltages at the onset of the synchronization process.

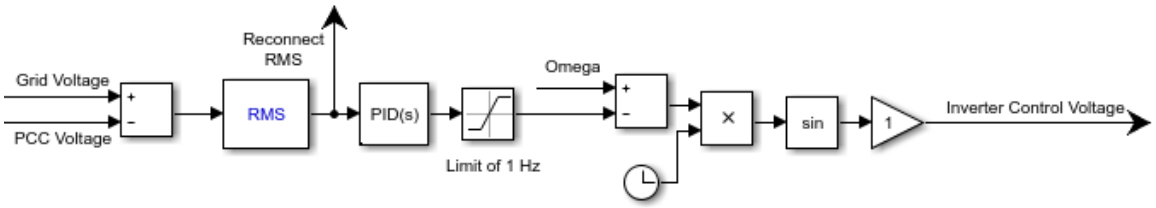

Figure 65. RMS Synchronization Control Algorithm

To reconnect the inverter to the AC grid two conditions must exist: 1) the RMS value of the restored grid voltage must be greater than 108 Volts or greater than 0.9 (p.u.). This value was chosen because it falls in the voltage range per Table 2 that requires continuous operation but also provides 0.02 (p.u.) tolerance for error to reach the next voltage range of 0.70 to 0.88. 2) The RMS value of the error between the grid voltage and PCC voltage, shown as “Reconnect RMS” in Figure 65 and Figure 66 must be less than 15 Volts. This value can be adjusted depending on the tolerance of phase difference between the grid voltage and PCC voltage required for reconnection to the grid. Once the two reconnection conditions are met the EMS reconnects to the grid and disconnects from the H-bridge inverter.

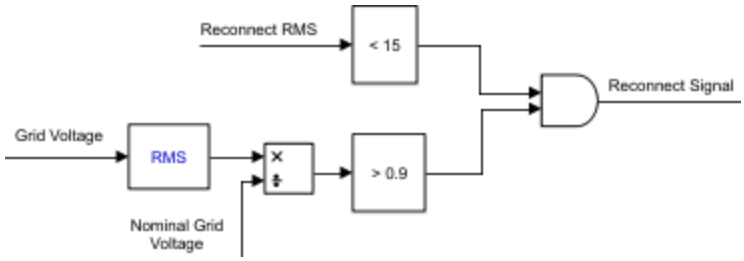

Figure 66. Grid Reconnection Algorithm

2. Simulation Results

The following simulations were run with the grid voltage initially at a nominal value of 120 Volts RMS, frequency of 60 Hz, and phase angle zero. The disturbance or fault occurs at 0.5 seconds in the simulation and mimics a voltage dip to approximately 0.6 (p.u.) of the nominal value. This disturbance value was chosen because it facilitated easier display of the data in this thesis but the disturbance could be set to any value shown in Table 2. After the voltage disturbance occurs and the appropriate ride-through time is allowed to pass, the grid voltage is restored to its nominal value of 120 Volts RMS, frequency of 60 Hz, and a phase angle of 180 degrees. Once the grid voltage is restored the synchronization and reconnection is initiated in the simulation and the reconnection occurs automatically once the conditions shown in Figure 66 have been met. These simulations were run with the worst case conditions, harmonics in the grid voltage and a non-linear load (diode rectifier circuit).

a. Extended SOGI Method

Figure 67 shows the load voltage during simulation. It can be observed from Figure 67 a grid voltage disturbance of 0.6 p.u. at 0.5 seconds and the load voltage decrease to approximately 0.6 volts of it nominal value. However, the standard implementation algorithm shown in Figure 63 does not allow the EMS to island itself from the grid until after the ride-through time, approximately 0.16 seconds, required by IEEE Standard 1547-2018 has been met.

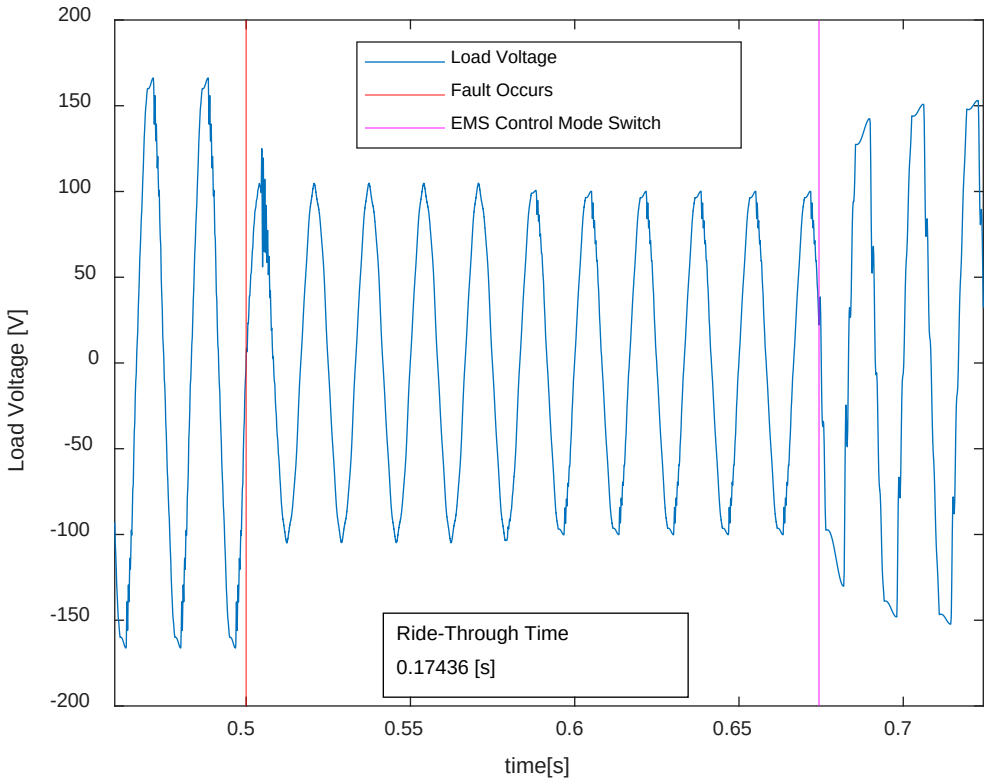

Figure 67. Load Voltage Ride-Through Time (Ext SOGI Method)

In Figure 67 the ride-through time was calculated to be 0.17436 seconds while Figure 63 shows the On/Off Delay block set to 0.16 seconds. Figure 68 shows the disconnection parameter during the transient and also shows the voltage range (p.u.) from Table 2 of the disturbance value (0.5 to 0.7 $V_{p.u.}$). The Ride-Through Difference calculation shows the amount of time required for the disconnection parameter to reach the voltage range of 0.50 to 0.70 (p.u.) after the disturbance occurs. The combination of the Ride-Through Time and Ride-Through Difference values were used to ensure that the standard implementation algorithm was working correctly. For verification purposes, 0.17436 – 0.014 = 0.16036 seconds which is approximately equal to 0.16 seconds, the setting of the On/Off delay and the appropriate ride-through time for the 0.50 to 0.70 voltage range required by Table 2.

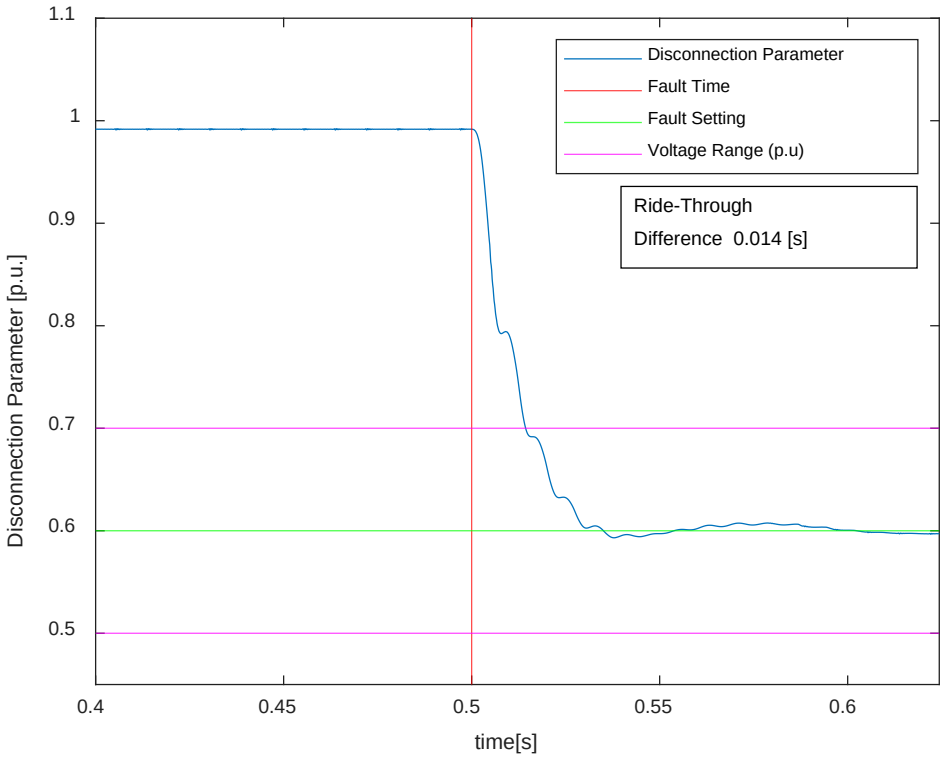

Figure 68. Disconnection Parameter (Ext SOGI Method)

Figure 69 shows the initialization of the synchronization of the grid to the PCC voltage with the grid voltage 180 degrees out of phase with respect to the PCC voltage. It can be observed from Figure 69 that the synchronization algorithm pictured in Figure 65 drives the difference between the phase voltage of the PCC and the grid voltage to zero by lowering the frequency of the H-bridge inverter to 59 Hz until the connection occurs. Figure 69 also shows virtually no transient in the load voltage during initialization and reconnection.

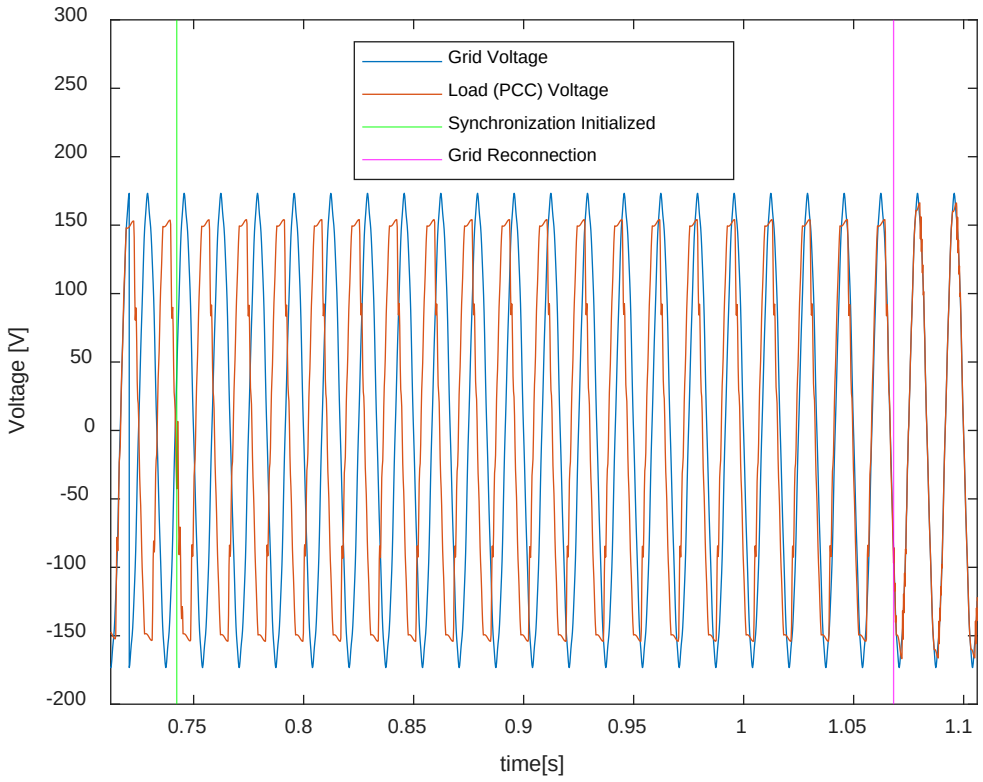

Figure 69. Voltage Comparison [Reconnect] (Ext SOGI Method)

Figure 70 shows the load current transient during the synchronization and reconnection with the grid. It can be observed from Figure 70 that a transient of approximately 20 Amps occurs during the reconnection to the grid. This transient at reconnection occurs only because of the difference in magnitude between the PCC voltage and grid voltage caused by the non-linear load shown in Figure 69.

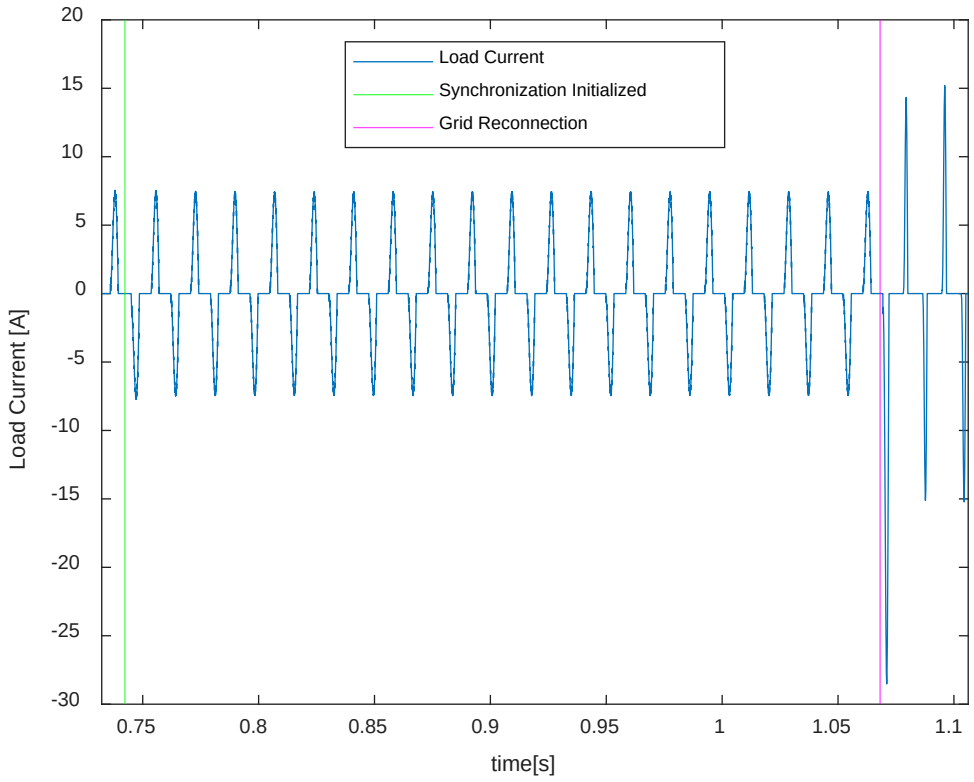

Figure 70. Load Current [Reconnect] (Ext SOGI Method)

For comparison purposes Figure 71 shows the same simulation presented in Figure 70 but with a linear load replacing the non-linear load. It can be observed that due to the frequency adjustment to 59 Hz of the H-bridge inverter (PCC) voltage a small transient occurs during the onset of synchronization and virtually no transient occurs when the grid is reconnected to the PCC.

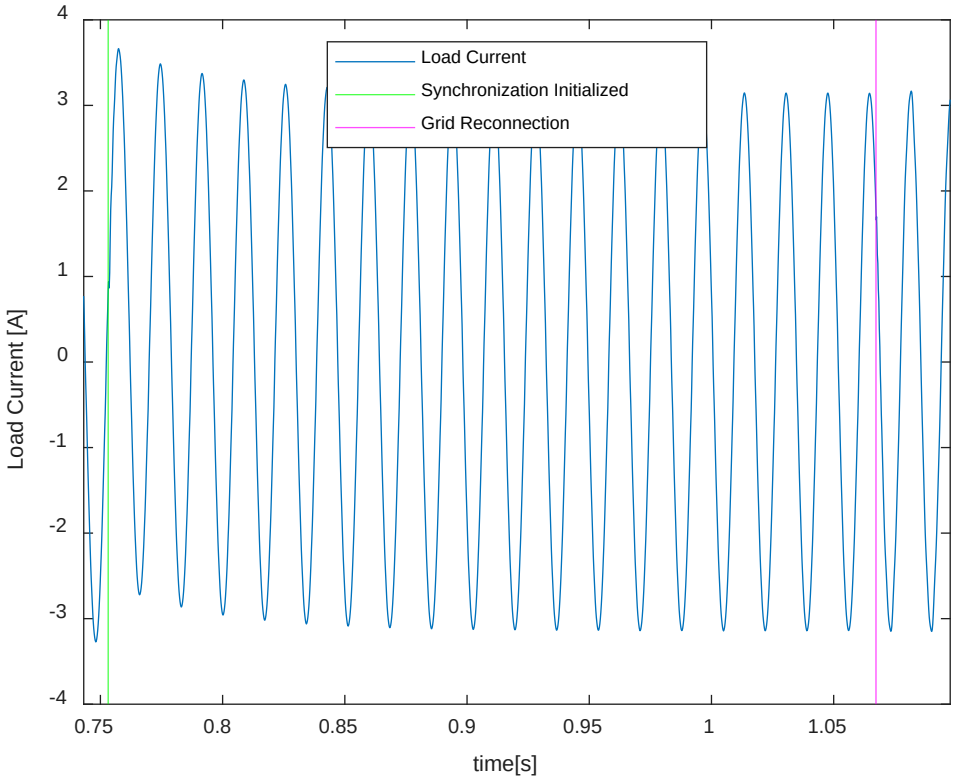

Figure 71. Load Current-Linear Load [Reconnect] (Ext SOGI Method)

Figure 72 shows the load voltage at the PCC with the associated ride-through time and Figure 73 shows the disconnection parameter during the transient for the true RMS method. With only a slight decrease in the Ride-Through Difference calculation in the true RMS simulation, the results of this test are very similar to the results of the extended SOGI method test.

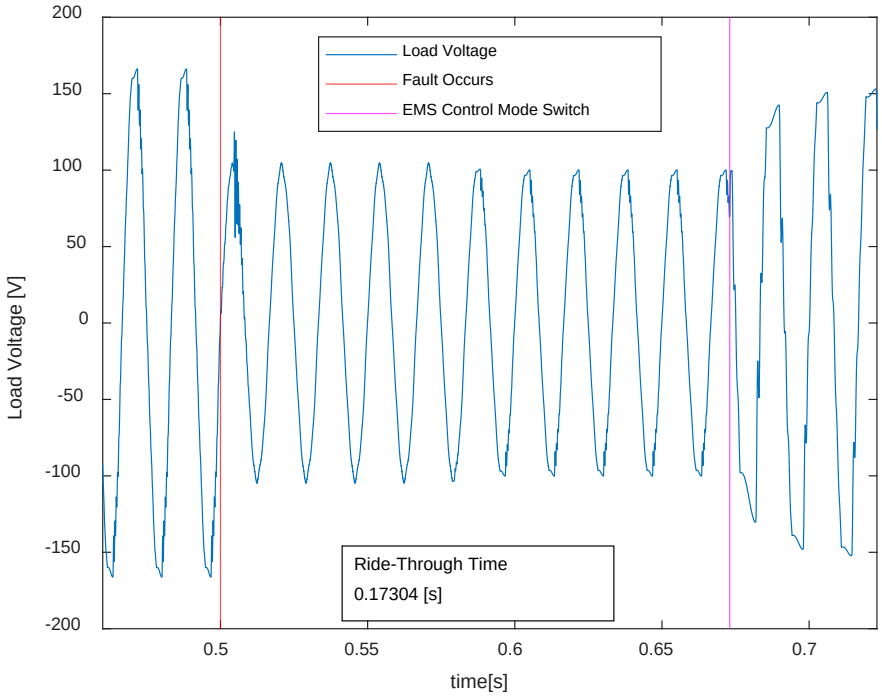

Figure 72. Load Voltage Ride-Through Time (True RMS Method)

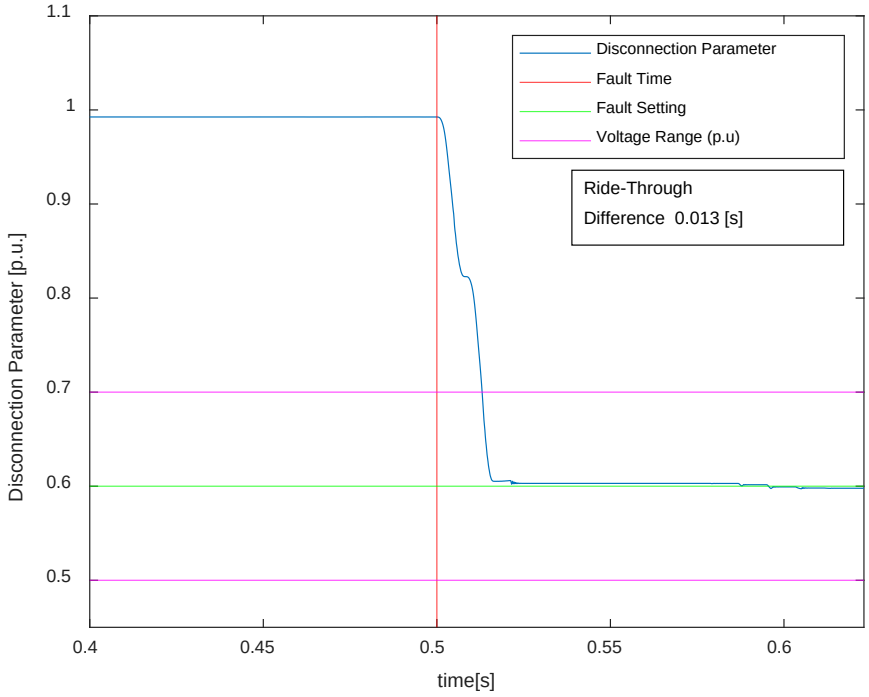

Figure 73. Disconnection Parameter (True RMS Method)

Both of these methods are shown to be viable options for implementation of IEEE Standard 1547-2018. The grid synchronization and reconnect method is shown to be efficient and accurate even under highly distorted conditions. Two key differences between these methods are worth noting. One, the true RMS method performs just as well as the extended MSOGI method but with far less calculations. Two, the extended MSOGI method provides almost instantaneous values of PCC voltage to the user while the true RMS method has an inherent 0.01667 seconds delay at 60 Hz. Depending on the requirements of the user one method may be more suitable than the other.

VII. CONCLUSIONS AND FUTURE WORK

A. CONCLUSIONS

This thesis had four main goals.

1. Develop a working model of the H-bridge inverter and EMS maintained in the laboratory at the Naval Postgraduate School.

2. Verify the model for testing and future work.

3. Use the model to test different disconnection control algorithms for speed and accuracy.

4. Perform a comparison of the different control strategies and the voltage ride-through times required by IEEE Standard 1547-2018.

Each of these goals were accomplished upon completion of this thesis. The key points to note from the research conducted in this thesis are as follows.

1. IEEE Standard 1547-2018 voltage ride-through requirements are not easily implemented. The standard is written such that there is no tolerance between the voltage categories listed in Table 2. This makes it very difficult to adhere to the standard when the voltage being measured is highly distorted by non-linear loads.

2. Non-linear loads have a negative effect on the operation of the control structures tested in this thesis. These non-linear loads are becoming more prevalent in household electronics and commercial industry. An example of this can be seen by comparing Figure 70 and Figure 71. The difference in the current spike between these two figures is caused simply by the addition of the non-linear load. This can also be seen when comparing the disconnection parameter values of the MSOGI method and the extended MSOGI method shown in Figure 58 and Figure 61 respectively. The introduction of the non-linear load required the addition of three tuned SOGI filters to smooth out the disconnection parameter in the extended MSOGI method.

3. Speed is not the ultimate goal. There must be a balance between speed and accuracy of the disconnection control topology being utilized. Ultimately, as shown in the Standard Implementation section the two control structures implemented in simulation were chosen for their accuracy following a transient and not the speed at which they reached the disturbance value. To continue this point, if a fault did occur that required an immediate islanding condition (0.50 or 1.20 p.u.) in accordance with Table 2 the minimum response time is 0.16 seconds which is approximately equal to 10 cycles of a 60 Hz signal.

4. Ultimately, the best control strategy is one that balances simplicity of implementation and the ability to meet the requirements of the user. For all the control strategies tested the true RMS method is the simplest to implement and allows adherence to IEEE Standard 1547-2018. Even though the true RMS method contains an inherent delay this thesis has shown that this has no negative repercussions on the effectiveness of this control method and therefore, the true RMS method is the best method to implement as an EMS disconnection control strategy.

B. FUTURE WORK

While the initial model for this thesis was verified using laboratory data the time was not allotted to further test each of the Standard Implementation models in the laboratory. Laboratory experiments could be set up to test these methods in actual hardware.

Only five control methods were tested in this thesis. The models developed for this thesis can be easily adapted for other control structures to facilitate further testing of different EMS islanding and grid synchronization methods.

IEEE Standard 1547-2018 also contains requirements for frequency ride-through which were not implemented in this thesis. The models built for this thesis could easily be adapted to include frequency ride through requirements for testing different control topologies.

APPENDIX. MATLAB CODE

```
close all

omega = 2*pi*60;
k = sqrt(2);
a = k*omega;
b = omega^2;
c = k*omega^2;

% Q(s)
num1 = [c];
dem1 = [1 a b];
H1 = tf(num1,dem1);

% E(s)
num = [1 0 b];
dem = [1 a b];
H = tf(num,dem);

opts = bodeoptions;
opts.Title.String = ''
bodeplot(H,H1,opts);
legend('qv''',[char(949),'v'],'location','northwest')

grid on
```

```
close all

omega = 2*pi*60;
k = sqrt(2)/2.8;
a = k*omega;
b = omega^2;
c = k*omega^2;

% D(s)
num = [a 0];
dem = [1 a b];
H = tf(num,dem);

% Q(s)
num1 = [c];
dem1 = [1 a b];
H1 = tf(num1,dem1);

opts = bodeoptions;
opts.Title.String = ''
```

```
bodeplot(H,H1,opts);
grid on
legend('D(s)','Q(s)')
```

```
close all

%Paramters to plot minimum or maximum peak voltage
X = controlSwitch_RMS_voltageFlux(end); %Defines when EMS switches control modes
Y = find(tout == fault_time); %Defines first index in tout to look at for voltage
Z = find(tout == X); %Defines index in tout for last value to look at for voltage

%Calculates min voltage reached after fault
A_RMS = abs(voltage_RMS_voltageFlux(Y:length(tout)));
B_RMS = findpeaks(A_RMS,'MinPeakDistance',8000);
min_VoltageFlux_RMS = min(B_RMS);

%Calculates max voltage reached

max_VoltageFlux_RMS = max(abs(voltage_RMS_voltageFlux(Y:length(tout))));

%Calculates max Load current reached

max_Load_CurrentFlux_RMS = max(abs(load_current_RMS_voltageFlux(Y:length(tout))));

%Calculates max EMS current reached

max_EMS_CurrentFlux_RMS = max(abs(ems_current_rms_voltageFlux(Y:length(tout))));

%Calculating Response time
responseTime_RMS_voltageFlux = (controlSwitch_RMS_voltageFlux(end))-fault_time;
responseTime_RMS_voltageFlux = round(responseTime_RMS_voltageFlux,4);

%plotting Connection Status and Response time
figure(1)
plot(tout,connection_RMS_voltageFlux)
xlim([0.495,0.55])
ylim([-0.1,1.1])
%title('RMS Connection Status')
xlabel('time [s]')
ylabel('Connection Status')

dim = [.707 .5 .3 .3];
str = '1 = Grid Connected';
annotation('textbox',dim,'String',str,'FitBoxToText','on');

dim = [.74 .42 .3 .3];
str = '0 = Island Mode';
annotation('textbox',dim,'String',str,'FitBoxToText','on');

dim = [.63 .34 .272 .3];
```

```
annotation('textbox',dim,'String',['Clearing Time = '
num2str(responseTime_RMS_voltageFlux) ' [s]'],'FitBoxToText','on');

hold on
xline(fault_time,'r');
legend('Connection Status','Fault Begins','Location','northeast')

ax = gca;
outerpos = ax.OuterPosition;
position = ax.Position;
ti = ax.TightInset;
left = position(1);
bottom = position(2);
ax_width = outerpos(3)-0.155;
ax_height = position(4);
ax.Position = [left bottom ax_width ax_height];
ax.OuterPosition;

%plotting Load Voltage
figure(2)
plot(tout,voltage_RMS_voltageFlux)
xlim([0.4,0.6])
ylim([-260,275])
%title('Load Voltage - RMS Model')
xlabel('time [s]')
ylabel('Load Voltage [V]')
hold on
xline(fault_time,'r');
xline(controlSwitch_RMS_voltageFlux(end),'g');
legend('Load Voltage','Fault Begins','EMS Mode Switch','Location','northwest')
%text box for minimum voltage reached
dim = [.135 .12 .274 .1];
annotation('textbox',dim,'String',['Min Voltage After Fault '
num2str(min_VoltageFlux_RMS) ' [V]']);

ax = gca;
outerpos = ax.OuterPosition;
position = ax.Position;
ti = ax.TightInset;
left = position(1);
bottom = position(2);
ax_width = outerpos(3)-0.155;
ax_height = position(4);
ax.Position = [left bottom ax_width ax_height];
ax.OuterPosition;

%plotting Load Current
figure(3)
plot(tout,load_current_RMS_voltageFlux)
%title('Load Current - RMS Model')
xlim([0.4,0.6])
ylim([-5,5.5])
```

```
xlabel('time [s]')
ylabel('Load Current [A]')
hold on
xline(fault_time,'r');
xline(controlSwitch_RMS_voltageFlux(end),'g');
legend('Load Current','Fault Begins','EMS Mode Switch','Location','northwest')
%textbox for max current reached
dim = [.135 .12 .3 .1];
annotation('textbox',dim,'String',['Max Current After Fault '
num2str(max_Load_CurrentFlux_RMS) ' [A]']);

ax = gca;
outerpos = ax.OuterPosition;
position = ax.Position;
ti = ax.TightInset;
left = position(1);
bottom = position(2);
ax_width = outerpos(3)-0.155;
ax_height = position(4);
ax.Position = [left bottom ax_width ax_height];
ax.OuterPosition;

%plotting EMS Current
figure(4)
plot(tout,ems_current_rms_voltageFlux)
%title('EMS Current - RMS Model')
xlim([0.4,0.6])
xlabel('time [s]')
ylabel('EMS Current [A]')
hold on
xline(fault_time,'r');
xline(controlSwitch_RMS_voltageFlux(end),'g');
legend('EMS Current','Fault Begins','EMS Mode Switch','Location','northwest')
%textbox for max current reached
dim = [.135 .12 .274 .1];
annotation('textbox',dim,'String',['Max Current After Fault '
num2str(max_EMS_CurrentFlux_RMS) ' [A]']);

ax = gca;
outerpos = ax.OuterPosition;
position = ax.Position;
ti = ax.TightInset;
left = position(1);
bottom = position(2);
ax_width = outerpos(3)-0.155;
ax_height = position(4);
ax.Position = [left bottom ax_width ax_height];
ax.OuterPosition;

%plotting Calculated RMS Voltage
figure(5)
plot(tout,rms_voltage_voltageFlux)
```

```
xline(fault_time,'r');
%title('Calculated RMS Voltage - RMS Model')
xlabel('time [s]')
ylabel('RMS Voltage [V]')
xlim([0.4,0.6])
ylim([55,135])
%yline(upperthreshold_RMS,'r');
yline(lowerthreshold_RMS,'m');
legend('RMS Calulated','Fault Begins','lowerthreshold')

ax = gca;
outerpos = ax.OuterPosition;
position = ax.Position;
ti = ax.TightInset;
left = position(1);
bottom = position(2);
ax_width = outerpos(3)-0.155;
ax_height = position(4);
ax.Position = [left bottom ax_width ax_height];
ax.OuterPosition;

%plotting RMS value from RMS block
figure(6)
plot(tout,voltage_RMS_voltageFlux_RMSvalue)
xlim([0.4,0.6])
ylim([50,135])
xlabel('time [s]')
ylabel('RMS Simscape Value [V]')
xline(fault_time,'r');
xline(controlSwitch_RMS_voltageFlux(end),'g');
legend('RMS Simscape Calulated','Fault Begins','EMS Mode Switch','location','best')
min_VoltageFlux_RMS_block = min(voltage_RMS_voltageFlux_RMSvalue(Y:length(tout)));
%textbox for min RMS reached
dim = [.135 .12 .31 .1];
annotation('textbox',dim,'String',['Min RMS Value After Fault '
num2str(min_VoltageFlux_RMS_block) ' [V]']);


ax = gca;
outerpos = ax.OuterPosition;
position = ax.Position;
ti = ax.TightInset;
left = position(1);
bottom = position(2);
ax_width = outerpos(3)-0.155;
ax_height = position(4);
ax.Position = [left bottom ax_width ax_height];
ax.OuterPosition;
```

```
close all

t1 = 0.34;
t2 = 0.38;
%plotting Calculated RMS Voltage
figure(1)

subplot(3,1,1)
plot(tout,rms_disconnection_baseline_p_u)
xlim([t1,t2])
ylim([0.94,1.08])
t1 = 0.34;
t2 = 0.38;
t_I = find(tout >= t1 & tout <= t2);
flux_rms_baseline = max(rms_disconnection_baseline_p_u(t_I)) -
min(rms_disconnection_baseline_p_u(t_I));

legend('No Harmonics / Linear Load')
dim = [.143 .61 .3 .3];
annotation('textbox',dim,'String',['pk-pk = '
num2str(flux_rms_baseline)],'FitBoxToText','on');


subplot(3,1,2)
plot(tout,rms_disconnection_harmonics_p_u,'r')
xlim([t1,t2])
ylim([0.94,1.08])
flux_rms_harmonics = max(rms_disconnection_harmonics_p_u(t_I))-
min(rms_disconnection_harmonics_p_u(t_I));

legend('Harmonics / Linear Load')
dim = [.143 .31 .3 .3];
annotation('textbox',dim,'String',['pk-pk = '
num2str(flux_rms_harmonics)],'FitBoxToText','on');

subplot(3,1,3)
plot(tout,rms_disconnection_nonLinear_p_u,'m')
xlim([t1,t2])
ylim([0.94,1.08])
xlabel('time [s]')
flux_rms_nonLinear = max(rms_disconnection_nonLinear_p_u(t_I))-
min(rms_disconnection_nonLinear_p_u(t_I));

legend('Harmonics / Non Linear Load')
dim = [.143 .014 .3 .3];
annotation('textbox',dim,'String',['pk-pk = '
num2str(flux_rms_nonLinear)],'FitBoxToText','on');

h1=subplot(3,1,1);
h2=subplot(3,1,2);
h3=subplot(3,1,3);
```

```
p1=get(h1,'position');
p2=get(h2,'position');
p3=get(h3,'position');
height=(p1(2)+p1(4))/3 - 0.1;
h3=axes('position',[p2(1)-0.03 p2(2) p2(3) height],'visible','off');
h_label=ylabel('Disconnection Parameter [p.u.]','visible','on');
```

```
close all

%plotting load voltage for ride-through
ride_through_trueRMS = controlSwitch_trueRMS_standardImp(end) - fault_time;
figure(1)
plot(tout,voltage_trueRMS_voltageFlux)
hold on
xline(fault_time,'r');
xline(controlSwitch_trueRMS_standardImp(end),'m');
xlim([0.46,(controlSwitch_trueRMS_standardImp(end)+0.05)])
xlabel('time [s]')
ylabel('PCC Voltage [V]')
legend('PCC Voltage','Fault Occurs','Inverter Control Mode Switch','location','north')
dim = [.37 .12 .272 .1];
annotation('textbox',dim,'String',['Ride-Through Time ' num2str(ride_through_trueRMS) '
[s]']);

%plotting disconnection parameter

%find difference between ride-through and time to range
a = find(trueRMS_disconnection <= 0.7);
b = a(1);
c = tout(b);
d = round(c - fault_time, 3);

%plot
figure(2)
plot(tout,trueRMS_disconnection)
xlabel('time [s]')
ylabel('Disconnection Parameter [p.u.]')
xline(fault_time,'r');
yline(0.6,'g');
yline(0.7,'m');
yline(0.50,'m');
xlim([(fault_time-0.1),(controlSwitch_trueRMS_standardImp(end)-0.05)])
ylim([0.45,1.1])
legend('Disconnection Parameter','Fault Time','Fault Setting','Voltage Range (p.u)')
dim = [.613 .62 .272 .1];
annotation('textbox',dim,'String',['Ride-Through Difference ' num2str(d) ' [s]']);

%plotting voltage comparison for reconnection
figure(3)
plot(tout,grid_Voltage)
```

```
hold on
plot(tout,voltage_trueRMS_voltageFlux)
xline(reconnect_initiate_trueRMS_standardImp(end),'g');
xline(reconnect_trueRMS_standardImp(end),'m');
xlabel('time [s]')
ylabel('Voltage [V]')
xlim([(reconnect_initiate_trueRMS_standardImp(end)-0.03), inf])
ylim([-200,300])
legend('Grid Voltage','Load (PCC) Voltage','Synchronization Initialized','Grid
Reconnection','location','north')

%plotting load current
figure(4)
plot(tout,load_current_trueRMS_voltageFlux)
xlabel('time [s]')
ylabel('Load Current [A]')
xlim([(reconnect_initiate_trueRMS_standardImp(end)-0.01), inf])
xline(reconnect_initiate_trueRMS_standardImp(end),'g');
xline(reconnect_trueRMS_standardImp(end),'m');
legend('Load Current','Synchronization Initialized','Grid
Reconnection','location','north')
```

```
close all

%plotting load voltage for ride-through
ride_through_extendedSOGI = controlSwitch_extendedSOGI_standardImp(end) - fault_time;
figure(1)
plot(tout,voltage_extendedSOGI_voltageFlux)
hold on
xline(fault_time,'r');
xline(controlSwitch_extendedSOGI_standardImp(end),'m');
xlim([0.46,(controlSwitch_extendedSOGI_standardImp(end)+0.05)])
xlabel('time [s]')
ylabel('Load Voltage [V]')
legend('Load Voltage','Fault Occurs','EMS Control Mode Switch','location','north')
dim = [.37 .12 .272 .1];
annotation('textbox',dim,'String',['Ride-Through Time '
num2str(ride_through_extendedSOGI) ' [s]']);

%plotting disconnection parameter

%find difference between ride-through and time to range
a1 = find(tout > 0.3);
a = find(estimated_voltage_extendedSOGI_p_u(a1) <= 0.7);
b = a(1);
c = tout(b+(length(tout)-length(a1)));
d = round(c - fault_time, 3);


%plot
```

```
figure(2)
plot(tout,estimated_voltage_extendedSOGI_p_u)
xlabel('time [s]')
ylabel('Disconnection Parameter [p.u.]')
xline(fault_time,'r');
yline(0.6,'g');
yline(0.7,'m');
yline(0.50,'m');
xlim([(fault_time-0.1),(controlSwitch_extendedSOGI_standardImp(end)-0.05)])
ylim([0.45,1.1])
legend('Disconnection Parameter','Fault Time','Fault Setting','Voltage Range (p.u)')
dim = [.613 .62 .272 .1];
annotation('textbox',dim,'String',['Ride-Through Difference ' num2str(d) ' [s]']);

%plotting voltage comparison for reconnection
figure(3)
plot(tout,grid_Voltage)
hold on
plot(tout,voltage_extendedSOGI_voltageFlux)
xline(reconnect_initiate_extendedSOGI_standardImp(end),'g');
xline(reconnect_extendedSOGI_standardImp(end),'m');
xlabel('time [s]')
ylabel('Voltage [V]')
xlim([(reconnect_initiate_extendedSOGI_standardImp(end)-0.03), inf])
ylim([-200,300])
legend('Grid Voltage','Load (PCC) Voltage','Synchronization Initialized','Grid
Reconnection','location','north')

%plotting load current
figure(4)
plot(tout,load_current_extendedSOGI_voltageFlux)
xlabel('time [s]')
ylabel('Load Current [A]')
xlim([(reconnect_initiate_extendedSOGI_standardImp(end)-0.01), inf])
xline(reconnect_initiate_extendedSOGI_standardImp(end),'g');
xline(reconnect_extendedSOGI_standardImp(end),'m');
legend('Load Current','Synchronization Initialized','Grid
Reconnection','location','north')
```

THIS PAGE INTENTIONALLY LEFT BLANK

LIST OF REFERENCES

[1] Office of the Assistant Secretary of Defense for Energy, Installations, and Environment, "Department of Defense annual energy management and resilience report (AEMRR) Fiscal Year 2017," Washington, DC, USA, Jul. 2018.

[2] A. Nicastri and A. Nagliero, "Comparison and evaluation of the PLL techniques for the design of the grid-connected inverter systems," in *2010 IEEE International Symposium on Industrial Electronics*, 2010, pp. 3865–3870, https://doi.org/10.1109/ISIE.2010.5637778

[3] D. Kanavaros, "Implementation of active and reactive power flow control in a single phase microgrid," Master's thesis, Monterey, CA; Naval Postgraduate School, 2019.

[4] G. Oriti, A. L. Julian, and N. J. Peck, "Power-electronics-based energy management system with storage," *IEEE Trans. Power Electron.*, vol. 31, no. 1, pp. 452–460, Jan. 2016, https://doi.org/10.1109/TPEL.2015.2407693

[5] J. Rocabert, G. M. S. Azevedo, A. Luna, J. M. Guerrero, J. I. Candela, and P. Rodríguez, "Intelligent connection agent for three-phase grid-connected microgrids," *IEEE Trans. Power Electron.*, vol. 26, no. 10, pp. 2993–3005, Oct. 2011, https://doi.org/10.1109/TPEL.2011.2116126

[6] P. Rodriguez, A. Luna, I. Candela, R. Mujal, R. Teodorescu, and F. Blaabjerg, "Multiresonant frequency-locked loop for grid synchronization of power converters under distorted grid conditions," *IEEE Trans. Ind. Electron.*, vol. 58, no. 1, pp. 127–138, Jan. 2011, https://doi.org/10.1109/TIE.2010.2042420

[7] Paul Krause, Oleg Wasynczuk, Scott Sudhoff, and Steven Pekarek, *Analysis of Electric Machinery and Drive Systems*, Third ed. Hoboken, NJ, USA: John Wiley & Sons, Inc, 2013.

[8] *IEEE Standard for interconnection and interoperability of distributed energy resources with associated electric power systems interfaces, IEEE* Std 1547-2018 Revis. IEEE Std 1547-2003, pp. 1–138, Apr. 2018, https://doi.org/10.1109/IEEESTD.2018.8332112

[9] Building microgrid. "Microgrid definitions." Accessed 27 Oct. 2019. [Online]. Available: https://building-microgrid.lbl.gov/microgrid-definitions

[10] Alexis Kwasinski, Wayne Weaver, and Robert S. Balog, *Microgrids and other Local Area Power and Energy Systems*, Cambridge, United Kingdom: Cambridge University Press, 2016.

[11] *IEEE guide for design, operation, and integration of distributed resource island systems with electric power systems, IEEE Std* 15474-2011, pp. 1–54, Jul. 2011, https://doi.org/10.1109/IEEESTD.2011.5960751.

[12] MathWorks. “Simscape electrical.” Accessed 19 Sep. 2019. [Online]. Available: https://www.mathworks.com/products/simscape-electrical.html

[13] A. Metzcus, “H-bridge inverter loading analysis for an Energy Management System,” Naval Postgraduate School, Monterey, California.

[14] MathWorks. “Simscape electrical block libraries - MATLAB & Simulink.” Accessed 19 Sep. 2019. [Online]. Available: https://www.mathworks.com/help/physmod/sps/ug/simscape-electrical-block-libraries.html

[15] MathWorks. “Environment block for Simscape Electrical Specialized Power Systems models - Simulink.” Accessed 19 Sep. 2019. [Online]. Available: https://www.mathworks.com/help/physmod/sps/powersys/ref/powergui.html

[16] Ned Mohan, Tore M. Undeland, and William P. Robbins, *Power Electronics, Converters, Applications, and Design 3rd Edition*, 3rd ed. Hoboken, NJ, USA: John Wiley & Sons, Inc, 2003.

[17] MathWorks. “csvread.” Accessed 19 Sep. 2019. [Online]. Available: https://www.mathworks.com/help/matlab/ref/csvread.html

[18] P. Rodriguez, A. Luna, M. Ciobotaru, R. Teodorescu, and F. Blaabjerg, “Advanced grid synchronization system for power converters under unbalanced and distorted operating conditions,” in *IECON 2006 - 32nd Annual Conference on IEEE Industrial Electronics*, Paris, 2006, pp. 5173–5178, https://doi.org/10.1109/IECON.2006.347807

[19] MathWorks. “Implement switch-on or switch-off delay - Simulink.” Accessed 02 Jan. 2020. [Online]. Available: https://www.mathworks.com/help/physmod/sps/powersys/ref/onoffdelay.html

INITIAL DISTRIBUTION LIST

1. Defense Technical Information Center
   Ft. Belvoir, Virginia

2. Dudley Knox Library
   Naval Postgraduate School
   Monterey, California